國 立 交 通 大 學

電信工程研究所

博 士 論 文

位元交錯編碼調變合作中繼網路之

效能分析與功率分配

Performance Analysis and Power Allocation for BICM-Coded Cooperative Relaying Networks

研 究 生：余倉緯

指導教授：沈文和 博士

王忠炫 博士

中 華 民 國 一 〇 一 年 六 月

位元交錯編碼調變合作中繼網路之效能分析與功率分配

Performance Analysis and Power Allocation for BICM-Coded Cooperative Relaying Networks

研 究 生：余倉緯　　Student：Tsang-Wei Yu
指導教授：沈文和 博士　　Advisor：Dr. Wern-Ho Sheen
王忠炫 博士　　Dr. Chung-Hsuan Wang

國立交通大學
電信工程研究所

博 士 論 文

A Dissertation
Submitted to Institute of Communication Engineering
College of Electrical and Computer Engineering
National Chiao Tung University
in Partial Fulfillment of the Requirements
for the Degree of Doctor of Philosophy
in
Communication Engineering
Hsinchu, Taiwan

2012 年 6 月

位元交錯編碼調變合作中繼網路之
效能分析與功率分配

研究生：余倉緯　　指導教授：沈文和 博士
王忠炫 博士

國 立 交 通 大 學
電 機 工 程 學 系

摘要

位元交錯編碼調變合作中繼網路(BICM-coded cooperative relaying network)是下世代無線通訊系統所使用的關鍵技術；它承襲了位元交錯編碼調變(bit-interleaved coded modulation, BICM)的頻寬與功率的高使用效率，並得益於合作式傳輸的使用，使得它可以在不需要實際裝置多天線的前提下，即能達到空間分集(space diversity)的效果。在本論文中，我們將探討此系統的效能分析與功率分配。

位元交錯編碼調變合作中繼網路的效能分析至今仍尚未有完整的探討，特別是針對選擇性解碼-轉傳(Selection decode-and-forward，S-DF)技術。S-DF 被認為是一實際的轉傳方式，因為它在可行的複雜度下，能提供比固定式解碼轉傳(Fixed DF)更好的效能。在現有的文獻中已有 S-DF 的相關分析結果，但皆僅侷限於無通道編碼的系統，並且皆採用一種以符元為單位的轉傳策略。在此策略中，各符元是分別地被檢測，而僅有正確的符元才允許被轉傳。實際上，此策略可能不適用於現今真實的系統上，因為它與循環冗餘校驗(cyclic redundancy check)本身特性有所矛盾，況且又需大量額外的信令耗損(signaling overhead)。本論文考慮的是一種以封包為單位的轉傳策略；包含了兩種 S-DF 方式：S-DF/RT(S-DF with source retransmission) 與 S-DF/Idle (S-DF with source idle) (依訊源端(source)是否在中繼站

解碼失敗時重傳封包來做區分)。在快速衰退(fast-fading)和區塊衰退(block-fading)的 Nakagami-*m* 通道下，本論文提出了在目的端(destination)的位元錯誤率(bit-error-rate，BER)分析，並且推導了該網路的分集階數(diversity order)，同時，也提供了模擬的結果來證實：在不同的調變、中繼站數量、及通道狀況下，所提出的分析方法的準確性。

在功率分配的部分，本論文考慮了四種的合作中繼模式：放大-轉傳(amplify-and-forward，AF)、S-DF/RT、S-DF/Idle 與 S-DF/AF，其中 S-DF/AF 代表中繼站在解碼失敗時，切換成以 AF 的模式進行轉傳。本論文的目標為：根據完美的通道狀態資訊(channel state information)，透過功率分配來最小化目的端的 BER。在 AF 模式中，本論文提出了一近似的 BER，並證明其為等效通道(equivalent channel)之嚴格遞減函數，因而可將此等效通道視為成本函數(cost function)來進行最佳化。在 S-DF 模式下，則提出了 PA-ABER 與 PA-MGEC 兩種功率分配的方式。PA-ABER 是採用近似的 BER 做為成本函數，經由證明得知此成本函數對於 S-DF 下的任一種中繼模式而言，皆是 convex 函數，因此可使用 gradient method 來對其進行最佳化。本論文又提出了 PA-MGEC 來進一步減化計算的複雜度，它將原本在 PA-ABER 的最佳化問題轉換成了一個 max-min 的問題，然後採用了最小廣義等效通道 (minimum generalized equivalent channel，MGEC)為其成本函數。對於不同的 S-DF 模式，我們皆提出了 PA-MGEC 下的特定解法。此外，本論文亦證明了 PA-ABER 與 PA-MGEC 皆可以被應用在解碼-重映射-轉傳(decode-remap-and-forward，DRF)的合作中繼系統上。其中 DRF 代表中繼站被允許使用與 source 不同的星座映射(constellation mapping)方式，來得到重映射的好處。本論文提供了數值的結果來證實，所提出的方法在效能上的確大幅地超越了等增益功率分配(equal gain power allocation)。

Performance Analysis and Power Allocation for BICM-Coded Cooperative Relaying Networks

Student: Tsang-Wei Yu Advisor: Dr. Wern-Ho Sheen

Dr. Chung-Hsuan Wang

Department of Electrical and Computer Engineering

National Chiao Tung University

Abstract

BICM (bit-interelaved coded modulation)-coded cooperative relaying network is one of the key technologies for the next-generation wireless communication systems. It inherits the bandwidth and power efficiency from BICM and also benefits from cooperative transmission for gaining space diversity yet without using multiple physical antennas. This dissertation investigates such a system from the aspects of performance analysis and power allocation.

The performance analysis of BICM-coded cooperative relaying network has not yet been fully explored, especially for selection decode-and-forward (S-DF) which has been regarded as a promising scheme that provides better performance over fixed DF with practical complexities. In fact, existing works are limited to un-coded S-DF with a symbol-by-symbol forwarding strategy, in which each symbol is detected separately, and only the correct symbols are forwarded. Unfortunately, this strategy may not be applicable to nowadays real systems due to the limitation of cyclic redundancy check and the requirement of additional signaling overhead. This dissertation is the first work that considers BICM-coded cooperative relaying network with a packet-by-packet forwarding strategy. In addition, two types of S-DF modes are investigated: S-DF/RT and S-DF/Idle, depending on whether or not the source re-transmits the packet again

when the relay fails to decode. The analysis of bit-error-rate (BER) at the destination and derivation of the diversity orders of the network are proposed for both fast-fading and block-fading Nakagami-*m* channels. Simulation results are given to show the effectiveness of our analyses in different modulations, number of relays and channel conditions.

This dissertation also provides a comprehensive investigation on transmit power allocation including 4 relaying modes, namely, amplify-and-forward (AF), S-DF/Idle, S-DF/RT and S-DF/AF in which the relay uses AF upon decoding failure. Based on perfect channel state information, the target is to allocate power to minimize the BER at the destination. To avoid the cumbersome (if not impossible) evaluation of the exact BER and an inefficient exhaustive search of the optimal power, this dissertation provides, for individual modes, a simplified cost function which can be optimized efficiently through existing algorithms. For AF, it is shown that the approximate BER monotonically decreases with the equivalent channel, which is then adopted as the cost function for optimization. For S-DF, two power allocation methods are proposed. The first, called PA-ABER, employs an approximate BER as a cost function, which is then proved to be convex for each relaying mode and then optimized through the gradient method. To further reduce the computation complexity, the second method, called PA-MGEC, first transforms PA-ABER to a max-min problem, and the cost function is named minimum generalized equivalent channel (MGEC) which can be optimized with existing algorithms for the 3 relaying schemes. Furthermore, this dissertation shows that these two methods are applicable to the network with decode-remap-and-forward (DRF) relays, which are allowed to choose different constellation mappings from that of source so as to obtain a remapping gain. Numerical results show that both of the proposed methods outperform the equal gain power allocation by large margins with or without remapping.

Acknowledgement

Foremost, I would like to express my sincere gratitude to my advisors, Prof. Wern-Ho Sheen. Thanks for teaching the right attitude on research, for helping me discover and deal with research problems, for patiently discussing with me again and again on details, and for reading and revising my draft papers, for supporting me throughout my Ph.D. studies. I could not have completed my Ph.D. degrees without their advice, guidance and valuable comments.

Second, I would like to express my heartfelt gratitude to Prof. Chung-Hsuan Wang, for giving valuable suggestions, and for instructing and helping me a lot in academic writing.

I would also like to thank my former student colleague Liang-Wei Huang for leading me to the start of my research, Shiang-Jiun Lin for encouraging me when I feel upset. Special thanks to all the student colleagues of Broadband Radio Access Systems Lab (BRASLAB) for their kind help in many aspects.

Finally, I am deeply indebted to my family who have supported me materially and mentally through this long journey.

Contents

List of Figures

List of Tables

Notations

- $\boldsymbol{j}$: $\sqrt{-1}$
- $(\cdot)^T$: transpose of a matrix or vector
- $\mathrm{E}_x[\ ]$: expectation operator with respect to variable x
- $\mathrm{Re}\{\cdot\}$: real parts
- $\mathbf{1}$: all 1 vector
- $\exp(\cdot)$: exponential function
- $\Gamma(\cdot)$: Gamma function
- $|\cdot|$: Norm of a complex number or cardinality of a set

Chapter 1

Introduction

Today, a wide variety of wireless communication systems have been deployed around the world to provide users with un-tethered telecommunication services. The users' ever increasing demands on better quality of service (QoS), higher transmission rate and lower cost, however, still keep driving the development of more advanced wireless communication technologies and systems. The design of future generations of wireless communication systems is aimed to provide users with low-power consumption, low-cost, high-quality multi-media services anytime, anywhere and at any mobility. Unfortunately, transmissions through wireless channels suffer from various radio impairments, including propagation loss, multi-path fading, shadowed fading and co-channel interference [1]-[4]. Such impairments will become even severer under high-rate and/or low-power constraints and have to be overcome before the design objective can become a reality.

To cope with multipath fading, diversity techniques are commonly considered. The idea is to transmit copies of the signals through multiple (independent) channels, which may be created in time, frequency, or space. Multiple-input multiple-output (MIMO) has been known as one of the most effective techniques [3]-[10]; by using multiple antennas at both transmitter and receiver, MIMO is able to provide not only diversity gain against multi-path fading, but also array gain

(power gain), and/or degree-of-freedom gain over the single-input and single-output (SISO) technique. However, since multiple antennas are usually installed on the same device, MIMO is not good at counteracting propagation loss or shadowed fading.

On the other hand, cooperative relaying [11]-[14] has emerged as a promising technique; by allowing other nodes to cooperate with the source to transmit data to the destination, the propagation loss and shadowed fading can be reduced, and the co-channel interference can be removed largely. In addition, the "virtual antenna array" formed by the source and the cooperative nodes can also be exploited to provide cooperative diversity to mitigate the effects of multi-path fading. Cooperative diversity has been regarded as the most practical space diversity technique for size-limited devices in which mounting multiple antennas is not feasible [15]-[18], and has been adopted in today commercial standards, such as 3GPP-LTE (long term evolution) [19] and IEEE 802.16j [20].

1.1 Cooperative Relaying

In the cooperative relaying, thanks to the broadcast nature of wireless communications, some other nodes (called relays) are allowed to overhear the packet transmitted from the source and help relay it to the destination to improve communication performance. Two relaying modes have been explored extensively in the literature: one is amplify-and-forward (AF, or non-regenerative) and the other decode-and-forward (DF, or regenerative). In the AF relaying, a relay simply forwards the signals received from the source to the destination without any decoding. To keep a constant transmit power at the relays, the signals are forwarded either with variable-gain normalization [16], [21]-[25] or fixed-gain normalization [26]-[28]. The AF relaying has been shown to achieve full diversity in Rayleigh fading channels [16] and in Nakagami-*m* fading channels [28].

In the DF relaying, a relay decodes the packet received from the source, re-encodes and forwards it to the destination. The relay can always forward the packet to the destination, or it

does the forwarding only if the packet is decoded correctly. The former is called the fixed DF (F-DF) and the latter the selection DF (S-DF) relaying. In [16], it was shown that the F-DF does not achieve a full diversity in Rayleigh fading channels, but S-DF does. In practice, S-DF can be implemented easily with a cyclic redundancy check (CRC) [30]. In addition, two modes of operation can be differentiated within the S-DF relaying: one is S-DF with source idle (S-DF/Idle) [31]-[40], and the other S-DF with source retransmission (S-DF/RT) [16]. In S-DF/Idle, the source keeps silent in the case of relay decoding failure whereas in the S-DF/RT, the source retransmits the packet on the relay's behave. Recently, a hybrid relaying method involving S-DF and AF (denoted by S-DF/AF) has been proposed in which a relay uses AF upon decoding failure [41]-[44] otherwise S-DF is used. Generally speaking, S-DF/AF and S-DF/RT outperform S-DF/Idle but with higher complexities on decoding and signaling.

Although DF relaying is more complex than AF due to the need of decoding and re-encoding before forwarding, it allows the relay to use a different channel code or modulation from source to acquire additional gains. The former is usually called coded cooperation [45][46] and the later the decode-remap-and-forward (DRF) relaying [47]-[50]. In DRF, the basic idea is to enlarge the minimum overall Euclidean distance seen at the destination by changing the mappers at relays so as to obtain a remapping gain. The concept of constellation-remapping was originally devised in the multiple-packet transmissions such as H-ARQ (hybrid automatic repeat request) and has been shown to offer significant gain over those without remapping for both coded and uncoded systems [51][52].

1.2 BICM

Coded modulation has been known as a high spectrum-efficient technique for high-data-rate transmission [53]-[58]. Trellis coded modulation (TCM) was first devised for AWGN (additive white Gaussian noise) channels in [53], where the Euclidean distance between coded sequences

is maximized. Its performance, however, significantly is degraded in fading channels because of its very low diversity order. In [57], a bit-wise interleaver is employed between the channel encoder and modulator to allow a coded modulation system to achieve a higher diversity order with a moderate complexity. The scheme is later known as the bit-interleaved coded modulation (BICM), and its diversity order was proved to be the free distance of the outer code, under the fast Rayleigh fading environment [58].

The main idea of BICM is to transmit the coded bits over independent channels for gaining the diversity. With the use of interleaving and de-interleaving, the independent channels can be obtained through time for high mobility users, through frequency for OFDM (orthogonal frequency-division multiplexing) systems, and/or through space for multi-antenna systems. As a result, BICM has been used widely in nowadays systems [59][60].

Very recently, studies have begun to look at the BICM-coded cooperative relaying networks [61]-[65]. For example, bit error rate (BER) performance of a BICM-coded cooperative network was analyzed in [61] with the F-DF relay being modeled by a post-BSC (binary symmetric channel). Reference [62] evaluated the achievable rates for different combinations of modulation and number of antennas used at the source and relay nodes. Pre-coding for a non-orthogonal AF was studied in [63] aiming to achieve maximum diversity order and high coding gains. For the BICM-coded cooperative OFDM systems, [64] considered the relay selection and sub-carrier allocation with AF relaying in order to minimize the asymptotic worst-case, pair-wise error probability, whereas [65] considered the issue of relay placement with DF relaying.

The objective of this dissertation is to investigate the BICM-coded cooperative relaying network in the aspects of performance analysis and power allocation.

1.3 Performance Analysis

The performance analysis of the cooperative relaying networks has been a topic of extensive research, e.g., [16]-[28] for AF and [31]-[40] for S-DF. The analyses were done over the Rayleigh fading channels from the aspects of capacity [21][31], outage probability [16][22][23][27][32][33] and un-coded symbol-error-rate (SER) [27][34][35], respectively. Very recently, the analysis has been extended to the Nakagami-*m* fading channels in [36]-[40] for the un-coded network. The Nakagami-m channel has been considered as a generalized channel model due to its great versatility, in the sense that it has better flexibility and accuracy in matching various real wireless environments than Rayleigh, log-normal or Rician distributions [29]. In particular, in [36], SER was analyzed for a single-relay network under the correlated and uncorrelated channels, and exact SER was provided in [37] for the multiple-relay networks. In [38], an asymptotic SER approximation is provided, and with that a power allocation was proposed. In [39], a close-form expression for the moment generating function of the received signal-to-noise ratio (SNR) at the destination was derived, and it was used to evaluate the average SER, outage probability and the average channel capacity. Lastly, in [40], SER and diversity order were investigated for the networks with inter-relay links.

For the BICM-coded cooperative relaying network, BER analyses with AF relays are provided in [66][67]. However, to the best of our knowledge, the existing works on S-DF provided the analysis only for the un-coded systems (cf. [34]-[40]). In addition, the S-DF was based on a symbol-by-symbol forwarding strategy, where symbols are detected separately, and only the correct symbols are forwarded to the destination. In real systems, nevertheless, a CRC can only detect whether a packet is in error rather than the exact erroneous locations. Furthermore, such a symbol-based forwarding requires additional signaling overheads to indicate the locations of the correct symbols, and that increases the complexity very significantly. Therefore, this dissertation considers BICM-coded cooperative relaying system with a packet-by-packet forwarding strategy

which is more practical in real systems.

1.4 Power Allocations

Transmit power allocation between source and relay nodes is a critical design issue in the cooperative networks where sources and relays are powered by batteries. An effective power allocation between transmit nodes could significantly lower the error rate at the destination so as to reduce the probability of re-transmission via (H-)ARQ [68] (which requires additional power/energy and radio resources). Moreover, a good transmit power allocation method should involve relay selection as well, e.g., allocate zero power to the useless relays. Recently, it has been widely discussed in the literature. For examples, the capacity is maximized for a 3-node F-DF relaying network in [69] based on full channel state information (CSI). The outage probability was minimized in [70] through joint power allocation and relay positioning for multiple DF or AF relays. Reference [71] proposed a relay selection and power allocation scheme to prolong the lifetime of the DF cooperative network under a non-outage constraint, whereas [72] aimed to maximize the sum-rate. Uncoded SER was analyzed and minimized via power allocation in [34] for a 3-node DF cooperative network, while [73] dealt with BER. Joint subcarrier and power allocation for an uncoded OFDM system with AF relays is investigated in [74].

In most of the existing works, power allocation was designed either from an information-theoretic viewpoint [69]-[72] or to minimize un-coded SER or BER [34][73][74]. As to the power allocation on BICM-coded cooperative systems, [64] considered the power allocation of a BICM-OFDM system with the AF relaying. Our previous work [75] considered a 3-node network with an S-DF/Idle relay, and which is then extended in [50] to a multiple-relay network with DRF relays. However, the power allocation is still an open question for S-DF/RT and S-DF/AF.

1.5 Dissertation Outline and Contributions

This dissertation focuses on performance analysis and power allocation for a BICM-coded cooperative relaying network. Since the performance analysis of AF has been discussed in [66][67], the performance analyses in this dissertation mainly focus on S-DF. For the performance analysis part, unlike the existing works which considered uncoded S-DF with symbol-by-symbol forwarding strategy, this dissertation is the first work that studies the BICM-coded cooperative relaying network with packet-by-packet forwarding strategy. The target is to provide the analysis of BER performance at the destination and the diversity order of the network for both S-DF/RT and S-DF/Idle over both fast-fading and block-fading Nakagami-*m* channels. For the power allocation part, a comprehensively investigation is proposed for not only the AF, S-DF/RT, S-DF/Idle and S-DF/AF relaying (based on a packet-by-packet forwarding) but also DRF relays. Based on the knowledge of perfect CSI, the target is to allocate power to minimize the BER at the destination, while taking into account the probability of decoding failure at relays. To avoid the cumbersome (if not impossible) evaluation of the exact BER and an inefficient exhaustive search of the optimal power, simplified cost functions which can be optimized efficiently through existing algorithms are proposed for individual modes. The objective is to determine the transmit power allocation that minimizes the BER at the destination. Outline and contributions of this dissertation are as follows.

Chapter 2 first describes the network model and the channel statistics. The BICM modulation at the source and the corresponding decoding at relays at the phase-I are given. Then, the model of signals forwarded at phase-II are introduced for AF, S-DF/RT, S-DF/Idle and S-DF/AF, following by a general formulation that is used to describe the decoding at the destination and will be further employed in the derivations of all the following chapters.

Chapter 3 investigates the BER performance and diversity order for S-DF/RT and S-DF/Idle over fast-fading Nakagami-*m* channels with a packet-by-packet forwarding strategy. Given a set

of active relays, this Chapter first derives the approximation of BER at the destination by extending the expurgated bound proposed in [58]. But, unlike [58] which employed the Chernoff bound to obtain the expurgated bound, a close-form evaluation is proposed. Such an evaluation can be degenerated to calculate the error rate at relays so that the overall BER at the destination is obtained. To find out the diversity of the network, the asymptotic upper and lower bounds are derived by considering only the worst case error events between coded sequences and signal point pairs with the shortest Euclidean distance in the constellation. By showing that both bounds achieve the same diversity order, the diversity order of the network is obtained. Numerical results show that our approximations are rather accurate (within a 0.4dB gap to the true BER) for different network setups.

Chapter 4 studies the BER performance and diversity order for block-fading Nakagami-*m* channels. For the BER analysis, the BER for a given active relay set can be obtained by first obtaining the BER in AWGN channels before averaging it over channel realizations. Unfortunately, a direct integration may lead to a non-trivial gap to the exact performance due to the severe loss at low SNR regions in AWGN case. As a result, the BER in AWGN is modified and the Monte Carlo method is used for the channel averaging. The diversity of the cooperative BICM network is also derived for both S-DF/RT and S-DF/Idle. Numerical results are given to show that our approximations are rather accurate for different network setups. An example is also provided to verify our proof of the diversity order.

Chapter 5 investigates the power allocation of the cooperative BICM relaying network. Four relaying schemes are considered: AF, S-DF/RT, S-DF/Idle and S-DF/AF with the general formulation given in Chapter 2. For AF, by simplifying the union bound, an approximate BER is derived and shown to be monotonically decreasing with an equivalent channel gain so that the power allocation method named PA-EC is proposed which takes the equivalent channel as the cost function. For the S-DF relaying modes, two power allocation methods are proposed: PA-ABER based on approximate BER and PA-MGEC based on minimum generalized equivalent

channel. In PA-ABER, the approximate BER is shown to be a convex function for S-DF/RT, S-DF/Idle and S-DF/AF. Therefore, gradient method can be adopted to find the solution. Then PA-MGEC transforms PA-ABER to a max-min problem, which can be optimized with even lower complexity. Examples are given to demonstrate how power is allocated for PA-EC and PA-MGEC on the AF and S-DF relaying modes. Simulation results confirm that our proposed methods have the ability to properly allocate power according to the SNR value and the channel realizations. The proposed methods outperform the equal gain power allocation (PA-EG) with large margins for different network setups.

Chapter 6 considers S-DRF relays which are allowed to change the mappers before forwarding so as to obtain an addition remapping gain. The proposed methods, PA-ABER and PA-MGEC, in Chapter 5 are extended in this chapter for the remapping case. Examples are provided to demonstrate how power is allocated, and numerical results confirm that the proposed method outperform PA-EG with large margins for different network setups.

Finally, Chapter 7 concludes the dissertation and discusses some possible extensions and future research topics.

Chapter 2

System Model

2.1 Network Model

This dissertation considers a cooperative relaying network as shown in Fig. 2.1 with one source, R relays and one destination, which are indexed by 0, 1, $\cdots$, R, and $R+1$, respectively. Each node is equipped with one antenna. Relays operate in the half-duplexing manner implying that they cannot transmit and receive simultaneously. Transmission of a packet is divided into two phases; at phase-I, the source broadcasts a packet to relays and the destination. In cases of the relaying mode used, at phase-II, either relays or the source forward(s) the received packet over orthogonal channels to the destination. In the following, the orthogonal channel allotted to relay j for transmission at phase-II will be called orthogonal-channel j (OC- j).

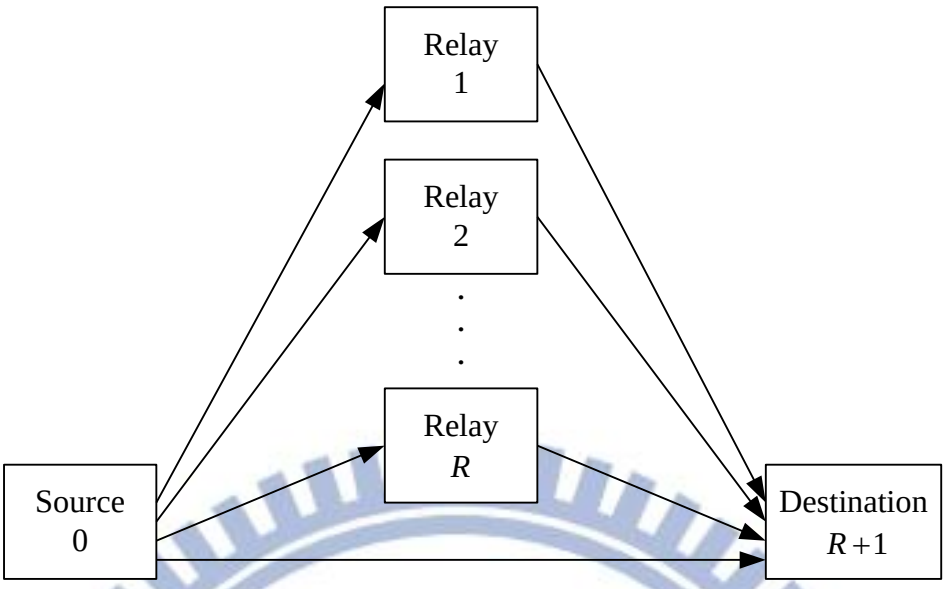

Fig. 2.1 A cooperative relaying network with one source, one destination and R relays

A frequency-nonselective fading channel is investigated. Define $h_{0,j}(k)$, $j=1,2,\cdots,R+1$, the channel gain between the source and node j at the k-th channel use, $h_{j,R+1}(k)$ $i=1,2,\cdots,R$ the channel gain between relay j and the destination (through orthogonal-channel j), and $h_{0,R+1}^{(j)}(k)$, $j=1,2,\cdots,R$ the channel gain between the source and destination at phase-II that uses orthogonal-channel j for retransmission. The channels are assumed to be mutually independent. When block-fading environments are considered, the channel gain of the same link is assumed constant during the transmission of a packet and changes from packet to packet. For fast-fading environments, under the assumption of a symbol interleaver with a depth larger than the channel coherent time, the channel gains of the same link are independent and identically distributed (i.i.d.) over different time index k.

The general Nakagami-*m* fading model is adopted, with the probability density function (PDF) [29]

$$p(h)=\frac{2m^m h^{2m-1}}{\Gamma(m)\Omega^m}\exp\left(-\frac{mh^2}{\Omega}\right) \tag{2.1}$$

for the channel gain h, where m is the shaping factor (assumed to be an integer), Ω is the average power, and $\Gamma(\cdot)$ is the Gamma function [76]. Perfect receiver CSI (CSI-R) is assumed available at all receiving nodes.

2.2 Bit-interleaved Coded Modulation (BICM)

BICM is employed at all nodes. At the source, an information bit sequence $\mathbf{b}$ of length K is encoded into a coded sequence $\mathbf{c}$ of length N, as shown in Fig. 2.2(a). After interleaving, the resulting sequence $\mathbf{v}$ is partitioned successively into groups of l bits, called the labels. The k-th label in $\mathbf{v}$, denoted by $v(k)$, is then mapped to a complex symbols $x(k)$ for transmission, according to a signal mapper μ and a signal constellation χ. At phase-I, the received signals at relays and the destination at time k are given by

$$y_{0,j}(k) = h_{0,j}(k)\sqrt{P_0}x(k) + \omega_{0,j}(k), \quad j = 1, 2, \cdots, R+1, \tag{2.2}$$

where P_0 is the source transmit power, and $\omega_{0,j}(k)$ is the AWGN (additive white Gaussian noise) at node j. All noises are modeled as i.i.d. zero-mean, circularly-symmetric complex Gaussian random variables with the variance $N_0/2$ per dimension.

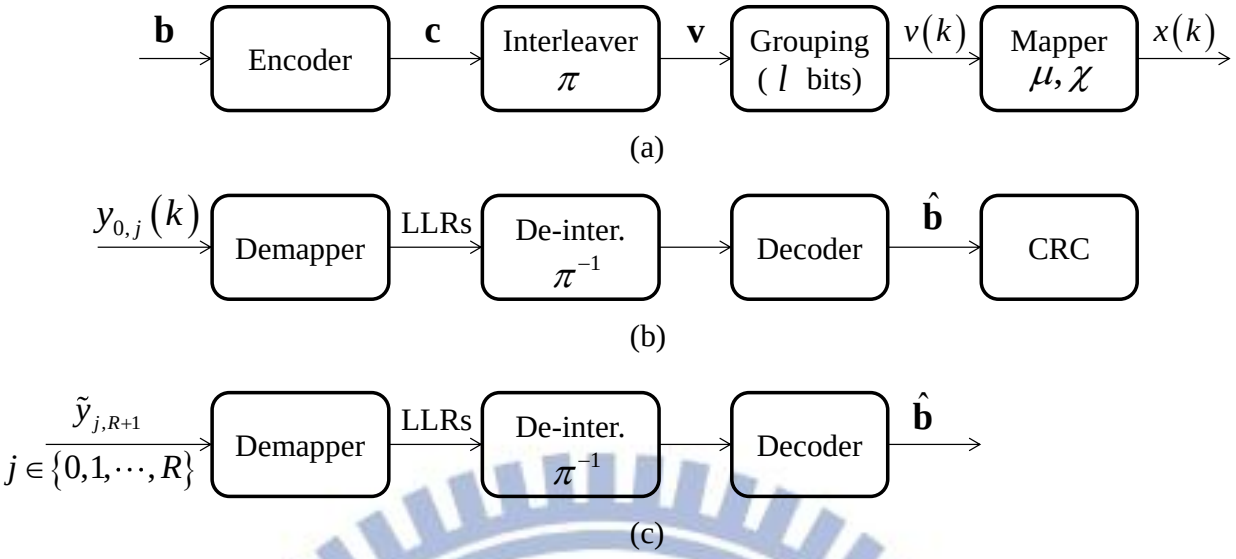

Fig. 2.2 Block diagrams of (a) the transmitter at source, (b) receivers at relay j and (c) receiver at destination

When AF relaying is considered, the received packet will be forwarded without decoding. For the S-DF relayings (S-DF/RT, S-DF/Idle, S-DF/AF), the packet is first decoded before forwarding. Specifically, upon receiving $y_{0,j}(k)$, relay j calculates the simplified log-likelihood ratio (LLR) for the i-th bit of the k-th symbol, according to

$$\min_{x\in\chi_0^i}\frac{\left|y_{0,j}(k)-h_{0,j}(k)\sqrt{P_0}x\right|^2}{N_0}-\min_{x\in\chi_1^i}\frac{\left|y_{0,j}(k)-h_{0,j}(k)\sqrt{P_0}x\right|^2}{N_0}, \tag{2.3}$$

where χ_b^i is the subset of signal points in χ with the binary value b at the i-th position of the label. The LLRs of coded sequence are then de-interleaved and decoded, as shown in Fig. 2.2(b). The Max-log MAP (maximum a posteriori probability) decoder [77] is employed at all receiving nodes.

2.3 Signals in Phase-II for different Relaying Schemes

2.3.1 Amplify-and-Forward (AF)

In the AF relaying, each relay forwards the received packet through the orthogonal-channel with a power normalization so as to keep a constant transmit power. In this case, the received signals at destination at phase-II are

$$y_{j,R+1}(k) = h_{j,R+1}(k)\sqrt{\frac{P_j}{P_0\left|h_{0,j}(k)\right|^2 + N_0}}\, y_{0,j}(k) + \omega_{j,R+1}(k), \quad j = 1,2,\cdots,R, \tag{2.4}$$

where P_j is the transmit power over orthogonal-channel j, and $\omega_{j,R+1}(k)$ is the corresponding AWGN at destination. In (2.4), the variable-gain normalization is adopted. The received signals at phase-I and phase-II are combined and decoded jointly at the destination, which will be described in Section 2.4.

2.3.2 S-DF with Source Re-transmission (S-DF/RT)

In S-DF/RT, relay j forwards the received packet to the destination if **b** is decoded correctly. Otherwise, it notifies the source to re-transmit the packet though OC-j. Define $\Theta \subseteq \{1,\cdots,R\}$ as the set of relays which have decoded successfully at phase-I. Then, at phase-II, the signals received at destination are expressed by

$$y_{j,R+1}(k) = h_{j,R+1}(k)\sqrt{P_j}\,x(k) + \omega_{j,R+1}(k), \ \ j \in \Theta, \tag{2.5}$$

and

$$y^{(j)}_{0,R+1}(k) = h^{(j)}_{0,R+1}(k)\sqrt{P_j}\,x(k) + \omega^{(j)}_{0,R+1}(k), \ \ j \notin \Theta, \tag{2.6}$$

where $\omega_{0,R+1}^{(j)}(k)$ is the corresponding AWGN at OC- j. Note that, in S-DF/RT, an ACK or NCK from relay j is required for the source before the beginning of Phase-II so as to know whether it should re-transmit the packet through OC- j or not.

2.3.3 S-DF with Source Idle (S-DF/Idle)

In S-DF/Idle, the source keeps silent at phase-II. Nothing is going to be sent in OC- j at phase-II, if relay j fails to decode. Thus, only the signals in (2.5) are received at the destination. Note that, for S-DF/Idle, the relays do not have to send ACK or NCK back to source, and neither to the destination. The destination is supposed to know whether signals are transmitted on OC- j through power detection.

2.3.4 Hybrid S-DF/AF (S-DF/AF)

In S-DF/AF, relay j forwards the received packet to the destination if **b** is decoded correctly. Otherwise, it amplifies the packet and forwards it though OC- j. Thus, at phase-II, the signals received at destination are expressed by

$$y_{j,R+1}(k) = h_{j,R+1}(k)\sqrt{P_j}x(k) + \omega_{j,R+1}(k),\ j \in \Theta, \tag{2.7}$$

and

$$y_{j,R+1}(k) = h_{j,R+1}(k)\sqrt{\frac{P_j}{P_0\left|h_{0,j}(k)\right|^2 + N_0}}y_{0,j}(k) + \omega_{j,R+1}(k),\quad j \notin \Theta. \tag{2.8}$$

Note that additional signaling is required for the decoding at the destination (in Section 2.4) to know whether the forwarding on OC- j is by DF or AF.

2.4 General Form and Decoding at Destination

For simplicity and convenience, we re-arrange the received signals of the above 4 relayings at phase-II into a general form, which is

$$\tilde{y}_{j,R+1}(k)=\tilde{h}_{j,R+1}(k)\sqrt{P_j}x(k)+\tilde{\omega}_{j,R+1}(k),\ \ j=1,2,\cdots,R. \tag{2.9}$$

In AF,

$$\begin{aligned}
&\tilde{y}_{j,R+1}(k)=y_{j,R+1}(k),\\
&\tilde{h}_{j,R+1}(k)=h_{j,R+1}(k)h_{0,j}(k)\sqrt{\frac{P_0}{P_0\left|h_{0,j}(k)\right|^2+N_0}},\\
&\tilde{\omega}_{j,R+1}(k)=h_{j,R+1}(k)\sqrt{\frac{P_j}{P_0\left|h_{0,j}(k)\right|^2+N_0}}\omega_{0,j}(k)+\omega_{j,R+1}(k)
\end{aligned} \tag{2.10}$$

with

$$\mathrm{var}\left[\tilde{\omega}_{j,R+1}(k)\right]=\left(\frac{\left|h_{j,R+1}(k)\right|^2P_j}{P_0\left|h_{0,j}(k)\right|^2+N_0}+1\right)N_0. \tag{2.11}$$

Define $\tilde{\Theta}\doteq\Theta\cup\{0\}$ as the set of all active nodes, including the source. In S-DF/RT, terms in (2.9) are replaced by

$$\begin{aligned}
\tilde{y}_{j,R+1}(k)&=\begin{cases}y_{j,R+1}(k), & \text{if } j\in\tilde{\Theta}\\ y_{0,R+1}^{(j)}(k), & \text{if } j\notin\tilde{\Theta}\end{cases},\\
\tilde{h}_{j,R+1}(k)&=\begin{cases}h_{j,R+1}(k), & \text{if } j\in\tilde{\Theta}\\ h_{0,R+1}^{(j)}(k), & \text{if } j\notin\tilde{\Theta}\end{cases},\\
\tilde{\omega}_{j,R+1}(k)&=\begin{cases}\omega_{j,R+1}(k), & \text{if } j\in\tilde{\Theta}\\ \omega_{0,R+1}^{(j)}(k), & \text{if } j\notin\tilde{\Theta}\end{cases}.
\end{aligned} \tag{2.12}$$

In S-DF/Idle,

$$\begin{aligned}
&\tilde{y}_{j,R+1}(k)=y_{j,R+1}(k),\ \text{for } j\in\tilde{\Theta},\\
&\tilde{h}_{j,R+1}(k)=h_{j,R+1}(k),\ \text{for } j\in\tilde{\Theta},\\
&\tilde{\omega}_{j,R+1}(k)=\omega_{j,R+1}(k),\ \text{for } j\in\tilde{\Theta}.
\end{aligned} \tag{2.13}$$

And in S-DF/AF,

$$\tilde{y}_{j,R+1}(k) = y_{j,R+1}(k),$$

$$\tilde{h}_{j,R+1}(k) = \begin{cases} h_{j,R+1}(k), & \text{if } j \in \tilde{\Theta} \\ h_{j,R+1}(k) h_{0,j}(k) \sqrt{\dfrac{P_0}{P_0 \left| h_{0,j}(k) \right|^2 + N_0}}, & \text{if } j \notin \tilde{\Theta} \end{cases}, \quad . \tag{2.14}$$

$$\tilde{\omega}_{j,R+1}(k) = \begin{cases} \omega_{j,R+1}(k), & \text{if } j \in \tilde{\Theta} \\ h_{j,R+1}(k) \sqrt{\dfrac{P_j}{P_0 \left| h_{0,j}(k) \right|^2 + N_0}} \omega_{0,j}(k) + \omega_{j,R+1}(k), & \text{if } j \notin \tilde{\Theta} \end{cases}.$$

With the general form in (2.9)-(2.14), the LLR for the i-th bit of the k-th symbol at the destination is evaluated by

$$\min_{x \in \chi_0^i} \sum_{j=0}^{R} \frac{\left| \tilde{y}_{j,R+1}(k) - \tilde{h}_{j,R+1}(k) \sqrt{P_j} x \right|^2}{\tilde{N}_0^{(j)}} - \min_{x \in \chi_1^i} \sum_{j=0}^{R} \frac{\left| \tilde{y}_{j,R+1}(k) - \tilde{h}_{j,R+1}(k) \sqrt{P_j} x \right|^2}{\tilde{N}_0^{(j)}}, \tag{2.15}$$

where

$$\tilde{N}_0^{(j)} = \begin{cases} \left(\dfrac{\left| h_{j,R+1}(k) \right|^2 P_j}{P_0 \left| h_{0,j}(k) \right|^2 + N_0} + 1 \right) N_0, & \text{for OC-}j\text{ with AF} \\ N_0, & \text{otherwise} \end{cases}. \tag{2.16}$$

Note that for S-DF/Idle, the summation in (2.15) only takes the terms with $j \in \tilde{\Theta}$. The LLRs of the coded sequence are then de-interleaved and passed to the decoder, as shown in Fig. 2.2(c).

Chapter 3

Performance and Diversity Analysis in Fast-fading Channels

In this chapter, the BER performance at the destination and the diversity order of the BICM-coded cooperative network in fast-fading Nakagami-*m* channels for both S-DF/RT and S-DF/Idle schemes are discussed. For fast-fading environments, we assume a symbol interleaver with a depth larger than the channel coherent time such that the channel gains of the same link are independent and identically distributed (i.i.d.) over different time index k. In what follows, the BER analyses are presented first, followed by the diversity analyses.

3.1 BER Analysis

This section provides the analyses of BER at destination for the BICM-coded cooperative network with packet-by-packet forwarding strategy. The analysis of S-DF/RT is provided first, and that of S-DF/Idle is given by indicating the differences.

3.1.1 S-DF/RT

Let $p_{b,R+1}^{\mathrm{RT}}$ denote the BER at the destination with the S-DF/RT relaying. Since $p_{b,R+1}^{\mathrm{RT}}$ depends on Θ, the decoding results at relays, it can be represented as

$$\begin{aligned} p_{b,R+1}^{RT} &= \sum_{\Theta\subseteq\{1,2,\cdots,R\}} p_{b,R+1}^{RT}(\Theta)\Pr[\Theta] \\ &= \sum_{\Theta\subseteq\{1,2,\cdots,R\}} p_{b,R+1}^{RT}(\Theta)\prod_{j\in\Theta}(1-p_{f,j})\prod_{j\notin\Theta} p_{f,j} \end{aligned}, \tag{3.1}$$

where $p_{b,R+1}^{\mathrm{RT}}(\Theta)$ is the BER at destination given the active set Θ, and $p_{f,j}$ is the packet-error-rate (PER) at relay j. Both $p_{b,R+1}^{\mathrm{RT}}(\Theta)$ and $p_{f,j}$ have experienced sufficient amount of channel realizations. It is worthy to remind that the BER in (3.1) is evaluated under the packet-by-packet based forwarding, rather than the impractical symbol-by-symbol based forwarding considered in [34]-[40]. In the following development, a close-form approximation of $p_{b,R+1}^{\mathrm{RT}}(\Theta)$ is derived first, followed by that of $p_{f,j}$.

Using the assumptions of ideal interleaving and symmetrization in [58], BICM can be regarded as a linear code such that the codeword pair-wise error probability (PEP) depends only on the Hamming distance between two coded sequences. In this case, the $p_{b,R+1}^{\mathrm{RT}}(\Theta)$ can be bounded by [78]

$$p_{b,R+1}^{\mathrm{RT}}(\Theta) \le \sum_{d_h=d_f}^{N} w_I(d_h) f^{\mathrm{RT}}(d_h,\Theta), \tag{3.2}$$

where $w_I(d_h)$ is the total information bits of the error events with Hamming weight d_h divided by K, d_f is the free distance of the code, and $f^{\mathrm{RT}}(d_h,\Theta)$ is the PEP between two coded sequences with Hamming distance d_h, averaged over the channel realizations.

In [58], $f^{\mathrm{RT}}(d_h,\Theta)$ was evaluated through a union bound $f_{ub}^{\mathrm{RT}}(d_h,\Theta)$ for a single-link Rayleigh fading channels. In this dissertation, where the parallel Nakagami-*m* fading channels are

considered, the union bound is extended as

$$f_{ub}^{\mathrm{RT}}\left(d_h,\Theta\right)=\frac{1}{2\pi \boldsymbol{j}}\int_{s_0-\boldsymbol{j}\infty}^{s_0+\boldsymbol{j}\infty}\prod_{k=1}^{d_h}\left[\frac{1}{l2^l}\sum_{i=1}^{l}\sum_{b=0}^{1}\sum_{x(k)\in\chi_b^i}\sum_{z(k)\in\chi_{\bar{b}}^i}\prod_{j=0}^{R}\Phi_{\Delta_j\left(x(k),z(k)\right)}\left(s\right)\right]\frac{ds}{s}, \tag{3.3}$$

where $\boldsymbol{j}=\sqrt{-1}$, and $\Phi_{\Delta_j\left(x(k),z(k)\right)}\left(s\right)$ is the moment generating function (MGF) of the metric difference

$$\begin{aligned}&\Delta_j\left(x(k),z(k)\right)\\&\doteq E_{\tilde{h}_{j,R+1}(k)}\left[\log p\left(\tilde{y}_{j,R+1}\left(k\right)\mid x\left(k\right),\tilde{h}_{j,R+1}\left(k\right)\right)-\log p\left(\tilde{y}_{j,R+1}\left(k\right)\mid z\left(k\right),\tilde{h}_{j,R+1}\left(k\right)\right)\right].\\&=E_{\tilde{h}_{j,R+1}(k)}\left[\exp\left[\left(-s+s^2\right)\frac{P_j}{\tilde{N}_0^{(j)}}\tilde{h}_{j,R+1}^2\left|x\left(k\right)-z\left(k\right)\right|^2\right]\right]\end{aligned} \tag{3.4}$$

Note that, in (3.4), $\tilde{N}_0^{(j)}=N_0$ for S-DF/RT and S-DF/Idle.

Unfortunately, as was discussed in [58], $f_{ub}^{\mathrm{RT}}\left(d_h,\Theta\right)$ is very loose at low-to-moderate SNRs due to that too many irrelevant z's are included in (3.3). To obtain a tighter bound, the expurgation proposed in [58] is proposed to provide a more accurate approximation, i.e.,

$$f_{ex}^{\mathrm{RT}}\left(d_h,\Theta\right)\doteq\frac{1}{2\pi \boldsymbol{j}}\int_{s_0-\boldsymbol{j}\infty}^{s_0+\boldsymbol{j}\infty}\prod_{k=1}^{d_h}\left[\frac{1}{l2^l}\sum_{i=1}^{l}\sum_{b=0}^{1}\sum_{x(k)\in\chi_b^i}\prod_{j=0}^{R}\Phi_{\Delta_j\left(x(k),\hat{z}(k)\right)}\left(s\right)\right]\frac{ds}{s}, \tag{3.5}$$

where all irrelevant $z\left(k\right)$'s in $\chi_{\bar{b}}^i$ are dropped, except $\hat{z}\left(k\right)$ which is the unique nearest neighbor of $x\left(k\right)$ in $\chi_{\bar{b}}^i$. In [58], the Chernoff bound was introduced in the evaluation of (3.5), which still introduces extra looseness on the bounds. Here, (3.5) is evaluated exactly through direct saddle point integration [79].

Firstly, we introduce Lemma-1 whose proof is given in Appendix A.

Lemma-1: Let h be a Nakagami-*m* random variable with shaping factor m and average power Ω, then

$$E_h\left[\exp\left[\left(-s+s^2\right)ah^2\right]\right]=\left(1-\left(-s+s^2\right)\frac{\Omega}{m}a\right)^{-m}, \tag{3.6}$$

providing that

$$\frac{1}{2}-\sqrt{\frac{m}{\Omega a}+\frac{1}{4}}<s<\frac{1}{2}+\sqrt{\frac{m}{\Omega a}+\frac{1}{4}}. \tag{3.7}$$

Applying Lemma-1, (3.4) is derived as

$$\Phi_{\Delta_j(x(k),\hat{z}(k))}(s)=\left(1-\left(-s+s^2\right)\frac{\tilde{\Omega}_{j,R+1}P_j\left|x(k)-\hat{z}(k)\right|^2}{\tilde{m}_{j,R+1}N_0}\right)^{-\tilde{m}_{j,R+1}} \tag{3.8}$$

with ROC given by

$$\frac{1}{2}-\sqrt{\frac{\tilde{m}_{j,R+1}N_0}{\tilde{\Omega}_{j,R+1}P_j\left|x(k)-\hat{z}(k)\right|^2}+\frac{1}{4}}<\mathrm{Re}\{s\}<\frac{1}{2}+\sqrt{\frac{\tilde{m}_{j,R+1}N_0}{\tilde{\Omega}_{j,R+1}P_j\left|x(k)-\hat{z}(k)\right|^2}+\frac{1}{4}}, \tag{3.9}$$

where

$$\tilde{m}_{j,R+1}=\begin{cases}m_{j,R+1}, & \text{if } j\in\tilde{\Theta}\\ m_{0,R+1}, & \text{if } j\notin\tilde{\Theta}\end{cases}\quad\text{and}\quad\tilde{\Omega}_{j,R+1}=\begin{cases}\Omega_{j,R+1}, & \text{if } j\in\tilde{\Theta}\\ \Omega_{0,R+1}, & \text{if } j\notin\tilde{\Theta}\end{cases}. \tag{3.10}$$

Since the saddle point 0.5 always falls in the ROC [79], the integration in (3.5) can be done along the vertical line $s=0.5+\boldsymbol{j}t$ for all real number t. By substituting $s=0.5+\boldsymbol{j}t$ and (3.8) into (3.5), one has

$$f_{\mathrm{ex}}^{\mathrm{RT}}(d_h,\Theta)=\frac{1}{4\pi}\int_{-\infty}^{\infty}\left[\frac{1}{l2^l}\sum_{i=1}^{l}\sum_{b=0}^{1}\sum_{x\in\chi_b^i}\prod_{j=0}^{R}\left(1+\left(t^2+\frac{1}{4}\right)\frac{\tilde{\Omega}_{j,R+1}P_j\left|x-\hat{z}\right|^2}{\tilde{m}_{j,R+1}N_0}\right)^{-\tilde{m}_{j,R+1}}\right]^{d_h}\frac{dt}{t^2+\frac{1}{4}}, \tag{3.11}$$

where the time index k has been dropped because $\tilde{m}_{j,R+1}$, $\tilde{\Omega}_{j,R+1}$ and the mapper are same for all k. In addition, (3.11) contains only the real part because, after rationalization, the imaginary part in the integral is an odd function of t.

Eq. (3.11) cares about only the Euclidean distance between x and $\hat{z}$, but not the actual locations of them. For the Gray mappings, some of $(x,\hat{z})$ pairs in (3.11) have the same squared Euclidean distance $\left|x-\hat{z}\right|^2$ and hence can be grouped together. By doing so, (3.11) is re-written as

$$f_{\text{ex}}^{\text{RT}}\left(d_h,\Theta\right)=\frac{1}{4\pi}\int_{-\infty}^{\infty}\left[\sum_{i=1}^{M}C_i\prod_{j=0}^{R}\left(1+\left(t^2+\frac{1}{4}\right)\frac{\tilde{\Omega}_{j,R+1}P_jD_i}{\tilde{m}_{j,R+1}N_0}\right)^{-\tilde{m}_{j,R+1}}\right]^{d_h}\frac{dt}{t^2+\frac{1}{4}},\tag{3.12}$$

where $D_i=\left|x-\hat{z}\right|^2$ is a squared Euclidean distance, C_i is the number of $\left(x,\hat{z}\right)$ pairs with $\left|x-\hat{z}\right|^2=D_i$ over $l2^l$, and M is the number of distinct D_i's. The values of M, C_i and D_i are listed in Table I for QPSK, 16-QAM and 64-QAM with Gray mappings.

Table I. Values of N_l, C_i and D_i for 3 square constellations with Gray mappings

QPSK	$M=1$	$C_1=1,\ D_1=4$
16-QAM	$M=2$	$C_1=3/4,\ D_1=4$
		$C_2=1/4,\ D_2=16$
64-QAM	$M=4$	$C_1=7/12,\ D_1=4$
		$C_2=1/4,\ D_2=16$
		$C_3=1/12,\ D_3=72$
		$C_4=1/12,\ D_4=128$

Now, applying the multinomial theorem, (3.12) becomes

$$f_{\text{ex}}^{\text{RT}}\left(d_h,\Theta\right)$$
$$=\frac{1}{4\pi}\sum_{u_1,u_2,\cdots,u_M}\frac{d_h!}{u_1!u_2!\cdots u_M!}\prod_{i=1}^{M}C_i^{u_i}\int_{-\infty}^{\infty}\prod_{i=1}^{M}\prod_{j=0}^{R}\left(1+\left(t^2+\frac{1}{4}\right)\frac{\tilde{\Omega}_{j,R+1}P_jD_i}{\tilde{m}_{j,R+1}N_0}\right)^{-u_i\tilde{m}_{j,R+1}}\frac{dt}{t^2+\frac{1}{4}}.\tag{3.13}$$

The integration in (3.13) can be evaluated with partial fraction decomposition (PFD). Re-arrange the integration (to make the coefficient of t^2 be 1) yields

$$\int_{-\infty}^{\infty}\prod_{i=1}^{M}\prod_{j=0}^{R}\left(1+\left(t^2+\frac{1}{4}\right)\frac{\tilde{\Omega}_{j,R+1}P_jD_i}{\tilde{m}_{j,R+1}N_0}\right)^{-u_i\tilde{m}_{j,R+1}}\frac{dt}{t^2+\frac{1}{4}}$$

$$=\int_{-\infty}^{\infty}\prod_{i=1}^{M}\prod_{j=0}^{R}\frac{1}{\left(1+\frac{1}{4}\frac{\tilde{\Omega}_{j,R+1}P_jD_i}{\tilde{m}_{j,R+1}N_0}+\frac{\tilde{\Omega}_{j,R+1}P_jD_i}{\tilde{m}_{j,R+1}N_0}t^2\right)^{u_i\tilde{m}_{j,R+1}}}\frac{dt}{t^2+\frac{1}{4}},$$

$$=\int_{-\infty}^{\infty}\prod_{i=1}^{M}\prod_{j=0}^{R}\frac{\left(\frac{\tilde{\Omega}_{j,R+1}P_jD_i}{\tilde{m}_{j,R+1}N_0}\right)^{-u_i\tilde{m}_{j,R+1}}}{\left(\frac{\tilde{m}_{j,R+1}N_0}{\tilde{\Omega}_{j,R+1}P_jD_i}+\frac{1}{4}+t^2\right)^{u_i\tilde{m}_{j,R+1}}}\frac{dt}{t^2+\frac{1}{4}} \qquad (3.14)$$

$$=\prod_{i=1}^{M}\prod_{j=0}^{R}\left(A_{i,j}-\frac{1}{4}\right)^{-B_{i,j}}\int_{-\infty}^{\infty}\prod_{i=1}^{M}\prod_{j=0}^{R}\left(A_{i,j}+t^2\right)^{-B_{i,j}}\left(t^2+\frac{1}{4}\right)^{-1}dt$$

where $A_{i,j}=\frac{\tilde{m}_{j,R+1}N_0}{\tilde{\Omega}_{j,R+1}P_jD_i}+\frac{1}{4}$ and $B_{i,j}=u_i\tilde{m}_{j,R+1}$. Using PFD yields

$$\prod_{i=1}^{M}\prod_{j=0}^{R}\left(A_{i,j}+t^2\right)^{-B_{i,j}}\left(t^2+\frac{1}{4}\right)^{-1}=\sum_{i=1}^{M}\sum_{j=0}^{R}\sum_{k=1}^{B_{i,j}}\frac{E_{i,j,k}}{\left(A_{i,j}+t^2\right)^k}+\frac{E'}{t^2+\frac{1}{4}}, \qquad (3.15)$$

where

$$E_{i,j,k}=\frac{1}{\left(B_{i,j}-k\right)!}\frac{d^{B_{i,j}-k}}{ds^{B_{i,j}-k}}\left(\left(A_{i,j}+s\right)^{B_{i,j}}G(s)\right)\Big|_{s=-A_{i,j}} \qquad (3.16)$$

$$E'=\left(\frac{1}{4}+s\right)G(s)\Big|_{s=-\frac{1}{4}} \qquad (3.17)$$

and

$$G(s)\triangleq\prod_{i=1}^{M}\prod_{j=0}^{R}\left(A_{i,j}+s\right)^{-B_{i,j}}\left(s+\frac{1}{4}\right)^{-1}, \qquad (3.18)$$

providing that $A_{i,j}$'s are different for distinct pairs (i,j).

Using (3.15), the remaining integrals in (3.14) becomes

$$\sum_{i=1}^{M}\sum_{j=0}^{R}\sum_{k=1}^{B_{i,j}}E_{i,j,k}\int_{-\infty}^{\infty}\frac{1}{\left(A_{i,j}+t^2\right)^k}dt+E'\int_{-\infty}^{\infty}\frac{1}{t^2+\frac{1}{4}}dt, \qquad (3.19)$$

which can be exactly evaluated by using [76]

$$\int_{-\infty}^{\infty}\frac{1}{\left(a^2+t^2\right)^k}dt=\frac{(2k-3)!!}{(2k-2)!!}\frac{\pi}{a^{2k-1}}. \tag{3.20}$$

Note that $k!!=1$, if $k=0$ or 1. So, the close form expression of (3.13) is

$$f_{\text{ex}}^{\text{RT}}(d_h,\Theta)=\frac{1}{4}\sum_{u_1,u_2,\cdots,u_M}\frac{d_h!}{u_1!u_2!\cdots u_M!}\prod_{i=1}^{M}\left[C_i^{u_i}\prod_{j=0}^{R}\left(A_{i,j}-\frac{1}{4}\right)^{B_{i,j}}\right] \cdot\left(\sum_{i=1}^{M}\sum_{j=0}^{R}\sum_{k=1}^{B_{i,j}}E_{i,j,k}\frac{(2k-3)!!}{2\cdot(2k-2)!!}A_{i,j}^{-\frac{2k-1}{2}}+2E'\right), \tag{3.21}$$

Bringing (3.21) back to (3.2) yields the approximation $\hat{p}_{b,R+1}^{\text{RT}}(\Theta)$ by

$$\hat{p}_{b,R+1}^{\text{RT}}(\Theta)=\sum_{d_h=d_f}^{N}w_I(d_h)\,f_{ex}^{\text{RT}}(d_h,\Theta). \tag{3.22}$$

As to the PER at relay j, unfortunately, the PER analysis for a BICM system is still an open question. Therefore, the following commonly-used approximation based on the BER is adopted

$$\hat{p}_{f,j}=\begin{cases}1, & \text{if } \hat{p}_{b,j}\ge 1\\ 1-\left(1-\hat{p}_{b,j}\right)^K, & \text{otherwise}\end{cases}, \tag{3.23}$$

where $\hat{p}_{b,j}$ is the approximate BER at relay j. Following the same steps as given in (3.2) -(3.22), $\hat{p}_{b,j}$ is given by

$$\hat{p}_{b,j}\triangleq\sum_{d_h=d_f}^{N}w_I(d_h)\frac{1}{4}\sum_{u_1,u_2,\cdots,u_M}\frac{d_h!}{u_1!u_2!\cdots u_M!}\prod_{i=1}^{M}\left[C_i^{u_i}\left(\tilde{A}_{i,j}-\frac{1}{4}\right)^{\tilde{B}_{i,j}}\right] \cdot\left(\sum_{i=1}^{M}\sum_{k=1}^{\tilde{B}_{i,j}}\tilde{E}_{i,j,k}\frac{(2k-3)!!}{(2k-2)!!}\tilde{A}_{i,j}^{-\frac{2k-1}{2}}+2\tilde{E}'\right), \tag{3.24}$$

where $\tilde{A}_{i,j}=\dfrac{m_{0,j}N_0}{\Omega_{0,j}P_0D_i}+\dfrac{1}{4}$, $\tilde{B}_{i,j}=u_i m_{0,j}$, and $\tilde{E}_{i,j,k}$ and $\tilde{E}'$ can be obtained as in (3.16)-(3.17) with $A_{i,j}$, $B_{i,j}$ and $G(s)$ replaced by $\tilde{A}_{i,j}$, $\tilde{B}_{i,j}$ and

$$\tilde{G}_j(s)\triangleq\prod_{i=1}^{M}\left(\tilde{A}_{i,j}+s\right)^{-\tilde{B}_{i,j}}\left(s+\frac{1}{4}\right)^{-1}, \tag{3.25}$$

respectively. Using $\hat{p}_{b,R+1}^{\mathrm{RT}}(\Theta)$ and $\hat{p}_{f,j}$, the approximation of $p_{b,R+1}^{\mathrm{RT}}$ is obtained by

$$\hat{p}_{b,R+1}^{\mathrm{RT}} \triangleq \sum_{\Theta\subseteq\{1,2,\cdots,R\}} \hat{p}_{b,R+1}^{\mathrm{RT}}(\Theta)\prod_{j\in\Theta}\left(1-\hat{p}_{f,j}\right)\prod_{j\notin\Theta}\hat{p}_{f,j} \tag{3.26}$$

Numerical results will be given in Section 3.3 to confirms the accuracy of (3.26).

3.1.2 S-DF/Idle

For S-DF/Idle, the BER analysis is similar to that of S-DF/RT, e.g., $\hat{p}_{f,j}$ is evaluated just the same as (3.23) and (3.24). The only difference is the evaluation of $\hat{p}_{b,R+1}^{\mathrm{Idle}}(\Theta)$ due to the fact that some orthogonal-channels are not used at phase-II, if the relays are inactive. Taking this into consideration leads to

$$\begin{aligned}\hat{p}_{b,R+1}^{\mathrm{Idle}}(\Theta) \triangleq \sum_{d_h=d_f}^{N} w_I(d_h)\frac{1}{4}\sum_{u_1,u_2,\cdots,u_M}\frac{d_h!}{u_1!u_2!\cdots u_M!}\prod_{i=1}^{M}\left[C_i^{u_i}\prod_{j\in\Theta}\left(A_{i,j}-\frac{1}{4}\right)^{B_{i,j}}\right]\cdot \\ \cdot\left(\sum_{i=1}^{M}\sum_{j\in\Theta}\sum_{k=1}^{B_{i,j}}E_{i,j,k}\frac{(2k-1)!!}{(2k)!!}A_{i,j}^{-\frac{2k-1}{2}}+2E'\right)\end{aligned}. \tag{3.27}$$

Following the same steps in the previous subsection with $\hat{p}_{b,R+1}^{\mathrm{RT}}(\Theta)$ replaced by $\hat{p}_{b,R+1}^{\mathrm{Idle}}(\Theta)$, the BER approximation for S-DF/Idle is obtained as

$$\hat{p}_{b,R+1}^{\mathrm{Idle}} \triangleq \sum_{\Theta\subseteq\{1,2,\cdots,R\}} \hat{p}_{b,R+1}^{\mathrm{Idle}}(\Theta)\prod_{j\in\Theta}\left(1-\hat{p}_{f,j}\right)\prod_{j\notin\Theta}\hat{p}_{f,j}\,. \tag{3.28}$$

The accuracy of (3.28) will also be verified in Section 3.3.

3.2 Diversity Analysis

This section provides the analysis of the diversity order of the considered BICM-coded cooperative network that characterizes how the average BER behaves with large SNRs in fast-fading Nakagami-*m* channels. Specifically, upper and lower bounds of BER are derived first, followed by showing that both bounds achieve the same diversity order. The diversity orders for

the S-DF/RT and the S-DF/Idle relaying will be denoted by $\mathrm{Div}^{\mathrm{RT}}$ and $\mathrm{Div}^{\mathrm{Idle}}$, respectively. For derivation simplicity, we will assume $P_0 = P_1 = \cdots = P_R = P$.

3.2.1 S-DF/RT

At high SNRs, $p_{b,R+1}^{\mathrm{RT}}$ in (3.1) is well-approximated by

$$p_{b,R+1}^{\mathrm{RT}} \approx \sum_{\Theta \subseteq \{1,2,\cdots,R\}} p_{b,R+1}^{\mathrm{RT}}(\Theta) \prod_{j \notin \Theta} p_{f,j}\,, \tag{3.29}$$

which is obtained because $1 - p_{f,j} \approx 1$. In the following, an asymptotic upper bound of $p_{b,R+1}^{\mathrm{RT}}$ is first provided through deriving the upper bounds of $p_{b,R+1}^{\mathrm{RT}}(\Theta)$ and $p_{f,j}$, then followed by those for the lower bounds.

For $p_{b,R+1}^{\mathrm{RT}}(\Theta)$, we first replace the PEP $f^{\mathrm{RT}}(d_h, \Theta)$ in (3.2) by $f_{ub}^{\mathrm{RT}}(d_h, \Theta)$. To make this upper bound even simpler, all error events in (3.2) are assumed to have the same worst PEP, i.e.,

$$\begin{aligned} p_{b,R+1}^{\mathrm{RT}}(\Theta) &\le \sum_{d_h = d_f}^{N} w_I(d_h)\, f_{ub}^{\mathrm{RT}}(d_h, \Theta) \\ &\le \left(\sum_{d_h = d_f}^{N} w_I(d_h) \right) f_{ub}^{\mathrm{RT}}(d_f, \Theta), \\ &= \bar{w} \cdot f_{ub}^{\mathrm{RT}}(d_f, \Theta) \end{aligned} \tag{3.30}$$

where $\bar{w} = \sum_{d_h = d_f}^{N} w_I(d_h)$. Eq. (3.30) helps us to focus on the worst-case PEP $f_{ub}^{\mathrm{RT}}(d_f, \Theta)$, which was defined in (3.3) with d_h replaced by d_f.

However, the union bound $f_{ub}^{\mathrm{RT}}(d_f, \Theta)$ is still too complicate to see how it decreases with the SNR. Thus, a further simplification is made by assuming that all (x, z) pairs have the shortest square Euclidean distance D_χ, e.g., D_1 for each Gray-mapped constellation in Table I, or

$$D_{\chi} = \min_{i=1,\cdots l,\ b=0,1,\ x\in\chi_b^i,\ z\in\chi_{\bar{b}}^i} |x-z|^2 \tag{3.31}$$

for arbitrary constellation with arbitrary mapping. This leads to a looser but simpler upper bound, i.e.,

$$\begin{aligned} & f_{ub}^{\mathrm{RT}}\left(d_f,\Theta\right) \\ &= \frac{1}{2\pi \boldsymbol{j}}\int_{s_0-\boldsymbol{j}\infty}^{s_0+\boldsymbol{j}\infty}\prod_{k=1}^{d_h}\left[\frac{1}{l2^l}\sum_{i=1}^{l}\sum_{b=0}^{1}\sum_{x(k)\in\chi_b^i}\sum_{z(k)\in\chi_{\bar{b}}^i}\prod_{j=0}^{R}\Phi_{\Delta_j(x(k),z(k))}(s)\right]\frac{ds}{s} \\ &\le \frac{\bar{\gamma}^{d_f}}{2\pi \boldsymbol{j}}\int_{s_0-\boldsymbol{j}\infty}^{s_0+\boldsymbol{j}\infty}\prod_{k=1}^{d_h}\prod_{j=0}^{R}\Phi_{\Delta_j(x(k),z(k))}(s)\frac{ds}{s} \\ &= \frac{\bar{\gamma}^{d_f}}{4\pi}\int_{-\infty}^{\infty}\prod_{j=0}^{R}\left(1+\left(t^2+\frac{1}{4}\right)\frac{\tilde{\Omega}_{j,R+1}PD_{\chi}}{\tilde{m}_{j,R+1}N_0}\right)^{-d_f\tilde{m}_{j,R+1}}\frac{ds}{t^2+\frac{1}{4}} \end{aligned}, \tag{3.32}$$

where $\bar{\gamma}=2^{l-1}$ which is the number of erroneous z's in $\chi_{\bar{b}}^i$ for a single x. Note that the third row of (3.32) is obtained by assuming that all (x,z) pairs have the shortest square Euclidean distance D_{χ}. The 4-th row is obtained by using (3.8) and the saddle point $s=0.5+\boldsymbol{j}t$.

To further evaluate (3.32), the following lemma is introduced with its proof provided in Appendix B.

Lemma-2: Given positive number $\{a_j\}_{j=0}^{R}$ and $\{b_j\}_{j=0}^{R}$, we have

$$\lim_{x\to\infty}\int_{-\infty}^{\infty}\prod_{j=0}^{R}\left(1+a_jx\left(t^2+\frac{1}{4}\right)\right)^{-b_j}\frac{dt}{t^2+\frac{1}{4}} = 4\pi\prod_{j=0}^{R}a_j^{-b_j}\cdot\frac{\left(\sum_{j=0}^{R}b_j-1\right)!!}{\left(\sum_{j=0}^{R}b_j\right)!!}2^{2\sum_{j=0}^{R}b_j-1}\cdot x^{-\sum_{j=0}^{R}b_j}. \tag{3.33}$$

Using Lemma-2 in (3.32) and bringing the result back to (3.30) yields

$$\begin{aligned} p_{b,R+1}^{\mathrm{RT}}(\Theta) &\le \bar{w}\bar{\gamma}^{d_f}\prod_{j=0}^{R}\left(\frac{\tilde{m}_{j,R+1}}{\tilde{\Omega}_{j,R+1}D_{\chi}}\right)^{d_f\tilde{m}_{j,R+1}}\frac{\left(2d_f\sum_{j=0}^{R}\tilde{m}_{j,R+1}-1\right)!!}{\left(2d_f\sum_{j=0}^{R}\tilde{m}_{j,R+1}\right)!!}2^{2d_f\sum_{j=0}^{R}\tilde{m}_{j,R+1}-1}\left(\frac{N_0}{P}\right)^{d_f\sum_{j=0}^{R}\tilde{m}_{j,R+1}} \\ &= \bar{\alpha}_{\Theta}\cdot\left(\frac{N_0}{P}\right)^{d_f\sum_{j=0}^{R}\tilde{m}_{j,R+1}} \end{aligned}, \tag{3.34}$$

where $\bar{\alpha}_{\Theta}$ contains all terms that are independent to P/N_0.

For the upper bound of PER $p_{f,j}$, similar (but not exact) to the assumptions used in (3.30), assume that all the 2^K-1 erroneous coded sequences have the same worst PEP so that $p_{f,j}$ is upper bounded by

$$\begin{aligned} p_{f,j} &\le \sum_{\hat{\mathbf{u}}\neq\mathbf{u}} \Pr\left[\mathbf{b}\to\hat{\mathbf{b}}\right] \\ &\le \left(2^K-1\right)\cdot f_{ub}\left(j,d_f\right) \end{aligned}, \tag{3.35}$$

where $f_{ub}\left(j,d_f\right)$ is the corresponding upper bound of the average PEP of Hamming distance d_f at relay j, which is further upper bounded by (similar to (3.32))

$$f_{ub}\left(j,d_f\right) \le \frac{\bar{\gamma}^{d_f}}{4\pi}\int_{-\infty}^{\infty}\left(1+\left(t^2+\frac{1}{4}\right)\frac{\Omega_{0,j}PD_\chi}{m_{0,j}N_0}\right)^{-d_f m_{0,j}}\frac{dt}{t^2+\frac{1}{4}}. \tag{3.36}$$

Then, using Lemma-2 again, $p_{f,j}$ can be upper bounded by

$$\begin{aligned} p_{f,j} &\le \left(2^K-1\right)\bar{\gamma}^{d_f}\left(\frac{m_{0,j}}{\Omega_{0,j}D_\chi}\right)^{d_f m_{0,j}}\frac{\left(2d_f m_{0,j}-1\right)!!}{\left(2d_f m_{0,j}\right)!!}2^{2d_f m_{0,j}-1}\left(\frac{N_0}{P}\right)^{d_f m_{0,j}} \\ &= \bar{\beta}_j\cdot\left(\frac{N_0}{P}\right)^{d_f m_{0,j}} \end{aligned}. \tag{3.37}$$

By bringing (3.34) and (3.37) together into (3.29), an upper bound of $p_{b,R+1}^{\mathrm{RT}}$ is obtained as

$$p_{b,R+1}^{\mathrm{RT}} \le \bar{p}_{b,R+1}^{\mathrm{RT}} \triangleq \sum_{\Theta\subseteq\{1,2,\ldots R\}}\left(\bar{\alpha}_\Theta\prod_{j\notin\Theta}\bar{\beta}_j\right)\left(\frac{N_0}{P}\right)^{d_f\left(\sum_{j=0}^{R}\tilde{m}_{j,R+1}+\sum_{j\notin\Theta}m_{0,j}\right)}. \tag{3.38}$$

At extremely high SNRs, e.g., $P/N_0\to\infty$, the summation in (3.38) will be dominated by the terms with the smallest exponents. Therefore, the diversity order [10] of $\bar{p}_{b,R+1}^{\mathrm{RT}}$ is

$$\begin{aligned} \overline{\mathrm{Div}}^{\mathrm{RT}} &= d_f\min_{\Theta\subseteq\{1,2,\ldots R\}}\left\{\sum_{j=0}^{R}\tilde{m}_{j,R+1}+\sum_{j\notin\Theta}m_{0,j}\right\} \\ &= d_f\left(m_{0,R+1}+\sum_{j=1}^{R}\min\left\{m_{0,j}+m_{0,R+1},m_{j,R+1}\right\}\right) \end{aligned}. \tag{3.39}$$

The lower bound of $p_{b,R+1}^{\mathrm{RT}}$ can be obtained similarly to the upper bound with some modi-

fications. First, $p_{b,R+1}^{\mathrm{RT}}(\Theta)$ is lower bounded by

$$\begin{aligned} p_{b,R+1}^{\mathrm{RT}}(\Theta) &\geq w_I(d_f) f^{RT}(d_f,\Theta) \\ &\geq f^{RT}(d_f,\Theta) \end{aligned}, \tag{3.40}$$

in which *only one* events with Hamming weight d_f is involved. The second row in (3.40) is obtained by assuming that the worst error event results in only one bit difference to $\mathbf{b}$. Moreover, the PEP $f^{RT}(d_f,\Theta)$ can be lower bounded by leaving *only one* (x,z) pair with D_χ, i.e.,

$$f(d_f,\Theta) \geq \frac{\underline{\gamma}^{d_f}}{2\pi \boldsymbol{j}} \int_{s_0-\boldsymbol{j}\infty}^{s_0+\boldsymbol{j}\infty} \prod_{j=0}^{R} \left(1-\left(-s+s^2\right)\frac{\tilde{\Omega}_{j,R+1}P_j D_\chi}{\tilde{m}_{j,R+1}N_0}\right)^{-d_f \tilde{m}_{j,R+1}} \frac{ds}{s} \tag{3.41}$$

where $\underline{\gamma} = 1/2^{l-1}$. Applying Lemma-2, (3.40) becomes

$$\begin{aligned} p_{b,R+1}^{\mathrm{RT}}(\Theta) &\geq \underline{\gamma}^{d_f} \prod_{j=0}^{R} \left(\frac{\tilde{\Omega}_{j,R+1}D_\chi}{\tilde{m}_{j,R+1}}\right)^{-d_f\tilde{m}_{j,R+1}} \frac{\left(2d_f\sum_{j=0}^{R}\tilde{m}_{j,R+1}-1\right)!!}{\left(2d_f\sum_{j=0}^{R}\tilde{m}_{j,R+1}\right)!!} 2^{2d_f\sum_{j=0}^{R}\tilde{m}_{j,R+1}-1}\left(\frac{N_0}{P}\right)^{d_f\sum_{j=0}^{R}\tilde{m}_{j,R+1}} \\ &= \underline{\alpha}_\Theta \cdot \left(\frac{N_0}{P}\right)^{d_f\sum_{j=0}^{R}\tilde{m}_{j,R+1}} \end{aligned}, \tag{3.42}$$

where $\underline{\alpha}_\Theta$ contains all the terms independent to P/N_0. Now, it is straightforward to show that $p_{f,j}$ is lower bounded by

$$p_{f,j} \geq \underline{\beta}_j \cdot \left(\frac{N_0}{P}\right)^{d_f m_{0,j}}, \tag{3.43}$$

where $\underline{\beta}_j$ contains all the terms independent to P/N_0. Using (3.42) and (3.43), an asymptotic lower bound of $p_{b,R+1}^{\mathrm{RT}}$ is,

$$p_{b,R+1}^{\mathrm{RT}} \geq \underline{p}_{b,R+1}^{\mathrm{RT}} \triangleq \sum_{\Theta\subset\{1,2,\cdots,R\}} \underline{\alpha}_\Theta \prod_{j\notin\Theta} \underline{\beta}_j \left(\frac{N_0}{P}\right)^{d_f\left(\sum_{j=0}^{R}\tilde{m}_{j,R+1}+\sum_{j\notin\Theta}m_{0,j}\right)} \tag{3.44}$$

Denote the diversity order of $\underline{p}_{b,R+1}$ by $\underline{\mathrm{Div}}^{\mathrm{RT}}$. Similarly, at extremely high SNRs, the summation is dominated by the terms with the smallest exponent. It turns out that $\underline{\mathrm{Div}}^{\mathrm{RT}} = \overline{\mathrm{Div}}^{\mathrm{RT}}$. Since

$\bar{p}_{b,R+1}^{\mathrm{RT}} \geq p_{b,R+1}^{\mathrm{RT}} \geq \underline{p}_{b,R+1}^{\mathrm{RT}}$ at all ranges of SNR, this implies $\overline{\mathrm{Div}}^{\mathrm{RT}} \leq \mathrm{Div}^{\mathrm{RT}} \leq \underline{\mathrm{Div}}^{\mathrm{RT}}$. Therefore, it is concluded that $\overline{\mathrm{Div}}^{\mathrm{RT}} = \mathrm{Div}^{\mathrm{RT}} = \underline{\mathrm{Div}}^{\mathrm{RT}}$, as provided in (3.39).

The result in (3.39) can be interpreted as follows. The total diversity order is the sum of diversity order contributed from the parallel transmission paths, including the direct source-destination and relaying paths. For the direct path, the diversity order is given by $d_f \cdot m_{0,R+1}$, where d_f accounts for the contribution from the channel codes under the assumption of independent fading on the coded bits, and $m_{0,R+1}$ the contribution from the Nakagami-*m* fading channel with shaping factor of $m_{0,R+1}$. For the relaying path through relay j, the diversity order is given by $d_f \cdot \min\left\{m_{0,j} + m_{0,R+1}, m_{j,R+1}\right\}$, where $m_{0,j} + m_{0,R+1}$ accounts for the diversity order contributed from the source-to-relay channel plus that from retransmission through direct path, and $m_{j,R+1}$ accounts for the diversity order contributed from the relay-to-destination channel.

3.2.2 S-DF/Idle

For S-DF/Idle, the only difference on diversity analysis from that of the S-DF/RT relaying is on the evaluation of the upper and lower bounds of $p_{b,R+1}^{\mathrm{Idle}}(\Theta)$, e.g., the upper bound becomes

$$p_{b,R+1}^{\mathrm{Idle}}(\Theta) \leq \bar{w}\bar{\gamma}^{d_f} \prod_{j\in\tilde{\Theta}} \left(\frac{m_{j,R+1}}{\Omega_{j,R+1} D_\chi} \right)^{d_f m_{j,R+1}} \frac{\left(2d_f \sum_{j\in\tilde{\Theta}} m_{j,R+1} - 1\right)!!}{\left(2d_f \sum_{j\in\tilde{\Theta}} m_{j,R+1}\right)!!} 2^{2d_f \sum_{j\in\tilde{\Theta}} m_{j,R+1} - 1} \left(\frac{N_0}{P}\right)^{d_f \sum_{j\in\tilde{\Theta}} m_{j,R+1}}, \quad (3.45)$$

and the lower bound

$$p_{b,R+1}^{\mathrm{Idle}}(\Theta) \geq \underline{\gamma}^{d_f} \prod_{j\in\tilde{\Theta}} \left(\frac{m_{j,R+1}}{\Omega_{j,R+1} D_\chi} \right)^{d_f m_{j,R+1}} \frac{\left(2d_f \sum_{j\in\tilde{\Theta}} m_{j,R+1} - 1\right)!!}{\left(2d_f \sum_{j\in\tilde{\Theta}} m_{j,R+1}\right)!!} 2^{2d_f \sum_{j\in\tilde{\Theta}} m_{j,R+1} - 1} \left(\frac{N_0}{P}\right)^{d_f \sum_{j\in\tilde{\Theta}} m_{j,R+1}}. \quad (3.46)$$

Note that the channels of inactive relays now have no contributions in (3.45) and (3.46). Following similar steps in the previous subsection, the diversity order for $p_{b,R+1}^{\mathrm{Idle}}$ is obtained as

$$\mathrm{Div}^{\mathrm{Idle}} = d_f\left(m_{0,R+1} + \sum_{j=1}^{R} \min\left\{m_{0,j}, m_{j,R+1}\right\}\right). \tag{3.47}$$

Note that $\mathrm{Div}^{\mathrm{Idle}}$ can also be obtained by replacing $m_{0,j} + m_{0,R+1}$ with $m_{0,j}$ in (3.39), because the source does not transmit when the relay is inactive

3.3 Numerical Results

This section shows the numerical results for the BER approximations proposed in Section 3.1. Since $\mathrm{Div}^{\mathrm{RT}}$ and $\mathrm{Div}^{\mathrm{Idle}}$ are derived theoretically, no simulation confirmation is needed for their accuracy. Besides, in a coded system, $\mathrm{Div}^{\mathrm{RT}}$ and $\mathrm{Div}^{\mathrm{Idle}}$ are often too large to be simulated with computer simulations (see (3.39) and (3.47)). In all the following simulations, a half-rate convolutional codes CC(171,133) with the generator matrix

$$\left(1 + D + D^2 + D^3 + D^6, 1 + D^2 + D^3 + D^5 + D^6\right) \tag{3.48}$$

is considered, the interleaver is S-random with length 1024 and depth 40, and the modulation is Gray-mapped 16-QAM (if not specified). For simplicity, let $P_0 = P_1 = \cdots = P_R = P$ with $P = E_b \cdot R_C \cdot l$ where E_b is the bit energy, and $R_C = 0.5$ is the channel code rate.

First, the proposed approximations in (3.22), (3.23), (3.24) and (3.27) are going to be verified . For simplicity, consider a 3-node network with the setups of S-R, S-D and R-D links shown as Network-1 in Table II. In this case, the BER at the destination is (from (3.1))

$$p_{b,2}^{\mathrm{mode}} = p_{b,2}^{\mathrm{mode}}\left(\{1\}\right)\left(1 - p_{f,1}\right) + p_{b,2}^{\mathrm{mode}}\left(\varnothing\right) p_{f,1} \tag{3.49}$$

where $\mathrm{mode} \in \{\mathrm{RT}, \mathrm{Idle}\}$. The BER/PER simulation results and approximations are plotted in Fig. 3.1. Note that when the relay decodes successfully, $p_{b,2}^{\mathrm{RT}}\left(\{1\}\right) = p_{b,2}^{\mathrm{Idle}}\left(\{1\}\right)$. As can be seen in Fig. 3.1, all the approximations provide very good predictions of the real BERs, except at very low SNRs. Unfortunately, the PER approximation $\hat{p}_{f,1}$, according (3.23), over-estimates $p_{f,1}$,

though $\hat{p}_{b,1}$ is very accurate in predicting $p_{b,1}$.

It is noteworthy to point out that $p_{b,2}^{\text{Idle}}(\varnothing)$ is, in fact, the BER at Rayleigh fading channels ($m_{0,2}=1$) without relay transmissions. In [58], $p_{b,2}^{\text{Idle}}(\varnothing)$ had been evaluated by using Chernoff bound, which provided a close approximation at high SNRs, but a non-trivial gap is observed at low SNRs, e.g., 1 dB gap is observed at BER of 10^{-2} for 16-QAM in Fig. 12 in [58]. On the other hand, our proposed close-form evaluation of $p_{b,2}^{\text{Idle}}(\varnothing)$ provides the approximation as good as that in [58] at high SNRs, but a trivial gap (less than 0.3 dB) is observed at BER of 10^{-2}, as shown in Fig. 3.1.

The over-estimation on PER becomes negligible when the S-R link is better than the other links. This is the typical case of relay network, e.g., when line-of-sight (LOS) is possible for S-R links. Consider Network-2 with setups shown in Table II with the value $n=2,\ 4$ and 8 to investigate the effect of different S-R link qualities to our approximations and plotted the results in Fig. 3.2 and Fig. 3.3 for S-DF/Idle and S-DF/RT relaying modes, respectively. In Fig. 3.2, the approximations (App.) are with about 0.5 dB gaps to the simulation results (Sim.) for $n=2$ and 4 at BER of 10^{-5}. For $n=8$, the approximation perfectly matches the simulation results since $E_b/N_0 \geq 0.5\,\text{dB}$. This is due to the fact that, when the S-R link is better than other links, $p_{f,1}$ is low enough such that $p_{b,2}^{\text{Idle}}(\varnothing)\,p_{f,1}$ is relatively smaller than the $p_{b,2}^{\text{Idle}}(\{1\})$ and that (3.49) is dominate by only $p_{b,2}^{\text{Idle}}(\{1\})$, which can be well approximated. For S-DF/RT in Fig. 3.3, a 0.5 dB gap is observed only for $n=2$, while approximations for $n=4$ and 8 are very close to the simulations. The approximations for S-DF/RT become more accurate, because $p_{b,2}^{\text{RT}}(\varnothing)$ is smaller than $p_{b,2}^{\text{Idle}}(\varnothing)$ such that $p_{b,2}^{\text{RT}}(\{1\})$ is more likely to dominate the error performance at destination.

Table II. Network Setups

Networks	S-D link	S-R link(s)	R-D link(s)
Network-1	$m_{0,2}=\Omega_{0,2}=1$	$m_{0,1}=\Omega_{0,1}=4$.	$m_{1,2}=\Omega_{1,2}=2$
Network-2	$m_{0,2}=\Omega_{0,2}=1$	$m_{0,1}=\Omega_{0,1}=n$	$m_{1,2}=\Omega_{1,2}=2$
Network-3	$m_{0,2}=\Omega_{0,2}=1$	$m_{0,1}=\Omega_{0,1}=4$ $m_{0,2}=\Omega_{0,2}=3$	$m_{1,3}=\Omega_{1,3}=1$ $m_{2,3}=\Omega_{2,3}=2$
Network-4	$m=2$, $\Omega=2$, for all links		
Network-5	$m_{0,R+1}=\Omega_{0,R+1}=1$	$m_{0,j}=1$, $\Omega_{0,j}=10$, $j=1, 2, \cdots, R$	$m_{j,R+1}=\Omega_{j,R+1}=1$, $j=1, 2, \cdots, R$

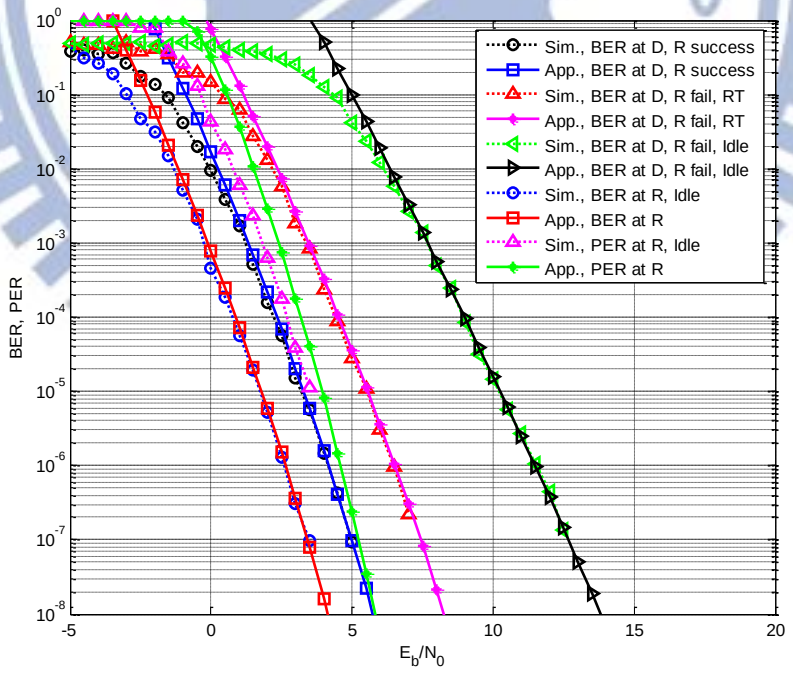

Fig. 3.1. BER/PER simulation results and approximations for Network-1

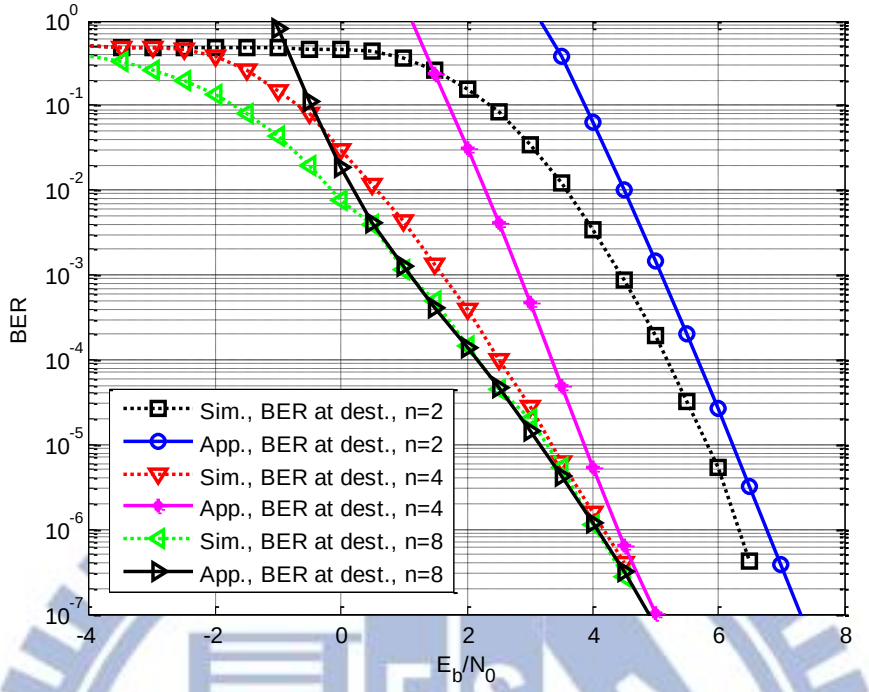

Fig. 3.2. BER simulations and approximations of Network-2 with the values of $n = 2,\ 4$, and 8 for S-DF/Idle

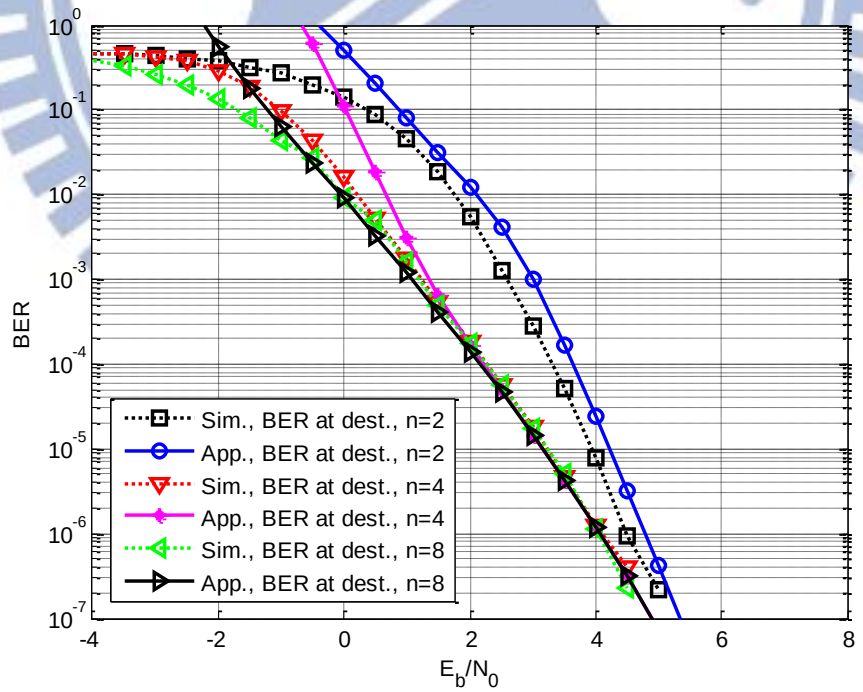

Fig. 3.3. BER simulations and approximations of Network-2 with the values of $n = 2,\ 4$, and 8 for S-DF/RT

The approximations with different modulations (4PSK, 16-QAM and 64-QAM) are verified in Fig. 3.4 and Fig. 3.5 for S-DF/RT and S-DF/Idle relaying modes, respectively. A network with 2 relays is considered with the setups shown as Network-3 in Table II. As shown in both figures, the approximations are quite close to the simulations, e.g., no larger than 0.3 dB and 0.5 dB gaps at BER of 10^{-5} are observed for S-DF/RT and S-DF/Idle, respectively.

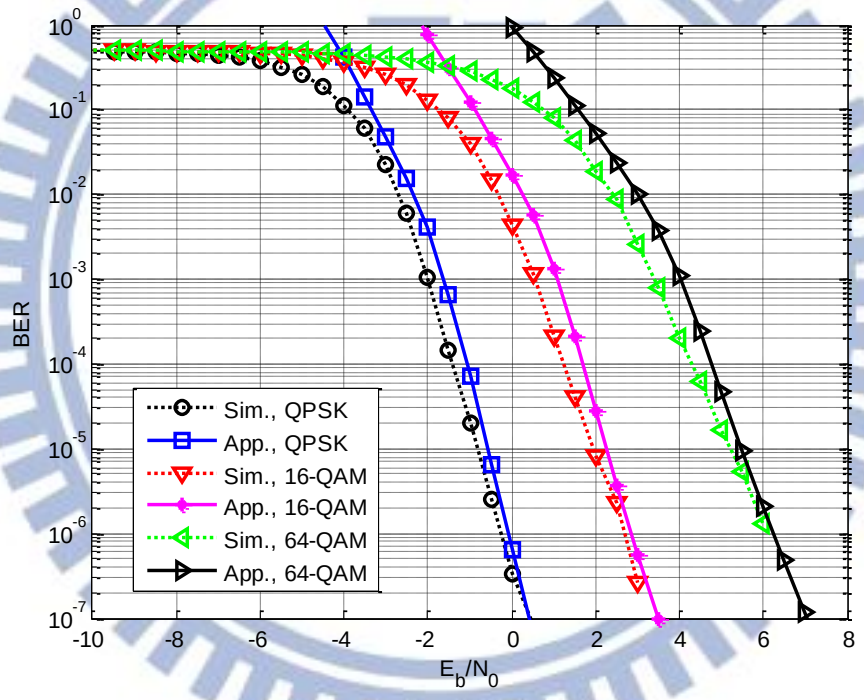

Fig. 3.4. BER simulations and approximations of Network-3 with S-DF/RT for 4PSK, 16-QAM and 64-QAM

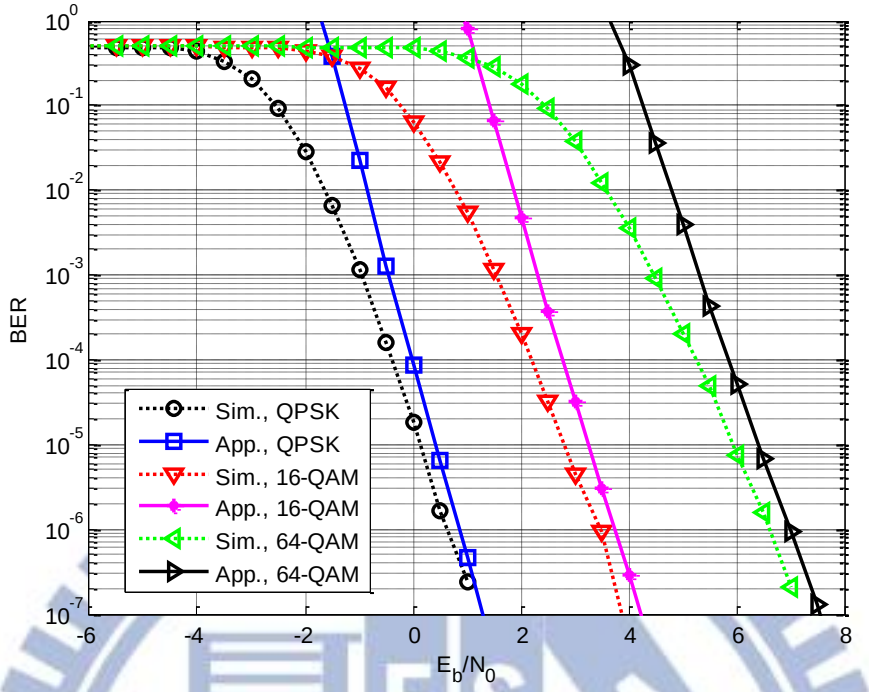

Fig. 3.5. BER simulations and approximations of Network-3 with S-DF/Idle for 4PSK, 16-QAM and 64-QAM

The results for different relay number $R = 1, 2, \cdots, 5$ are provided in Fig. 3.6 and Fig. 3.7 . In Fig. 3.6, Network-4 with S-DF/RT and i.i.d. channel statistics ($m = 2$ and $\Omega = 2$ for all links in Table II) is considered. As is seen from Fig. 3.6, the proposed approximations are very close to the simulation results, since BER $\le 10^{-2}$ for all R . In Fig. 3.7, we examine another network with S-DF/Idle for Rayleigh fading channels in which the shaping factors of all links are set to 1 ($m = 1$), and the S-R links have better average power gain than the others, cf. Network-5 in Table II. As shown in Fig. 3.7, the approximations are quite accurate at BER of 10^{-5} for all R . Note that a larger R may lead to gaps at low SNRs because $p_{f,j}$'s are large at low SNRs.

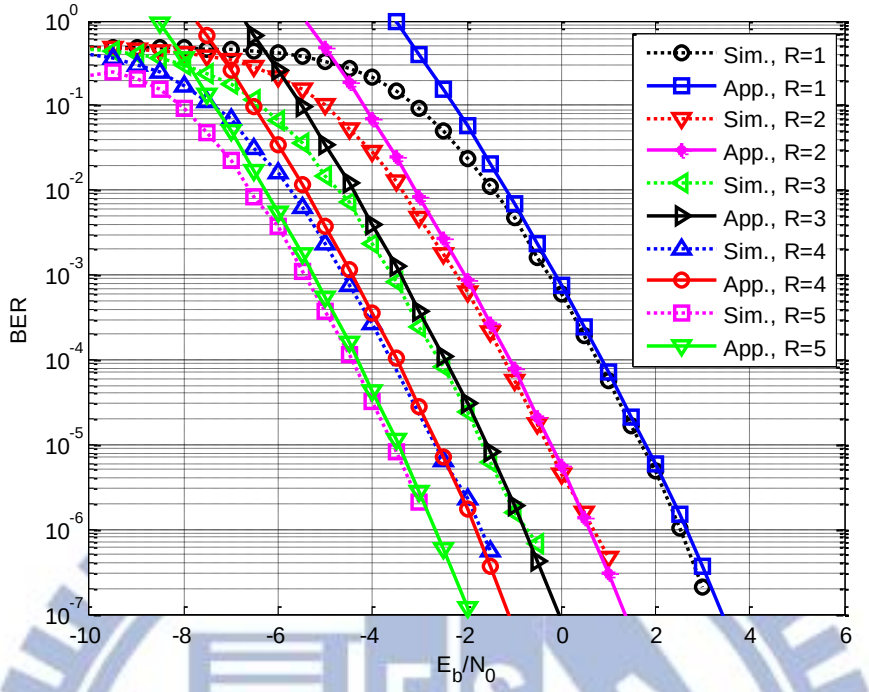

Fig. 3.6. BER simulations and approximations of Network-4 with S-DF/RT for $R = 1, 2, \cdots, 5$ and i.i.d channel conditions ($m = 2$ and $\Omega = 2$ for all links)

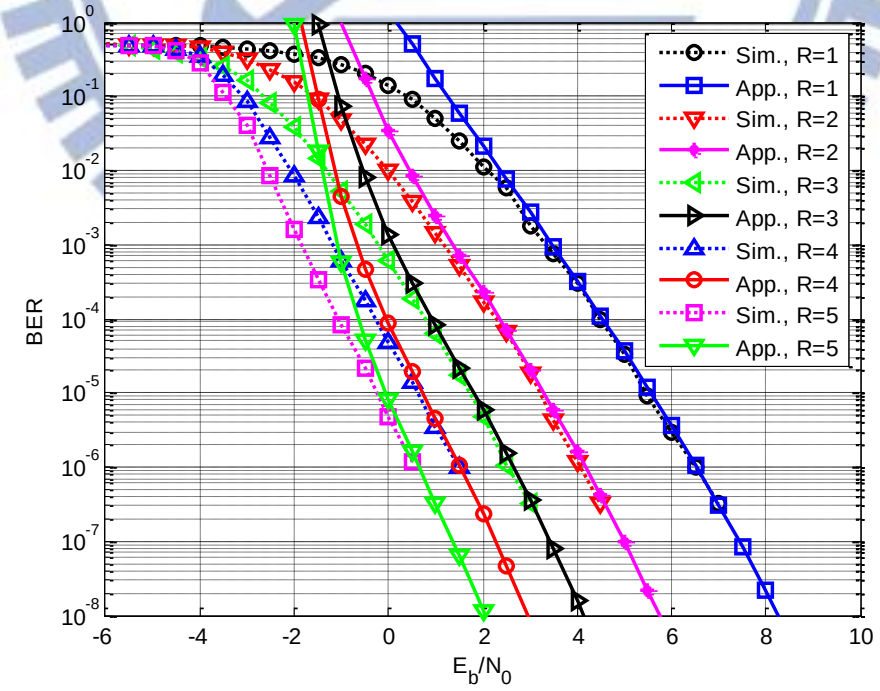

Fig. 3.7. BER simulations and approximations of Network-5 with S-DF/Idle for $R = 1, 2, \cdots, 5$

over Rayleigh fading channels

3.4 Summary

In Chapter 3, the BER performance and diversity order of a cooperative BICM networks are investigated for the S-DF/RT and S-DF/Idle relaying over fast-fading Nakagami-*m* channels. Unlike most of the existing works, this chapter considers a packet-by-packet forwarding strategy. For the BER analysis, the BER based on a given set of active relays is approximated based on extending the expurgating bound proposed in [47]. But, instead of using a Chernoff bound (as in [47]) to evaluate it, a close-form evaluation is proposed and verified to be very accurate in numerical results. Based on this approximation and together with a BER-to-PER approximation, approximate the BER at the destination can be obtained. The diversity of the cooperative BICM network is also provided for both S-DF/RT and S-DF/Idle in fast Nakagami-*m* fading channels through deriving the asymptotic upper and lower bounds of the BER at destination. Numerical results show that, though the BER-to-PER approximation may not be accurate, it does not seriously degrade our approximations, especially in some typical case where the S-R links are better than the other links.

Chapter 4

Performance and Diversity Analysis in Block-fading Channels

This chapter proposes the BER analyses and the diversity derivations for BICM-coded cooperative networks with the S-DF/RT and S-DF/Idle relaying over block-fading Nakagami-*m* channels. Different from the previous chapter, in block-fading environments, the channel gains are constant during the transmission of a packet. Thus, the time index k will be dropped for simplicity. In what follows, the BER analyses are presented first, followed by the diversity analyses.

4.1 BER Analysis

In this section, the BER at the destination for BICM-coded cooperative network with the S-DF/RT and S-DF/Idle relaying over block-fading Nakagami-*m* channels is discussed. Different from the results in fast-fading channels, an effective close-form approximation in block-fading channels is difficult to obtain. As a result, a semi-analytic method is provided.

4.1.1 S-DF/RT

At the destination, the average BER is

$$p_{b,R+1}^{\mathrm{RT}} = \sum_{\Theta \subseteq \{1,2,\cdots,R\}} p_{b,R+1}^{\mathrm{RT}}(\Theta) \prod_{j \in \Theta} \left(1 - p_{f,j}\right) \prod_{j \notin \Theta} p_{f,j} \,. \tag{4.1}$$

Note that $p_{b,R+1}^{\mathrm{RT}}(\Theta)$ and $p_{f,j}$ are now BER and PER which have been averaged over sufficient frames (channel realizations). In the following development, $p_{b,R+1}^{\mathrm{RT}}(\Theta)$ is discussed first, followed by that of $p_{f,j}$.

The BER $p_{b,R+1}^{\mathrm{RT}}(\Theta)$ can be obtained by first obtain the BER with given channel realizations, followed by averaging the result w.r.t. the realizations, e.g.,

$$p_{b,R+1}^{\mathrm{RT}}(\Theta) \le E_{\tilde{\mathbf{h}}_{R+1}}\left[p_{b,R+1}^{\mathrm{RT}}\left(\Theta, \tilde{\mathbf{h}}_{R+1}\right)\right], \tag{4.2}$$

where $p_{b,R+1}^{\mathrm{RT}}\left(\Theta, \tilde{\mathbf{h}}_{R+1}\right)$ is the BER at destination with given active set Θ and the channel realizations $\tilde{\mathbf{h}}_{R+1} = \left\{\tilde{h}_{j,R+1}\right\}_{j=0}^{R}$. Using the assumptions of ideal interleaving and symmetrization in [47], the $p_{b,R+1}^{\mathrm{RT}}\left(\Theta, \tilde{\mathbf{h}}_{R+1}\right)$ can be bounded by

$$p_{b,R+1}^{\mathrm{RT}}\left(\Theta, \tilde{\mathbf{h}}_{R+1}\right) \le \sum_{d_h = d_f}^{N} w_I\left(d_h\right) f^{\mathrm{RT}}\left(d_h, \Theta, \tilde{\mathbf{h}}_{R+1}\right), \tag{4.3}$$

where $f^{\mathrm{RT}}\left(d_h, \Theta, \tilde{\mathbf{h}}_{R+1}\right)$ is the PEP between two coded sequences with Hamming distance d_h.

Given $\tilde{\mathbf{h}}_{R+1}$, $f^{\mathrm{RT}}\left(d_h, \Theta, \tilde{\mathbf{h}}_{R+1}\right)$ can be evaluated through a union bound $f_{ub}^{\mathrm{RT}}\left(d_h, \Theta, \tilde{\mathbf{h}}_{R+1}\right)$ by following the steps in [47] for AWGN channels, e.g.,

$$f_{ub}^{\mathrm{RT}}\left(d_h, \Theta, \tilde{\mathbf{h}}_{R+1}\right) = \frac{1}{2\pi \boldsymbol{j}} \int_{s_0 - \boldsymbol{j}\infty}^{s_0 + \boldsymbol{j}\infty} \left[\frac{1}{l 2^l} \sum_{i=1}^{l} \sum_{b=0}^{1} \sum_{x \in \chi_b^i} \sum_{z \in \chi_{\bar{b}}^i} \prod_{j=0}^{R} \Phi_{\Delta_{\tilde{h}_{j,R+1}}(x,z)}(s) \right]^{d_h} \frac{ds}{s}, \tag{4.4}$$

where $\Phi_{\Delta_{\tilde{h}_{j,R+1}}(x,z)}(s)$ is the MGF of the difference metric

$$\Delta_{\tilde{h}_{j,R+1}}(x,z) \doteq \log p\left(\tilde{y}_{j,R+1} \mid x, \tilde{h}_{j,R+1}\right) - \log p\left(\tilde{y}_{j,R+1} \mid z, \tilde{h}_{j,R+1}\right). \tag{4.5}$$

With given the channel realization $\tilde{h}_{j,R+1}$, $\Delta_{\tilde{h}_{j,R+1}}(x,z)$ is a Gaussian random variable with the MGF

$$\Phi_{\Delta_{\tilde{h}_{j,R+1}}(x,z)}(s)=\exp\left[\left(-s+s^2\right)\frac{P_j}{\tilde{N}_0^{(j)}}\tilde{h}_{j,R+1}^2\left|x-z\right|^2\right]. \tag{4.6}$$

Note that, for S-DF/RT and S-DF/Idle relaying modes, $\tilde{N}_0^{(j)}=N_0$.

Unfortunately, as was discussed in [47], $f_{ub}^{\mathrm{RT}}\left(d_h,\Theta,\tilde{\mathbf{h}}_{R+1}\right)$ is very loose at low-to-moderate SNRs. As a result, the expurgation proposed in [47] is adopted to provide a more accurate approximation, i.e.,

$$f_{\mathrm{ex}}^{\mathrm{RT}}\left(d_h,\Theta,\tilde{\mathbf{h}}_{R+1}\right)\doteq\frac{1}{2\pi\boldsymbol{j}}\int_{s_0-\boldsymbol{j}\infty}^{s_0+\boldsymbol{j}\infty}\left[\frac{1}{l2^l}\sum_{i=1}^{l}\sum_{b=0}^{1}\sum_{x\in\chi_b^i}\prod_{j=0}^{R}\Phi_{\Delta_{\tilde{h}_{j,R+1}}(x,\hat{z})}(s)\right]^{d_h}\frac{ds}{s}, \tag{4.7}$$

where all irrelevant z's in χ_b^i are dropped, except $\hat{z}$ which is the unique nearest neighbor of x in χ_b^i.

The inverse Laplace transform in (4.7) can be evaluated through the saddle point [79], which occurs at $s=0.5$ because $-s+s^2=\left(s-0.5\right)^2-0.25$. By substituting $s=0.5+\boldsymbol{j}t$ into (4.6) and (4.7) leads to

$$f_{\mathrm{ex}}^{\mathrm{RT}}\left(d_h,\Theta,\tilde{\mathbf{h}}_{R+1}\right)=\frac{1}{4\pi}\int_{-\infty}^{\infty}\left[\frac{1}{l2^l}\sum_{i=1}^{l}\sum_{b=0}^{1}\sum_{x\in\chi_b^i}\prod_{j=0}^{R}\exp\left[-\left(t^2+\frac{1}{4}\right)\frac{P_j}{N_0}\tilde{h}_{j,R+1}^2\left|x-\hat{z}\right|^2\right]\right]^{d_h}\frac{dt}{t^2+\frac{1}{4}}. \tag{4.8}$$

Note that (4.8) contains only the real part because the imaginary part in the integral is an odd function of t. For the Gray mappings, some of $(x,\hat{z})$ pairs in the summation of (4.8) have the same squared Euclidean distance $\left|x-\hat{z}\right|^2$ and hence can be grouped together. By doing so, (4.8) is rewritten as

$$f_{\mathrm{ex}}^{\mathrm{RT}}\left(d_h,\Theta,\tilde{\mathbf{h}}_{R+1}\right)=\frac{1}{4\pi}\int_{-\infty}^{\infty}\left[\sum_{i=1}^{M}C_i\prod_{j=0}^{R}\exp\left[-\left(t^2+\frac{1}{4}\right)\frac{P_j}{N_0}\tilde{h}_{j,R+1}^2D_i\right]\right]^{d_h}\frac{dt}{t^2+\frac{1}{4}}, \tag{4.9}$$

where the values M, C_i and D_i are listed in Table I for QPSK, 16-QAM and 64-QAM with Gray mappings.

In [47], (4.9) is evaluated numerically for AWGN channels. However, the approximation in AWGN channels is still loose at low SNRs. In fact, it is exponentially increasing as SNR decreases, although the actual BER is upper bounded by 0.5. Therefore, when averaging the BER over channel realizations (as in (4.2)), such a loss could leads to a non-trivial gap. To mitigate this gap, some modification is required. The modification adopted is to limit the BER at AWGN channel to no greater than 0.5, i.e.,

$$\min\left\{\sum_{d_h=d_f}^{N} w_I\left(d_h\right) f_{ex}^{\mathrm{RT}}\left(d_h,\Theta,\tilde{\mathbf{h}}_{R+1}\right),\ 0.5\right\}. \tag{4.10}$$

With this modification, the loose at high SNR in AWGN channels can be mitigated. However, such a modification prohibits an analytic expression. As a result, channel averaging is carried out by the Monte Carlo method which evaluates

$$\hat{p}_{b,R+1}^{\mathrm{RT}}\left(\Theta\right)=E_{\tilde{\mathbf{h}}_{R+1}}\left[\min\left\{\sum_{d_h=d_f}^{N} w_I\left(d_h\right) f_{ex}^{\mathrm{RT}}\left(d_h,\Theta,\tilde{\mathbf{h}}_{R+1}\right),\ 0.5\right\}\right]. \tag{4.11}$$

To speed up the evaluation, Eq. (4.10) can be obtained efficiently by using table look-up with interpolation. Such a table can be pre-built to provide the mapping from the SNR to the resulting BER at AWGN channels, e.g. from $E_b/N_0=0$ to 30 [1] with grid spacing 0.01. Then, given the channel realizations $\tilde{\mathbf{h}}_{R+1}$, one has $\sum_{j=0}^{R} P_j\tilde{h}_{j,R+1}^2/N_0$ as the equivalent SNR in AWGN channels. With the help of linear interpolation, the desired BER under $\tilde{\mathbf{h}}_{R+1}$ can be obtained fast with low-complexity.

To obtain an approximation for the PER at relay, i.e., $\hat{p}_{f,j}$, a commonly-used approximation is adopted to obtain the PER with given the channel state $h_{0,j}$, i.e.,

---

[1] The maximum $E_b/N_0=30$ is enough for 16-QAM to provide BER lower than 10^{-27} in AWGN channels.

$$\hat{p}_{f,j}\left(h_{0,j}\right)=1-\left(1-\hat{p}_{b,j}\left(h_{0,j}\right)\right)^{K} \tag{4.12}$$

with

$$\hat{p}_{b,j}\left(h_{0,j}\right)=\min\left\{\sum_{d_h=d_f}^{N} w_I\left(d_h\right) f_{ex}\left(j,d_h,h_{0,j}\right),\ 0.5\right\}, \tag{4.13}$$

where $f_{ex}\left(j,d_h,h_{0,j}\right)$ is the expurgated approximation for PEP of two coded sequences with Hamming distance d_h at relay j with the channel state $h_{0,j}$. This approximation can be obtained according to the results for AWGN channels in [47], or by through a look-up table as described early.

To obtain $\hat{p}_{f,j}$ in block-fading channels, the last step is to average $\hat{p}_{f,j}\left(h_{0,j}\right)$ with respect to $h_{0,j}$, i.e.,

$$\hat{p}_{f,j}=E_{h_{0,j}}\left[\hat{p}_{f,j}\left(h_{0,j}\right)\right]. \tag{4.14}$$

However, a close-form expression of (4.14) is prohibited, and Monte Carlo method is used again to numerically evaluate this expectation. Bringing (4.11) and (4.14) back to (4.1), the average PER at destination for S-DF/RT is obtained. Numerical results will be provided in Section 4.3.

4.1.2 S-DF/Idle

Let $p_{b,R+1}^{\text{Idle}}$ denote the average BER at destination for the S-DF/Idle relaying scheme, which is

$$p_{b,R+1}^{\text{Idle}}=\sum_{\Theta\subseteq\{1,2,\cdots,R\}} p_{b,R+1}^{\text{Idle}}(\Theta)\prod_{j\in\Theta}\left(1-p_{f,j}\right)\prod_{j\notin\Theta}p_{f,j}\,, \tag{4.15}$$

where $p_{b,R+1}^{\text{Idle}}\left(\Theta\right)$ is the BER at destination given the active set Θ. Note that $p_{f,j}$'s for are the same as those in S-DF/RT so that they can be directly obtained through (4.12)-(4.14). The only difference is $p_{b,R+1}^{\text{Idle}}\left(\Theta\right)$, in which the orthogonal-channels of inactive relays are not used at

phase-II.

Following similar steps in the previous subsection, $p_{b,R+1}^{\text{Idle}}(\Theta)$ can be approximated by

$$\hat{p}_{b,R+1}^{\text{Idle}}(\Theta) = E_{\tilde{\mathbf{h}}_{R+1}}\left[\min\left\{\sum_{d_h=d_f}^{N} w_I(d_h)\, f_{ex}^{\text{Idle}}\left(d_h,\Theta,\tilde{\mathbf{h}}_{R+1}\right),\ 0.5\right\}\right], \tag{4.16}$$

where $f_{ex}^{\text{Idle}}\left(d_h,\Theta,\tilde{\mathbf{h}}_{R+1}\right)$ is

$$\begin{aligned} f_{ex}^{\text{Idle}}\left(d_h,\Theta,\tilde{\mathbf{h}}_{R+1}\right) &= \frac{1}{2\pi \boldsymbol{j}}\int_{s_0-\boldsymbol{j}\infty}^{s_0+\boldsymbol{j}\infty}\left[\frac{1}{l2^l}\sum_{i=1}^{l}\sum_{b=0}^{1}\sum_{x\in\chi_b^i}\prod_{j\in\tilde{\Theta}}\Phi_{\Delta_{\tilde{h}_{j,R+1}}(x,\hat{z})}(s)\right]^{d_h}\frac{ds}{s} \\ &= \frac{1}{4\pi}\int_{-\infty}^{\infty}\left[\sum_{i=1}^{M}C_i\prod_{j\in\tilde{\Theta}}\exp\left[-\left(t^2+\frac{1}{4}\right)\frac{P_j}{N_0}h_{j,R+1}^2 D_i\right]\right]^{d_h}\frac{dt}{t^2+\frac{1}{4}}, \end{aligned} \tag{4.17}$$

where the second line is obtained similarly to that for (4.9). Note that the product in (4.17) contains only the MGFs corresponding to active relays (and source). Through either a direct numeric integration or a table looking up, $\hat{p}_{b,R+1}^{\text{Idle}}(\Theta)$ can be obtained. Bringing (4.14) and (4.15) back to (4.15), the average PER at destination for S-DF/Idle is obtained. Numerical results will be provided in Section 4.3.

4.2 Diversity Analysis

This subsection provides the proof of the diversity orders of the considered BICM systems that characterizes how the average BER behaves with large SNRs. Specifically, upper and lower bounds of BER are derived first, followed by showing that both bounds achieve the same diversity order. The diversity orders for the S-DF/RT and S-DF/Idle relaying schemes will be denoted by Div^{RT} and Div^{Idle}, respectively. For simplicity, an equal gain power allocation among source and all relays is assumed, i.e., $P_0 = P_{01} = \cdots = P_R = P$.

4.2.1 S-DF/RT

At high SNRs, $p_{b,R+1}^{\mathrm{RT}}$ in (4.1) is well-approximated by

$$p_{b,R+1}^{\mathrm{RT}} \approx \sum_{\Theta \subseteq \{1,2,\cdots,R\}} p_{b,R+1}^{\mathrm{RT}}(\Theta) \prod_{j \notin \Theta} p_{f,j}\,, \tag{4.18}$$

which is obtained because $1-p_{f,j} \approx 1$. In the following, an asymptotic upper bound of $p_{b,R+1}^{\mathrm{RT}}$ is provided by deriving the upper bounds of $p_{b,R+1}^{\mathrm{RT}}(\Theta)$ and $p_{f,j}$.

Similar to (3.30), $p_{b,R+1}^{\mathrm{RT}}(\Theta)$ is upper-bounded by

$$p_{b,R+1}^{\mathrm{RT}}(\Theta) \le \bar{w} \cdot f_{ub}^{\mathrm{RT}}(d_f, \Theta), \tag{4.19}$$

where

$$\begin{aligned}
&f_{ub}^{\mathrm{RT}}(d_f,\Theta) \\
&= E_{\tilde{\mathbf{h}}_{R+1}}\left[\frac{1}{2\pi \boldsymbol{j}}\int_{s_0-\boldsymbol{j}\infty}^{s_0+\boldsymbol{j}\infty}\left[\frac{1}{l2^l}\sum_{i=1}^{l}\sum_{b=0}^{1}\sum_{x\in\chi_b^i}\sum_{z\in\chi_{\bar{b}}^i}\prod_{j=0}^{R}\exp\left[\left(-s+s^2\right)\frac{P}{N_0}\tilde{h}_{j,R+1}^2|x-z|^2\right]\right]^{d_f}\frac{ds}{s}\right] \\
&\le E_{\tilde{\mathbf{h}}_{R+1}}\left[\frac{1}{2\pi \boldsymbol{j}}\int_{s_0-\boldsymbol{j}\infty}^{s_0+\boldsymbol{j}\infty}\left[\bar{\gamma}\prod_{j=0}^{R}\exp\left[\left(-s+s^2\right)\frac{P}{N_0}\tilde{h}_{j,R+1}^2 D_\chi\right]\right]^{d_f}\frac{ds}{s}\right] \\
&= \frac{\bar{\gamma}^{d_f}}{2\pi \boldsymbol{j}}\int_{s_0-\boldsymbol{j}\infty}^{s_0+\boldsymbol{j}\infty} E_{\tilde{\mathbf{h}}_{R+1}}\left[\prod_{j=0}^{R}\exp\left[\left(-s+s^2\right)\frac{Pd_f D_\chi}{N_0}\tilde{h}_{j,R+1}^2\right]\right]\frac{ds}{s} \\
&= \frac{\bar{\gamma}^{d_f}}{2\pi \boldsymbol{j}}\int_{s_0-\boldsymbol{j}\infty}^{s_0+\boldsymbol{j}\infty}\prod_{j=0}^{R} E_{\tilde{h}_{j,R+1}^2}\left[\exp\left[\left(-s+s^2\right)\frac{Pd_f D_\chi}{N_0}\tilde{h}_{j,R+1}^2\right]\right]\frac{ds}{s} \\
&= \frac{\bar{\gamma}^{d_f}}{2\pi}\int_{-\infty}^{\infty}\prod_{j=0}^{R} E_{\tilde{h}_{j,R+1}^2}\left[\exp\left[-\left(t^2+\frac{1}{4}\right)\frac{Pd_f D_\chi}{N_0}\tilde{h}_{j,R+1}^2\right]\right]\frac{dt}{t^2+\frac{1}{4}}
\end{aligned}, \tag{4.20}$$

where $\bar{\gamma} = 2^{l-1}$ is the number of erroneous z's in $\chi_{\bar{b}}^i$ for a single x. The inequality in (4.20) is obtained by assuming all (x,z) pairs achieve D_χ, and the last line is obtained by bringing the saddle point $s = 0.5 + \boldsymbol{j}t$.

According to Lemma-1, the expectation in (4.20) is evaluated as

$$E_{\tilde{h}_{j,R+1}}\left[\exp\left[-\left(t^2+\frac{1}{4}\right)\frac{Pd_fD_\chi}{N_0}\tilde{h}_{j,R+1}^2\right]\right]=\left(1+\left(t^2+\frac{1}{4}\right)\frac{\tilde{\Omega}_{j,R+1}Pd_fD_\chi}{\tilde{m}_{j,R+1}N_0}\right)^{-\tilde{m}_{j,R+1}}. \tag{4.21}$$

It is important to note that, in block fading channels, the SNR is multiplied by free distance d_f, while in fast-fading case, d_f appears in the exponent (see Section 3.2). Now, (4.20) becomes

$$\begin{aligned} &f_{ub}^{\mathrm{RT}}\left(d_f,\Theta\right)\\ &\le\frac{\bar{\gamma}^{d_f}}{2\pi}\int_{-\infty}^{\infty}\prod_{j=0}^{R}\left(1+\left(t^2+\frac{1}{4}\right)\frac{\tilde{\Omega}_{j,R+1}Pd_fD_\chi}{\tilde{m}_{j,R+1}N_0}\right)^{-\tilde{m}_{j,R+1}}\frac{dt}{t^2+\frac{1}{4}}. \end{aligned} \tag{4.22}$$

Furthermore, using Lemma-2, (4.22) is approximated at high SNRs by

$$f_{ub}^{\mathrm{RT}}\left(d_f,\Theta\right)\le\bar{\gamma}^{d_f}\prod_{j=0}^{R}\left(\frac{\tilde{\Omega}_{j,R+1}d_fD_\chi}{\tilde{m}_{j,R+1}}\right)^{-\tilde{m}_{j,R+1}}\frac{\left(2\sum_{j=0}^{R}\tilde{m}_{j,R+1}-1\right)!!}{\left(2\sum_{j=0}^{R}\tilde{m}_{j,R+1}\right)!!}2^{2\sum_{j=0}^{R}\tilde{m}_{j,R+1}-1}\left(\frac{N_0}{P}\right)^{\sum_{j=0}^{R}\tilde{m}_{j,R+1}}. \tag{4.23}$$

Binging (4.23) back to (4.19), $p_{b,R+1}^{\mathrm{RT}}(\Theta)$ is upper bounded by

$$\begin{aligned} p_{b,R+1}^{\mathrm{RT}}(\Theta)&\le\bar{w}\bar{\gamma}^{d_f}\prod_{j=0}^{R}\left(\frac{\tilde{\Omega}_{j,R+1}d_fD_\chi}{\tilde{m}_{j,R+1}}\right)^{-\tilde{m}_{j,R+1}}\frac{\left(2\sum_{j=0}^{R}\tilde{m}_{j,R+1}-1\right)!!}{\left(2\sum_{j=0}^{R}\tilde{m}_{j,R+1}\right)!!}2^{2\sum_{j=0}^{R}\tilde{m}_{j,R+1}-1}\left(\frac{N_0}{P}\right)^{\sum_{j=0}^{R}\tilde{m}_{j,R+1}},\\ &=\bar{\alpha}_\Theta\cdot\left(\frac{N_0}{P}\right)^{\sum_{j=0}^{R}\tilde{m}_{j,R+1}} \end{aligned} \tag{4.24}$$

where $\bar{\alpha}_\Theta$ contains all terms that are independent to P/N_0.

The upper bound of PER $p_{f,j}$ is obtained similarly from. Assume that all the 2^K-1 erroneous coded sequences have the same worst PEP so that $p_{f,j}$ is upper bounded by

$$p_{f,j}\le\left(2^K-1\right)\cdot f_{ub}\left(j,d_f\right), \tag{4.25}$$

where $f_{ub}\left(j,d_f\right)$ is the corresponding upper bound of the average PEP of Hamming distance d_f at relay j, which is further upper bounded by (similar to (4.20)-(4.23))

$$
\begin{aligned}
& f_{ub}\left(j, d_f\right) \\
&= E_{h_{0,j}}\left[\frac{1}{2\pi \boldsymbol{j}} \int_{s_0-\boldsymbol{j}\infty}^{s_0+\boldsymbol{j}\infty}\left[\frac{1}{l 2^l} \sum_{i=1}^{l} \sum_{b=0}^{1} \sum_{x \in \chi_b^i} \sum_{z \in \chi_{\bar{b}}^i} \exp\left[\left(-s+s^2\right) \frac{P}{N_0} h_{0,j}^2|x-z|^2\right]\right]^{d_f} \frac{ds}{s}\right] \\
&\leq E_{h_{0,j}}\left[\frac{1}{2\pi \boldsymbol{j}} \int_{s_0-\boldsymbol{j}\infty}^{s_0+\boldsymbol{j}\infty}\left[\bar{\gamma} \exp\left[\left(-s+s^2\right) \frac{P}{N_0} h_{0,j}^2 D_\chi\right]\right]^{d_f} \frac{ds}{s}\right] \\
&\leq \frac{\bar{\gamma}^{d_f}}{2\pi} \int_{-\infty}^{\infty} E_{h_{0,j}}\left[\exp\left[-\left(t^2+\frac{1}{4}\right) \frac{P d_f D_\chi}{N_0} h_{0,j}^2\right]\right] \frac{dt}{t^2+\frac{1}{4}}
\end{aligned}
\quad . \tag{4.26}
$$

Then, applying Lemma-1 and Lemma-2 yields the upper bound $p_{f,j}$ as

$$
\begin{aligned}
p_{f,j} &\leq \tilde{w} \bar{\gamma}^{d_f}\left(\frac{\Omega_{0,j} d_f D_\chi}{m_{0,j}}\right)^{-m_{0,j}} \frac{\left(2m_{0,j}-1\right)!!}{\left(2m_{0,j}\right)!!} 2^{2m_{0,j}-1}\left(\frac{N_0}{P}\right)^{m_{0,j}} \\
&= \bar{\beta}_j \cdot\left(\frac{N_0}{P}\right)^{m_{0,j}}
\end{aligned}
\quad , \tag{4.27}
$$

where $\bar{\beta}_j$ contains all terms that are independent to P/N_0.

By bringing (4.24) and (4.27) into (4.18), an asymptotic upper bound of $p_{b,R+1}^{\mathrm{RT}}$ is obtained as

$$
p_{b,R+1}^{\mathrm{RT}} \leq \bar{p}_{b,R+1}^{\mathrm{RT}} \triangleq \sum_{\Theta \subseteq\{1,2,\ldots R\}}\left(\bar{\alpha}_\Theta \prod_{j \notin \Theta} \bar{\beta}_j\right)\left(\frac{N_0}{P}\right)^{\sum_{j=0}^{R} \tilde{m}_{j,R+1}+\sum_{j \notin \Theta} m_{0,j}} . \tag{4.28}
$$

At extremely high SNRs, e.g., $P/N_0 \to \infty$, the summation in (4.28) will be dominated by the terms with the smallest exponents. Therefore, the diversity order [10] of $\bar{p}_{b,R+1}^{\mathrm{RT}}$ is

$$
\begin{aligned}
\overline{\mathrm{Div}}^{\mathrm{RT}} &= \min_{\Theta \subseteq\{1,2,\ldots R\}}\left\{\sum_{j=0}^{R} \tilde{m}_{j,R+1}+\sum_{j \notin \Theta} m_{0,j}\right\} \\
&= m_{0,R+1}+\sum_{j=1}^{R} \min\left\{m_{0,j}+m_{0,R+1}, m_{j,R+1}\right\}
\end{aligned}
\quad . \tag{4.29}
$$

The lower bound of $p_{b,R+1}^{\mathrm{RT}}$ can be obtained similarly to the upper bound with some modifications. First, $p_{b,R+1}^{\mathrm{RT}}(\Theta)$ is lower bounded by

$$p_{b,R+1}^{\mathrm{RT}}(\Theta) \geq f^{RT}\left(d_f, \Theta\right), \tag{4.30}$$

in which only the error events with Hamming weight d_f is involved. Moreover, The PEP $f^{RT}\left(d_f, \Theta\right)$ can be lower bounded by leaving only one (x, z) pair with D_χ, i.e.,

$$\begin{aligned} & f^{\mathrm{RT}}\left(d_f, \Theta\right) \\ & \geq E_{\tilde{\mathbf{h}}_{R+1}}\left[\frac{1}{2\pi \boldsymbol{j}} \int_{s_0-\boldsymbol{j}\infty}^{s_0+\boldsymbol{j}\infty}\left[\underline{\gamma} \prod_{j=0}^{R} \exp\left[\left(-s+s^2\right) \frac{P}{N_0} \tilde{h}_{j,R+1}^2 D_\chi\right]\right]^{d_f} \frac{ds}{s}\right] \\ & = \frac{\underline{\gamma}^{d_f}}{2\pi} \int_{-\infty}^{\infty} \prod_{j=0}^{R} E_{\tilde{h}_{j,R+1}^2}\left[\exp\left[-\left(t^2+\frac{1}{4}\right) \frac{P d_f D_\chi}{N_0} \tilde{h}_{j,R+1}^2\right]\right] \frac{dt}{t^2+\frac{1}{4}} \end{aligned} \tag{4.31}$$

where $\underline{\gamma} = 1/2^{l-1}$, the second row is obtained by considering only one single (x, z) pair with squared Euclidean distance D_χ, and the other rows are obtained similar to (4.20).

Since the remaining integration in (4.31) is exactly the same with that in (4.20), we have

$$\begin{aligned} p_{b,R+1}^{\mathrm{RT}}(\Theta) & \geq \underline{\gamma}^{d_f} \prod_{j=0}^{R}\left(\frac{\tilde{\Omega}_{j,R+1} d_f D_\chi}{\tilde{m}_{j,R+1}}\right)^{-\tilde{m}_{j,R+1}} \frac{\left(2\sum_{j=0}^{R} \tilde{m}_{j,R+1}-1\right)!!}{\left(2\sum_{j=0}^{R} \tilde{m}_{j,R+1}\right)!!} 2^{2\sum_{j=0}^{R} \tilde{m}_{j,R+1}-1}\left(\frac{N_0}{P}\right)^{\sum_{j=0}^{R} \tilde{m}_{j,R+1}} \\ & = \underline{\alpha}_\Theta \cdot\left(\frac{N_0}{P}\right)^{\sum_{j=0}^{R} \tilde{m}_{j,R+1}} \end{aligned}, \tag{4.32}$$

where $\underline{\alpha}_\Theta$ contains all the terms independent to P/N_0. Now, it is straightforward to show that $p_{f,j}$ is lower bounded by

$$p_{f,j} \geq \underline{\beta}_j \cdot\left(\frac{N_0}{P}\right)^{m_{0,j}}, \tag{4.33}$$

where $\underline{\beta}_j$ contains all the terms independent to P/N_0. Using (4.32) and (4.33), an asymptotic lower bound of $p_{b,R+1}^{\mathrm{RT}}$ is

$$p_{b,R+1}^{\mathrm{RT}} \geq \underline{p}_{b,R+1}^{\mathrm{RT}} \triangleq \sum_{\Theta \subset\{1,2,\cdots,R\}} \underline{\alpha}_\Theta \prod_{j \notin \Theta} \underline{\beta}_j\left(\frac{N_0}{P}\right)^{\sum_{j=0}^{R} \tilde{m}_{j,R+1}+\sum_{j \notin \Theta} m_{0,j}} \tag{4.34}$$

Denote the diversity order of $\underline{p}_{b,R+1}^{\mathrm{RT}}$ by $\underline{\mathrm{Div}}^{\mathrm{RT}}$. Similarly, at extremely high SNRs, the summation is dominated by the terms with the smallest exponent. It turns out that $\underline{\mathrm{Div}}^{\mathrm{RT}}=\overline{\mathrm{Div}}^{\mathrm{RT}}$. Since $\bar{p}_{b,R+1}^{\mathrm{RT}} \geq p_{b,R+1}^{\mathrm{RT}} \dot{\geq} \underline{p}_{b,R+1}^{\mathrm{RT}}$ at all ranges of SNR, this implies $\overline{\mathrm{Div}}^{\mathrm{RT}} \leq \mathrm{Div}^{\mathrm{RT}} \leq \underline{\mathrm{Div}}^{\mathrm{RT}}$. Therefore, it can be concluded that $\overline{\mathrm{Div}}^{\mathrm{RT}}=\mathrm{Div}^{\mathrm{RT}}=\underline{\mathrm{Div}}^{\mathrm{RT}}$, as provided in (4.29). Compared with (3.39), the diversity in fast-fading channel is just d_f times of that in the block-fading channels. The reason is rather straightforward. Since all coded bits in a packet suffer the same channel realization, the diversity does not increase with the free distance.

4.2.2 S-DF/Idle

For S-DF/Idle relaying scheme, the BER at destination is first approximated by

$$p_{b,R+1}^{\mathrm{Idle}} \approx \sum_{\Theta \subseteq \{1,2,\cdots,R\}} p_{b,R+1}^{\mathrm{Idle}}(\Theta) \prod_{j \notin \Theta} p_{f,j} \,. \tag{4.35}$$

Since the upper and lower bounds of $p_{f,j}$ have been provided in the previous subsection. This subsection focuses on $p_{b,R+1}^{\mathrm{Idle}}(\Theta)$.

The derivation of the upper bound of $p_{b,R+1}^{\mathrm{Idle}}(\Theta)$ is very similar to that of $p_{b,R+1}^{\mathrm{RT}}(\Theta)$. The only difference comes from the fact that the orthogonal-channels of inactive relays are not used for S-DF/Idle relaying scheme. Following the same steps in (4.19)-(4.24), $p_{b,R+1}^{\mathrm{Idle}}(\Theta)$ is upper bounded by

$$\begin{aligned} p_{b,R+1}^{\mathrm{Idle}}(\Theta) &\leq \bar{w}\bar{\gamma}^{d_f} \prod_{j \in \tilde{\Theta}} \left(\frac{\Omega_{j,R+1} d_f D_{\chi}}{m_{j,R+1}} \right)^{-m_{j,R+1}} \frac{\left(2\sum_{j=0}^{R} m_{j,R+1}-1\right)!!}{\left(2\sum_{j=0}^{R} m_{j,R+1}\right)!!} 2^{2\sum_{j \in \tilde{\Theta}} m_{j,R+1}-1} \left(\frac{N_0}{P}\right)^{\sum_{j \in \tilde{\Theta}} m_{j,R+1}} \\ &= \bar{\alpha}_{\Theta} \cdot \left(\frac{N_0}{P}\right)^{\sum_{j \in \tilde{\Theta}} m_{j,R+1}} \end{aligned}, \tag{4.36}$$

where $\bar{\alpha}_{\Theta}$, which contains all terms that are independent to P/N_0, is slightly different from that

in Section 3.2. Now $p_{b,R+1}^{\text{Idle}}$ is upper bounded by

$$p_{b,R+1}^{\text{Idle}} \le \bar{p}_{b,R+1}^{\text{Idle}} \triangleq \sum_{\Theta \subseteq \{1,2,\ldots R\}} \left(\bar{\alpha}_{\Theta} \prod_{j \notin \Theta} \bar{\beta}_j \right) \left(\frac{N_0}{P} \right)^{\sum_{j \in \Theta} m_{j,R+1} + \sum_{j \notin \Theta} m_{0,j}} \tag{4.37}$$

and is lower bounded by

$$p_{b,R+1}^{\text{Idle}} \ge \bar{p}_{b,R+1}^{\text{Idle}} \triangleq \sum_{\Theta \subseteq \{1,2,\ldots R\}} \left(\underline{\alpha}_{\Theta} \prod_{j \notin \Theta} \underline{\beta}_j \right) \left(\frac{N_0}{P} \right)^{\sum_{j \in \Theta} m_{j,R+1} + \sum_{j \notin \Theta} m_{0,j}} . \tag{4.38}$$

Thus, similarly to that in the previous subsection, it is concluded that the diversity of $p_{b,R+1}^{\text{Idle}}$ is

$$\text{Div}^{\text{Idle}} = m_{0,R+1} + \sum_{j=1}^{R} \min\left\{ m_{0,j}, m_{j,R+1} \right\}. \tag{4.39}$$

4.3 Numerical Results

This section verifies the numerical results for the BER approximations in Section 4.1 and diversity order proposed in Section 4.2. In the following simulations, a half-rate convolutional code CC(171,133) is considered, the interleaver is S-random with length 1024 and depth 20, and the modulation is Gray-mapped 16-QAM. For simplicity, let $P_0 = P_1 = \cdots = P_R = P$ (orthogonal channels in the time domain) with $P = E_b \cdot R_C \cdot l$ where E_b is the bit energy, and $R_C = 0.5$ is the channel code rate.

We first verify the proposed approximations in (4.11), (4.14) and

$$\hat{p}_{b,j} = E_{h_{0,j}} \left[\min\left\{ \sum_{d_h = d_f}^{N} w_I\left(d_h\right) f_{ex}\left(j, d_h, h_{0,j}\right),\ 0.5 \right\} \right]. \tag{4.40}$$

For simplicity, consider a 3-node network with the setups shown as Network-1 in Table II. In this case, the BER at the destination is (from (4.1))

$$p_{b,2}^{\text{mode}} = p_{b,2}^{\text{mode}}\left(\{1\}\right)\left(1 - p_{f,1}\right) + p_{b,2}^{\text{mode}}\left(\varnothing\right) p_{f,1}, \tag{4.41}$$

where $\text{mode} \in \{\text{RT}, \text{Idle}\}$. Note that when the relay decodes successfully, $p_{b,2}^{\text{RT}}\left(\{1\}\right) = p_{b,2}^{\text{Idle}}\left(\{1\}\right)$.

The simulation results and approximations are plotted in Fig. 4.1 for $p_{b,2}^{\mathrm{RT}}(\{1\})$, $p_{b,2}^{\mathrm{RT}}(\varnothing)$, $p_{b,2}^{\mathrm{Idle}}(\varnothing)$ and in Fig. 4.2 for $p_{b,1}$ and $p_{f,1}$. As can be seen in Fig. 4.1, all approximations provide very good predictions of the real BERs. Unfortunately, in Fig. 4.2, the PER approximation $\hat{p}_{f,1}$, according (4.12), over-estimates $p_{f,1}$, but $\hat{p}_{b,1}$ obtained by (4.40) is rather accurate in predicting $p_{b,1}$. Thus, (4.12) is the main reason that leads to the gap on predicting PER.

The over-estimation on PER could become negligible when the S-R link is better than the other links. This is the typical case of relay network, e.g., when LOS is possible for S-R links. Consider Network-2 with setups shown in Table II with $n=1$, 2 and 4 to investigate the effect of different S-R link qualities to our approximations and plotted the results in Fig. 4.3 and Fig. 4.4 for S-DF/Idle and S-DF/RT relaying MODES, respectively. In Fig. 4.3, non-trivial gaps (about 1 dB) are observed between the approximations (App.) and the simulation results (Sim.) for both $n=1$ and 2. For $n=4$, the approximation matches the simulation results with a smaller gap. This is due to the fact that, when the S-R link is better than other links, $p_{f,1}$ is low enough such that $p_{b,2}^{\mathrm{Idle}}(\varnothing)\,p_{f,1}$ is relatively smaller than the $p_{b,2}^{\mathrm{Idle}}(\{1\})$ and that (4.41) is dominate by only $p_{b,2}^{\mathrm{Idle}}(\{1\})$, which can be well approximated. For S-DF/RT in Fig. 4.4, a 0.5 dB gap is observed only for $n=1$, while approximations for $n=2$ and 4 are very close to the simulations. The approximations for S-DF/RT become more accurate, because $p_{b,2}^{\mathrm{RT}}(\varnothing)$ is smaller than $p_{b,2}^{\mathrm{Idle}}(\varnothing)$ such that $p_{b,2}^{\mathrm{RT}}(\{1\})$ is more likely to dominate the error performance at destination.

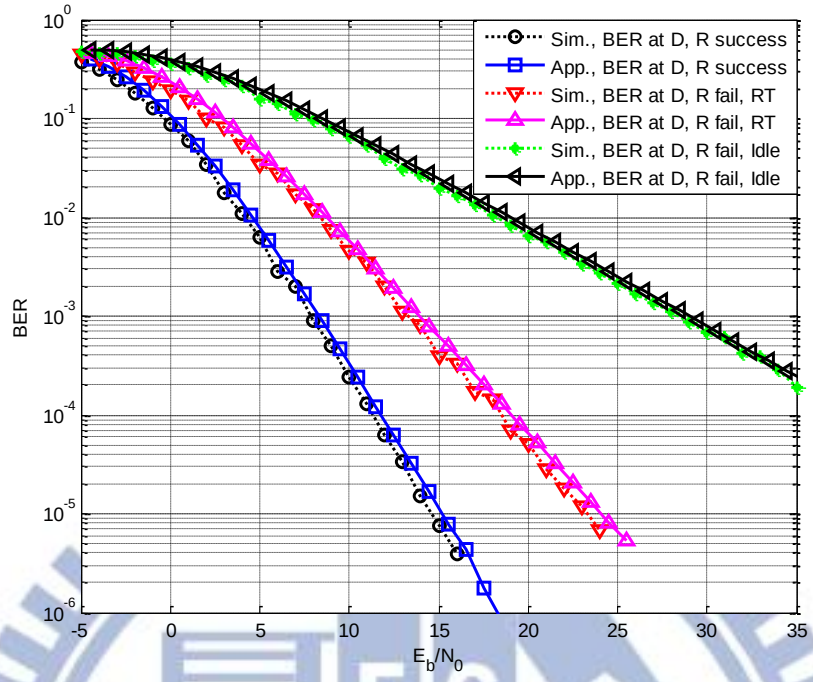

Fig. 4.1. Destination BER simulation results and approximations for Network-1

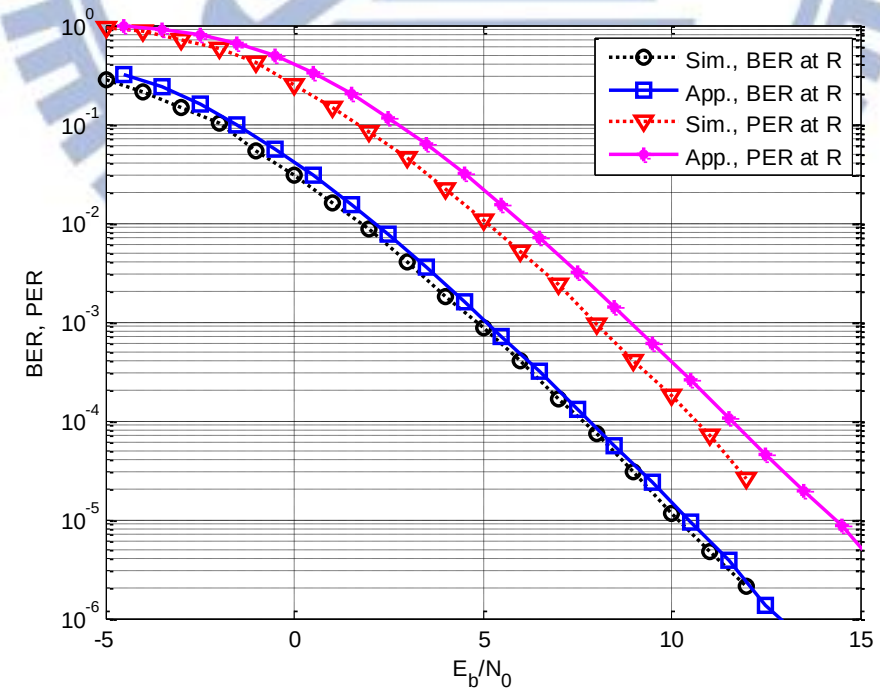

Fig. 4.2. Relay BER/PER simulation results and approximations for Network-1

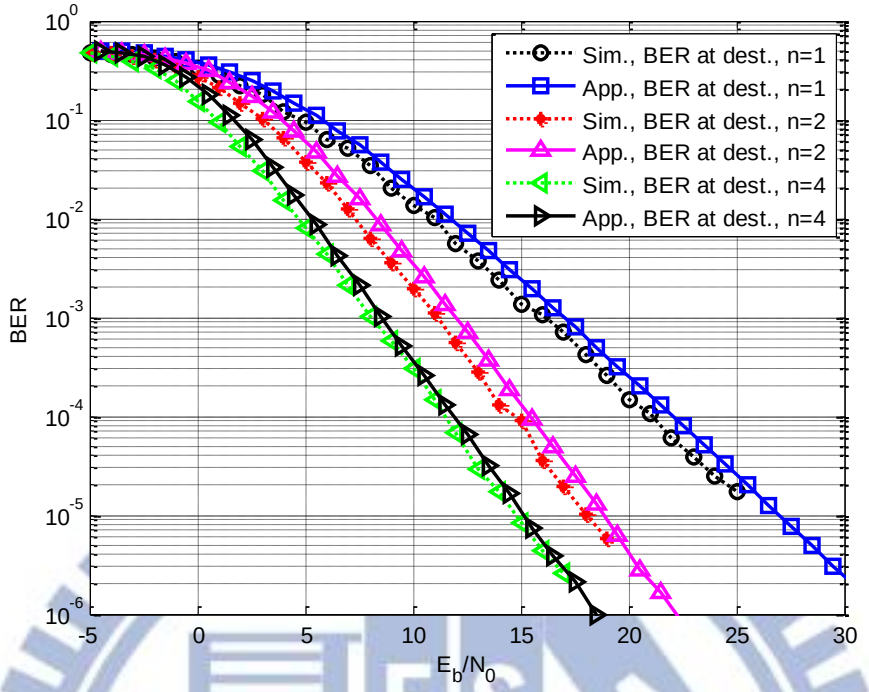

Fig. 4.3. BER simulations and approximations of Network-2 with the values of $n = 1,\ 2$ and 4 for S-DF/Idle

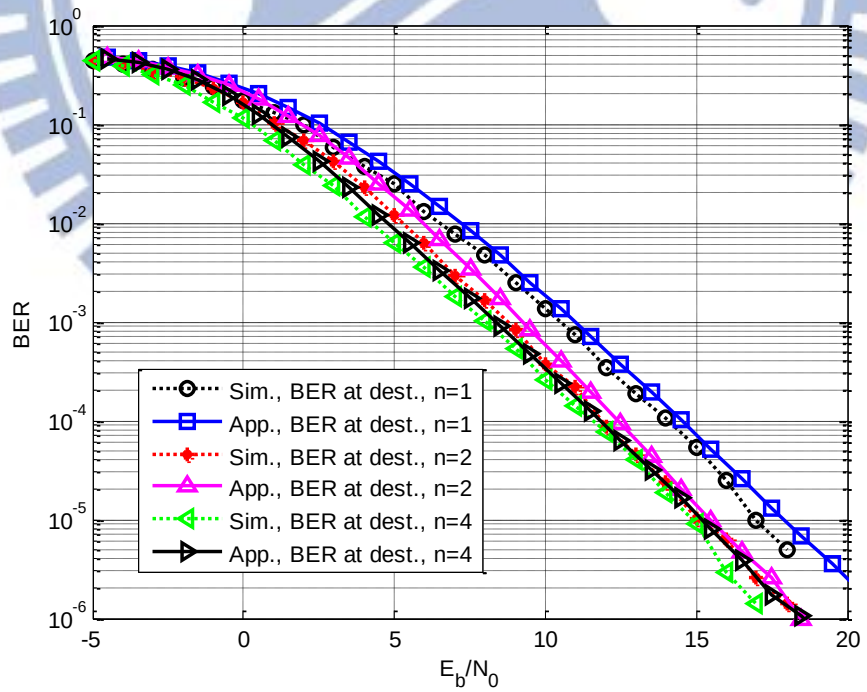

Fig. 4.4. BER simulations and approximations of Network-2 with the values of $n = 1,\ 2$ and 4 for S-DF/RT

The results for different relay number $R=1,\ 2,\ 3$ and 4 is provided for S-DF/RT and S-DF/Idle in Fig. 4.5 and Fig. 4.6, respectively. Fig. 4.5 considers Network-4 in Table II, and Fig. 4.6 provides another results for Rayleigh fading channels, cf. Network-5 in Table II. As is seen from both figures, the proposed approximations are very close to the simulation results for all R at BER of 10^{-5}.

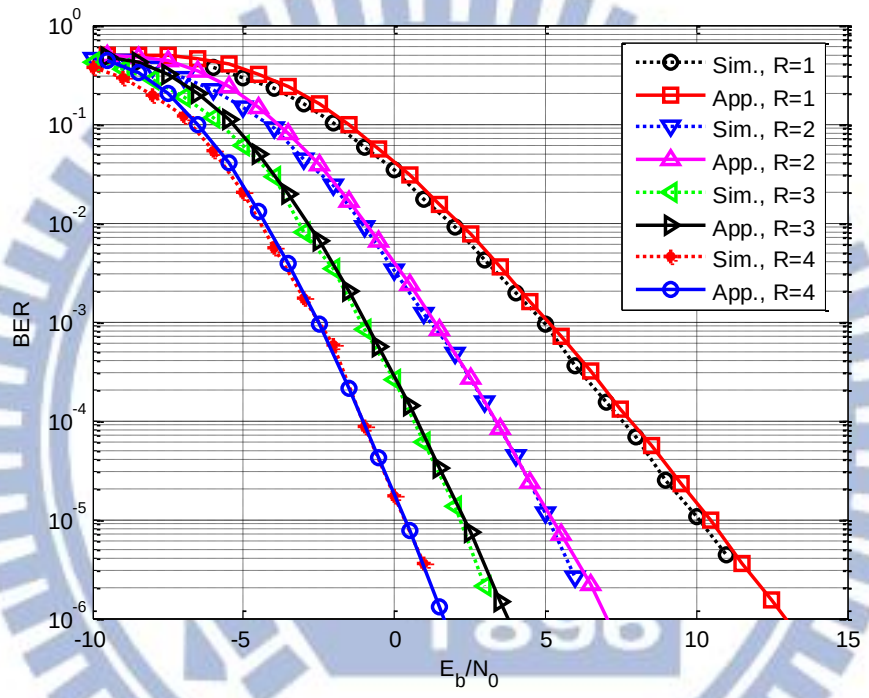

Fig. 4.5. BER simulations and approximations of Network-4 with S-DF/RT for $R=1,\ 2,\ 3$ and 4 and i.i.d channel conditions ($m=2$ and $\Omega=2$ for all links)

Table III. Network setups

Networks	S-D link	S-R link	R-D link	Div^{RT}	Div^{Idle}
Network-6	$m_{0,2}=\Omega_{0,2}=1$	$m_{0,1}=\Omega_{0,1}=3$	$m_{1,2}=\Omega_{1,2}=1$	2	2
Network-7	$m_{0,2}=\Omega_{0,2}=1$	$m_{0,1}=\Omega_{0,1}=1$	$m_{1,2}=\Omega_{1,2}=3$	3	2
Network-8	$m_{0,2}=\Omega_{0,2}=1$	$m_{0,1}=\Omega_{0,1}=2$	$m_{1,2}=\Omega_{1,2}=2$	3	3

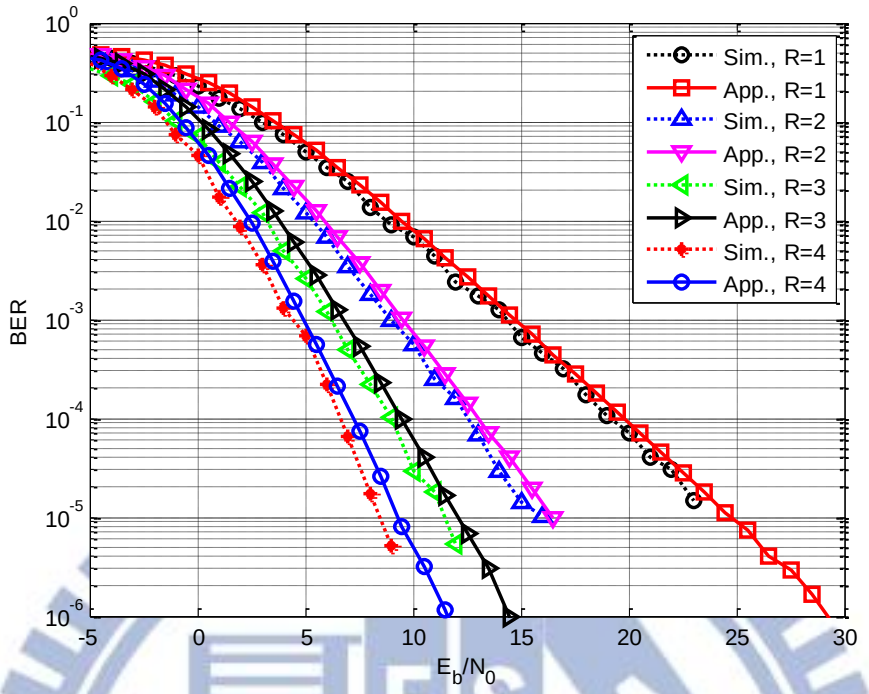

Fig. 4.6. BER simulations and approximations of Network-5 with S-DF/Idle for $R=1,\ 2,\ 3$ and 4 over Rayleigh fading channels

To verify the diversity results in Section 4.2, we now compare the PER performance of 3 different networks (Network-6, 7 and 8 in Table III) with the channel statistics. All networks have 1 relay and are with $m_{0,2}=\Omega_{0,2}=1$ on the source-to-destination link. Network-6 has a better source-to-relay link $(m_{0,1}=\Omega_{0,1}=3)$, Network-7 has a better relay-to-destination link $(m_{1,2}=\Omega_{1,2}=3)$, and Network-8 has $(m_{0,1}=\Omega_{0,1}=m_{1,2}=\Omega_{1,2}=2)$. The PER performances for S-DF/RT are plotted in Fig. 4.7, wherein the PER curves of Network-7 and 8 decrease with the same slope which is steeper than that of Network-6 at high SNRs. This coincides the diversity orders shown in Table III which are calculated according to (4.29). The diversity orders for S-DF/Idle are also provided in Table III according to (4.39) and the verification through simulations in Fig. 4.8. It can be clearly seen in Fig. 4.8, Network-8 with diversity order 3 outperforms Network-6 and 7 with diversity order 2 at high SNRs.

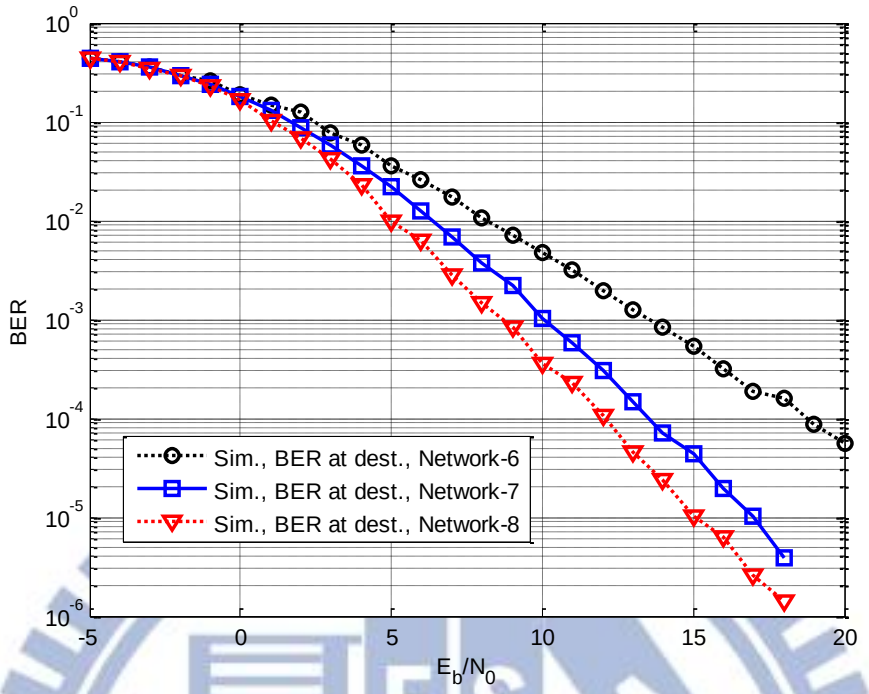

Fig. 4.7. PER performance of Network-6, 7 and 8 in Table III with S-DF/RT

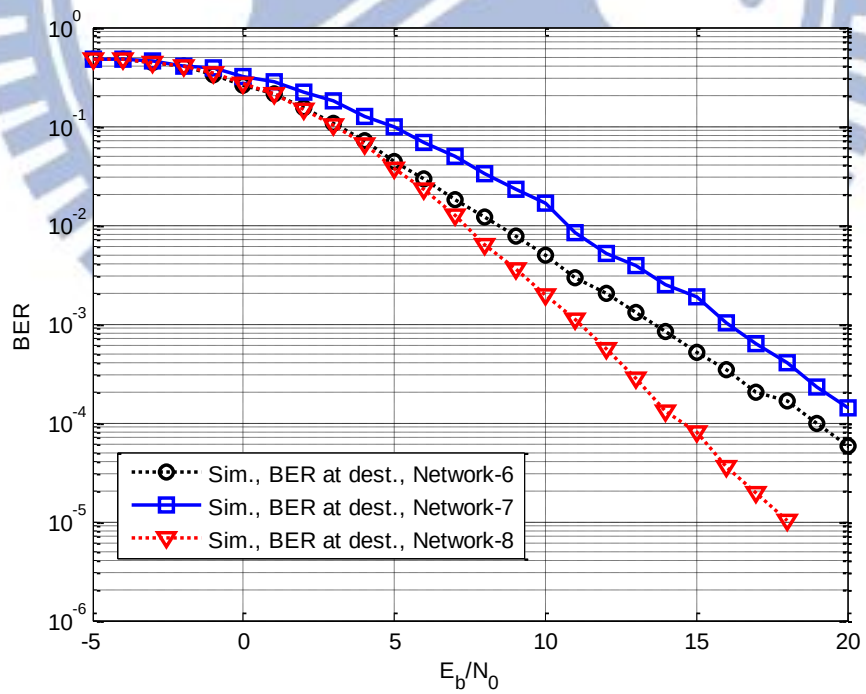

Fig. 4.8. PER performance of Network-6, 7 and 8 in Table III with S-DF/Idle

4.4 Summary

In Chapter 4, the BER performance and diversity order of BICM-coded cooperative networks is investigated for the S-DF/RT and S-DF/Idle relaying over block-fading Nakagami-*m* channels. Unlike most of the existing works, this chapter considers a packet-by-packet forwarding strategy. For the BER analysis, the BER over block-fading channels can be obtained by first obtaining the BER in AWGN channels and then averaging it over channel realizations. Unfortunately, a direct integration may introduce non-trivial gap to the exact performance. To overcome this, a modification on the AWGN BER is adopted. But such a modification prohibits a close-form solution. As a result, the Monte Carlo method is used for the channel averaging. The diversity of the cooperative BICM network is also derived for both S-DF/RT and S-DF/Idle in fast Nakagami-*m* fading channels. The ideas of derivations are the same as those in 3.2, though the details are different. Numerical results show that our approximations are rather accurate for different network setups. An example is also provided to verify our proof of the diversity order.

Chapter 5

Power Allocation

The objective of this Chapter is to determine the transmit power allocation $\mathbf{P} = [P_0, P_1, ..., P_R]^T$ that minimizes BER at the destination under the sum power constraint $\sum_{j=0}^{R} P_j \le P_T$ [2]. An effective power allocation between transmit nodes could significantly lower the error rate at the destination so as to reduce the probability of re-transmission via (H-)ARQ (which requires additional power/energy and radio resources). Moreover, a good power allocation should also involve relay selection as well, e.g., allocate zero power to the useless relays.

This chapter assumes a slowly fading environment so that the channels remain constants for several following frames and assume that full channel state information (CSI) is available. For simplicity, the time index k will be dropped in this chapter. Since every link remains unchanged over the transmission of a packet, it can be treated as an AWGN (additive white Gaussian noise) channel from the power allocation perspective. Note that power allocation can be done either at source or destination depending on the required signaling overhead and where the complexity of

[2] The sum power constraint can also be interpreted as a sum energy constraint.

power allocation is to be placed. From the signaling overhead aspect, allocation at destination seems favorable because only the CSIs of the source-to-relay links have to be reported to the destination.

In the following sections, power allocation for the AF relaying is firstly discussed, followed by those for the S-DF relaying modes (RT, Idle and AF).

5.1 Power Allocation for AF Relaying: PA-EC

For the AF relaying, all relays forward the received packet without decoding. All orthogonal channels are used by relays at phase-II. The destination decodes the packet based on all received signals from all orthogonal channels. It can be regarded that $\Theta = \{1, 2, \cdots R\}$ in (4.1). Thus, the BER at the destination is expressed as

$$p_{b,R+1}^{\mathrm{AF}} \le \sum_{d_h = d_f}^{N} w_I(d_h) f_{ub}^{\mathrm{AF}}(d_h, \boldsymbol{\alpha}), \tag{5.1}$$

where $\mathbf{P}$ is replaced by $\boldsymbol{\alpha} = [\alpha_0 \ \alpha_1 \ \ldots \ \alpha_R]^T$ with $\alpha_j = P_j / P_T$, and $f_{ub}^{\mathrm{AF}}(d_h, \boldsymbol{\alpha})$ is the union bound of PEP between two coded sequences with Hamming distance d_h and depends on a power allocation $\boldsymbol{\alpha}$, which is to be determined.

At high SNRs, (5.1) is dominated by the error events that have the smallest Hamming weight, i.e., the free distance d_f. Thus, (5.1) can be approximated by

$$p_{b,R+1}^{\mathrm{AF}} \approx w_I(d_f) f_{ub}^{\mathrm{AF}}(d_f, \boldsymbol{\alpha}). \tag{5.2}$$

By following the steps in previous chapters, $f_{ub}^{\mathrm{AF}}(d_f, \boldsymbol{\alpha})$ is evaluated by (similar to that in (4.4))

$$f_{ub}^{\mathrm{AF}}(d_f, \boldsymbol{\alpha}) = \frac{1}{2\pi \boldsymbol{j}} \int_{s_0 - \boldsymbol{j}\infty}^{s_0 + \boldsymbol{j}\infty} \left[\frac{1}{l 2^l} \sum_{i=1}^{l} \sum_{b=0}^{1} \sum_{x \in \chi_b^i} \sum_{z \in \chi_{\bar{b}}^i} \prod_{j=0}^{R} \Phi_{\Delta_{\tilde{h}_{j,R+1}}(x,z)}(s) \right]^{d_f} \frac{ds}{s}. \tag{5.3}$$

With given $\tilde{h}_{j,R+1}$, the metric difference is a Gaussian random variable with the MGF

$$\Phi_{\Delta_{\tilde{h}_{j,R+1}}(x,z)}(s)=\exp\left[\left(-s+s^2\right)P_T\left|x-z\right|^2\frac{\alpha_j\left|\tilde{h}_{j,R+1}\right|^2}{\tilde{N}_0^{(j)}}\right]. \tag{5.4}$$

After substituting the saddle point $s=0.5+\boldsymbol{j}t$ into (5.4), (5.3) becomes

$$f_{ub}^{\mathrm{AF}}\left(d_f,\boldsymbol{\alpha}\right)=\frac{1}{4\pi}\int_{-\infty}^{\infty}\left[\frac{1}{l2^l}\sum_{i=1}^{l}\sum_{b=0}^{1}\sum_{x\in\chi_b^i}\sum_{z\in\chi_{\bar{b}}^i}\exp\left[-\left(t^2+\frac{1}{4}\right)P_T\left|x-z\right|^2\sum_{j=0}^{R}\frac{\alpha_j\left|\tilde{h}_{j,R+1}\right|^2}{\tilde{N}_0^{(j)}}\right]\right]^{d_f}\frac{dt}{t^2+\frac{1}{4}}. \tag{5.5}$$

Note that the imaginary part in the integral of (5.5) disappears because it is an odd function of t.

Eq. (5.5) is too complicated for power allocation. To simplify it, note that the summation of real exponential functions in (5.5) is dominated by the (x,z) pairs with the minimum squared Euclidean distance (MSWD) $\left|x-z\right|^2$, which is D_χ as was defined in (3.31). By just considering the (x,z) pairs that achieve D_χ, (5.5) is approximated as

$$\begin{aligned}f_{ub}^{\mathrm{AF}}\left(d_f,\boldsymbol{\alpha}\right)&\approx\frac{1}{4\pi}\int_{-\infty}^{\infty}\left[N_\chi\exp\left[-\left(t^2+\frac{1}{4}\right)P_TD_\chi\sum_{j=0}^{R}\frac{\alpha_j\left|\tilde{h}_{j,R+1}\right|^2}{\tilde{N}_0^{(j)}}\right]\right]^{d_f}\frac{dt}{t^2+\frac{1}{4}},\\&=\frac{N_\chi^{d_f}}{4\pi}\int_{-\infty}^{\infty}\exp\left[-\left(t^2+\frac{1}{4}\right)\frac{d_fP_TD_\chi}{N_0}M_{AF}\left(\boldsymbol{\alpha}\right)\right]\frac{dt}{t^2+\frac{1}{4}}\end{aligned} \tag{5.6}$$

where N_χ is the number of (x,z) pairs that achieves $\left|x-z\right|^2=D_\chi$ divided by $l2^l$ (or C_1 in Table I), and $M_{AF}\left(\boldsymbol{\alpha}\right)$ is the equivalent channel seen at the destination, expressed as

$$M_{AF}(\boldsymbol{\alpha}) = N_0\left(\frac{\alpha_0\left|\tilde{h}_{0,R+1}\right|^2}{\tilde{N}_0^{(0)}} + \sum_{j=1}^{R}\frac{\alpha_j\left|\tilde{h}_{j,R+1}\right|^2}{\tilde{N}_0^{(j)}}\right)$$

$$= \alpha_0\left|h_{0,R+1}\right|^2 + N_0\sum_{j=1}^{R}\frac{\alpha_j\left|h_{j,R+1}\right|^2\left|h_{0,j}\right|^2\dfrac{P_T\alpha_0}{P_T\alpha_0\left|h_{0,j}\right|^2+N_0}}{\left(\dfrac{\left|h_{j,R+1}\right|^2 P_T\alpha_j}{P_T\alpha_0\left|h_{0,j}\right|^2+N_0}+1\right)N_0} \quad . \tag{5.7}$$

$$= \alpha_0\left|h_{0,R+1}\right|^2 + \sum_{j=1}^{R}\frac{\alpha_j\left|h_{j,R+1}\right|^2\left|h_{0,j}\right|^2 P_T\alpha_0}{\left|h_{j,R+1}\right|^2 P_T\alpha_j + P_T\alpha_0\left|h_{0,j}\right|^2 + N_0}$$

$$= \alpha_0\left|h_{0,R+1}\right|^2 + \sum_{j=1}^{R}\frac{\alpha_j\left|h_{j,R+1}\right|^2\left|h_{0,j}\right|^2\alpha_0}{\left|h_{j,R+1}\right|^2\alpha_j + \alpha_0\left|h_{0,j}\right|^2 + N_0/P_T}$$

Furthermore, at high SNRs, i.e., $P_T/N_0 \to \infty$, the integral in (5.6) is dominated by the value integrated over a small interval $[-\tau,\tau]$, where $0<\tau\ll 1$. Thus, (5.6) can be approximated by ignoring the term t^2 in the denominator, i.e.,

$$f_{ub}^{\mathrm{AF}}(d_f,\boldsymbol{\alpha}) \approx \frac{N_\chi^{d_f}}{\pi}\int_{-\infty}^{\infty}\exp\left[-\left(t^2+\frac{1}{4}\right)\frac{d_f P_T D_\chi}{N_0}M_{AF}(\boldsymbol{\alpha})\right]dt$$

$$= \frac{N_\chi^{d_f}}{\pi}\exp\left[-\frac{d_f P_T D_\chi \hat{M}_{AF}(\boldsymbol{\alpha})}{4N_0}\right]\int_{-\infty}^{\infty}\exp\left[-\frac{d_f P_T D_\chi}{N_0}M_{AF}(\boldsymbol{\alpha})t^2\right]dt \quad . \tag{5.8}$$

Re-arranging the remaining integral in (5.8) into a form of Gaussian PDF leads to

$$f_{ub}^{\mathrm{AF}}(d_f,\boldsymbol{\alpha}) \approx N_\chi^{d_f}\sqrt{\frac{N_0}{\pi d_f P_T D_\chi M_{AF}(\boldsymbol{\alpha})}}\exp\left[-\frac{d_f P_T D_\chi M_{AF}(\boldsymbol{\alpha})}{4N_0}\right], \tag{5.9}$$

and

$$p_{b,R+1}^{\mathrm{AF}} \approx w_I(d_f)N_\chi^{d_f}\sqrt{\frac{N_0}{\pi d_f P_T D_\chi M_{AF}(\boldsymbol{\alpha})}}\exp\left[-\frac{d_f P_T D_\chi M_{AF}(\boldsymbol{\alpha})}{4N_0}\right]. \tag{5.10}$$

Now, the power $\boldsymbol{\alpha}$ can be allocated so as to minimize (5.10), i.e.,

$$\min_{\boldsymbol{\alpha}} \quad w_I(d_f)N_\chi^{d_f}\sqrt{\frac{N_0}{\pi d_f P_T D_\chi M_{AF}(\boldsymbol{\alpha})}}\exp\left[-\frac{d_f P_T D_\chi M_{AF}(\boldsymbol{\alpha})}{4N_0}\right]. \tag{5.11}$$

$$\text{s.t.} \quad \mathbf{1}^T\boldsymbol{\alpha}\le 1,\ 0\le\alpha_j\le 1,\ j=0,1,\cdots,R$$

In fact, (5.10) is monotonically decreasing with $M_{AF}(\boldsymbol{\alpha})$. This can be proved by examining the first derivative of the function $S(x) = a_1 x^{-a_2/2} e^{-a_3 x}$ for $x > 0$, $a_1 > 0$ and $a_3 > 0$. Therefore, the problem of minimizing (5.11) can be simplified by maximizing $M_{AF}(\boldsymbol{\alpha})$. This leads to our power allocation for AF relaying mode, call PA-EC ('EC' stands for equivalent channel), as

$$\begin{aligned} \max_{\boldsymbol{\alpha}} \quad & M_{AF}(\boldsymbol{\alpha}) \\ \text{s.t.} \quad & \mathbf{1}^T \boldsymbol{\alpha} \le 1,\ 0 \le \alpha_j \le 1,\ j = 0,1,\cdots,R \end{aligned} . \tag{5.12}$$

The optimization problem in (5.12) can be conducted by first showing that $M_{AF}(\boldsymbol{\alpha})$ is a concave function in the feasible region of $\boldsymbol{\alpha}$. The proof is provided in Appendix C. Since $M_{AF}(\boldsymbol{\alpha})$ is differentiable, such an optimization of a concave differentiable cost function can be done by using existing optimization algorithms, e.g. the Gradient descent method. The results of power allocation will be provided in Section 5.4.

5.2 Power Allocation for S-DF Relayings

This section provides the power allocation for the S-DF relayings (S-DF/RT, SDF/Idle and S-DF/AF). Two methods with different cost functions are going to be proposed. One employs an approximate BER as the cost functions (PA-ABER), and the other employs a minimum generalized equivalent channel as the cost function (PA-MGEC). Both methods are first derived based on the general form in (2.9), followed by specific methods for optimizing the cost functions.

5.2.1 PA-ABER

Different from those of AF in Section 5.1, for S-DF, the signals received by the destination at phase-II depends on the decoding results of relays, or namely, the active relay set Θ. Therefore, the BER at the destination is evaluated by

$$p_{b,R+1}^{\text{S-DF}} = \sum_{\Theta\subseteq\{1,2,\cdots,R\}} p_{b,R+1}^{\text{S-DF}}(\Theta)\prod_{j\in\Theta}\left(1-p_{f,j}\right)\prod_{j\notin\Theta} p_{f,j} \approx \sum_{\Theta\subseteq\{1,2,\cdots,R\}} p_{b,R+1}^{\text{S-DF}}(\Theta)\prod_{j\notin\Theta} K\cdot p_{b,j} \quad , \tag{5.13}$$

where $p_{b,R+1}^{\text{S-DF}}(\Theta)$ is the conditional BER at destination for the S-DF relaying scheme, given the active relay set Θ. In (5.13), the approximation is obtained with the assumptions that $p_{f,j} \ll 1$ in practical systems and that $p_{f,j} \approx K\cdot p_{b,j}$ for a small $p_{b,j}$ at high SNRs. The conditional BER at the destination, under the assumptions of ideal interleaving and symmetrization, is evaluated by (similar to (5.1))

$$p_{b,R+1}^{\text{S-DF}}(\Theta) \le \sum_{d_h=d_f}^{N} w_I(d_h)\, f_{ub}^{\text{S-DF}}(d_h,\Theta,\boldsymbol{\alpha}) \approx w_I(d_f)\, f_{ub}^{\text{S-DF}}(d_f,\Theta,\boldsymbol{\alpha}) \quad , \tag{5.14}$$

where the second line is obtained because the error events with the smallest Hamming weight will dominate the BER performance at high SNRs. The union bound of PEP, $f_{ub}^{\text{S-DF}}(d_f,\Theta,\boldsymbol{\alpha})$, is given by

$$f_{ub}^{\text{S-DF}}(d_f,\Theta,\boldsymbol{\alpha}) = \frac{1}{2\pi \boldsymbol{j}}\int_{s_0-\boldsymbol{j}\infty}^{s_0+\boldsymbol{j}\infty}\left[\frac{1}{l2^l}\sum_{i=1}^{l}\sum_{b=0}^{1}\sum_{x\in\chi_b^i}\sum_{z\in\chi_b^i}\prod_{j=0}^{R}\Phi_{\Delta_{\tilde{h}_{j,R+1}}(x,z)}(s)\right]^{d_f}\frac{ds}{s}, \tag{5.15}$$

where $\Phi_{\Delta_{\tilde{h}_{j,R+1}}(x,z)}(s)$ was defined in (5.4) with different $\tilde{h}_{j,R+1}$ and $\tilde{N}_0^{(j)}$ corresponding to the actual mode, e.g., S-DF/RT, S-DF/Idle or S-DF/AF, is adopted..

After replacing the saddle point $s = 0.5+\boldsymbol{j}t$ into (5.15) and the approximation with MSED, we have

$$f_{ub}^{\text{S-DF}}(d_f,\Theta,\boldsymbol{\alpha}) \approx \frac{N_\chi^{d_f}}{4\pi}\int_{-\infty}^{\infty}\exp\left[-\left(t^2+\frac{1}{4}\right)\frac{d_f P_T D_\chi}{N_0} M_\Theta(\boldsymbol{\alpha})\right]\frac{dt}{t^2+\frac{1}{4}}, \tag{5.16}$$

where

$$M_\Theta(\boldsymbol{\alpha}) = N_0\sum_{j=0}^{R}\frac{\alpha_j\left|\tilde{h}_{j,R+1}\right|^2}{\tilde{N}_0^{(j)}}. \tag{5.17}$$

Note that for S-DF/Idle, the summation $\sum_{j=0}^{R}(\cdot)$ is replaced by $\sum_{\tilde{j}}(\cdot)$. Following the same steps from (5.6) to (5.10), the conditional BER at the destination is approximated by

$$p_{b,R+1}^{\text{S-DF}}(\Theta) \approx w_I\left(d_f\right) N_\chi^{d_f} \sqrt{\frac{N_0}{\pi d_f P_T D_\chi M_\Theta(\boldsymbol{\alpha})}} \exp\left[-\frac{d_f P_T D_\chi M_\Theta(\boldsymbol{\alpha})}{4N_0}\right]. \tag{5.18}$$

On the other hand, the BER at the relay can be approximated similarly as

$$p_{b,j} \approx w_I\left(d_f\right) N_\chi^{d_f} \sqrt{\frac{N_0}{\pi d_f P_T D_\chi \alpha_0 \left|h_{0,j}\right|^2}} \exp\left[-\frac{d_f P_T}{4N_0} D_\chi \alpha_0 \left|h_{0,j}\right|^2\right]. \tag{5.19}$$

Note that $M_\Theta(\boldsymbol{\alpha})$ is replaced by $\alpha_0\left|h_{0,j}\right|^2$ in (5.19), because the decoding at relay depends on only the source transmit power and the S-R channel.

Bringing (5.18) and (5.19) into (5.13) leads to an approximation of $p_{b,R+1}$ as

$$p_{b,R+1} \approx w_I\left(d_f\right) N_\chi^{d_f} G(\boldsymbol{\alpha}), \tag{5.20}$$

where

$$G(\boldsymbol{\alpha}) = \sum_{\Theta \subset \{1,2,\ldots R\}} g_\Theta \prod_{j \notin \Theta} K W_I\left(d_f\right) N_\chi^{d_f} g_j, \tag{5.21}$$

$$g_\Theta = \sqrt{\frac{N_0}{\pi d_f P_T D_\chi M_\Theta(\boldsymbol{\alpha})}} \exp\left[-\frac{d_f P_T D_\chi}{4N_0} M_\Theta(\boldsymbol{\alpha})\right], \tag{5.22}$$

and

$$g_j = \sqrt{\frac{N_0}{\pi d_f P_T D_\chi \alpha_0 \left|h_{0,j}\right|^2}} \exp\left[-\frac{d_f P_T D_\chi}{4N_0} \alpha_0 \left|h_{0,j}\right|^2\right]. \tag{5.23}$$

Now, the first power allocation method for S-DF, called PA-ABER is introduced as

$$\boldsymbol{\alpha}^* = \arg\min_{\boldsymbol{\alpha}} G(\boldsymbol{\alpha}),\ \text{s.t.}\ \mathbf{1}^T\boldsymbol{\alpha} \le 1,\ 0 \le \alpha_j \le 1,\ j = 0,1,\cdots,R, \tag{5.24}$$

where $\mathbf{1}$ is the all-one vector of dimension $R+1$. In the following, the specific optimization methods for different modes are provided.

S-DF/RT and S-DF/Idle

For convenience, we focus on the power allocation for S-DF/RT, while that for S-DF/Idle can be straightforwardly obtained through degeneration. To solve the problem in (5.24), $G(\boldsymbol{\alpha})$ is shown to be a convex function of $\boldsymbol{\alpha}$ in Appendix D. Therefore, some existing algorithms can be applied to solve the optimization problem in (5.24), e.g., the Gradient descent method. The numerical results will be given in Section 5.4.

S-DF/AF

For S-DF/AF, the cost function $G(\boldsymbol{\alpha})$ in (5.24) is also convex. This can be proved by following the same steps of proof in Appendix D. The main difference is that in S-DF/AF, $M_{\Theta}(\boldsymbol{\alpha})$ is not a linear functions of $\boldsymbol{\alpha}$. Actually, it is

$$M_{\Theta}(\boldsymbol{\alpha}) = \sum_{j\in\Theta} \alpha_j \left|\tilde{h}_{j,R+1}\right|^2 + \sum_{j\notin\Theta} \frac{\alpha_j \left|h_{j,R+1}\right|^2 \left|h_{0,j}\right|^2 \alpha_0}{\left|h_{j,R+1}\right|^2 \alpha_j + \alpha_0 \left|h_{0,j}\right|^2 + N_0/P_T}. \tag{5.25}$$

In (5.25), source and relays with correct decoding contribute in the first summation, while those with incorrect decoding contribute to the second one. In S-DF/AF, the term $M_{\Theta}(\boldsymbol{\alpha})$ is still concave because the first summation is linear and the second is the sum of concave functions, as proved in Appendix C. Therefore, the cost function for S-DF/AF is still convex.

In summary, for all 3 S-DF relaying schemes, the cost function $G(\boldsymbol{\alpha})$ are all convex and can be optimized with existing algorithms.

5.2.2 PA-MGEC

In PA-ABER, $G(\boldsymbol{\alpha})$ needs to be evaluated repeatedly when the gradient decent method is carried out, and there are total of 2^R Θ's (each has different $g_\Theta \prod_{j\notin\Theta} KW_I(d_f) N_\chi^{d_f} g_j$) needed to be included in the evaluation of $G(\boldsymbol{\alpha})$ in (5.21). As a consequence, it can be quite complex in some cases. In this subsection, an alternative method is proposed to further reduce the complexity of power allocation. The performance and complexity of the two methods will be compared in Section 5.4 for some examples.

The first idea is that instead of minimizing $G(\boldsymbol{\alpha})$ in (5.21), an $\boldsymbol{\alpha}$ is searched to minimize $\max_{\Theta\subset\{1,2,\ldots R\}} g_\Theta \prod_{j\notin\Theta} KW_I(d_f) N_\chi^{d_f} g_j$, the largest term in the summation of (5.21). Equivalently, an $\boldsymbol{\alpha}$ is searched to minimize

$$\max_{\Theta\subset\{1,2,\ldots R\}} \left\{\ln A_\Theta(\boldsymbol{\alpha}) + \ln B_\Theta(\boldsymbol{\alpha})\right\}, \tag{5.26}$$

where

$$\ln A_\Theta(\boldsymbol{\alpha}) = -\frac{1}{2}\ln\left[M_\Theta(\boldsymbol{\alpha})\prod_{j\notin\Theta}\alpha_0\left|h_{0,j}\right|^2 D_\chi\right], \tag{5.27}$$

and

$$\ln B_\Theta(\boldsymbol{\alpha}) = \ln\left(KW_I(d_f)N_\chi^{d_f}\sqrt{\frac{N_0}{\pi d_f P_T D_\chi}}\right)^{R-|\Theta|} - \frac{d_f P_T D_\chi}{4N_0}\left(M_\Theta(\boldsymbol{\alpha}) + \alpha_0\sum_{j\notin\Theta}\left|h_{0,j}\right|^2\right). \tag{5.28}$$

The term $|\Theta|$ denotes the cardinality of the set Θ. Note that (i) $\ln A_\Theta(\boldsymbol{\alpha})$ does not change with P_T/N_0, (ii) $\left|\ln B_\Theta(\boldsymbol{\alpha})\right| \to \infty$ as $P_T/N_0 \to \infty$, and (iii) $\left|\ln A_\Theta(\boldsymbol{\alpha})\right| \to \infty$ as $\alpha_0 \to 0$ for $|\Theta| < R$. Using a very small α_0, however, is impractical because the source power will be too small to activate any relay in this case. Therefore, in practical systems, $\ln A_\Theta(\boldsymbol{\alpha}) + \ln B_\Theta(\boldsymbol{\alpha})$ is dominated by $\ln B_\Theta(\boldsymbol{\alpha})$ at high SNRs, and it can be employed in search for good $\boldsymbol{\alpha}$ with a reduced com-

plexity.

Now, the optimization problem for PA-MGEC is cast as follows.

$$\begin{aligned}\boldsymbol{\alpha}^{*} &= \arg\min_{\boldsymbol{\alpha}} \max_{\Theta\subset\{1,2,\ldots R\}} \ln B_{\Theta}(\boldsymbol{\alpha}) \\ &= \arg\max_{\boldsymbol{\alpha}} \min_{\Theta\subset\{1,2,\ldots R\}} \left\{ M_{\Theta}(\boldsymbol{\alpha}) + \alpha_0 \sum_{j\notin\Theta} \left|h_{0,j}\right|^2 - \eta_{R-|\Theta|} \right\},\end{aligned} \tag{5.29}$$

where

$$\eta_{R-|\Theta|} = \frac{4N_0}{d_f P_T D_{\chi}} \ln\left(KW_I(d_f) N_{\chi}^{d_f} \sqrt{\frac{N_0}{\pi d_f P_T D_{\chi}}} \right)^{R-|\Theta|}. \tag{5.30}$$

In (5.29), $M_{\Theta}(\boldsymbol{\alpha})$ is the equivalent channel seen by the destination, $\alpha_0 \sum_{j\notin\Theta} \left|h_{0,j}\right|^2$ accounts for the effect the S-R link of inactive relays, and $\eta_{R-|\Theta|}$, which is independent to $\boldsymbol{\alpha}$, is a term relating to the coded modulation $\left(K, d_f, W_I(d_f), N_{\chi}, D_{\chi}\right)$, the number of inactive relays $(R-|\Theta|)$ and the SNR $\left(P_T/N_0\right)$. Note that $\eta_{R-|\Theta|}$ decreases with P_T/N_0 and that $\eta_{R-|\Theta|}=0$ when $P_T/N_0 \to \infty$ or $|\Theta| = R$.

S-DF/RT and S-DF/Idle

For S-DF/RT (which can be degenerated to S-DF/Idle straightforwardly), bringing $M_{\Theta}(\boldsymbol{\alpha})$ in (5.17) into (5.29) yields

$$\begin{aligned}&M_{\Theta}(\boldsymbol{\alpha}) + \alpha_0 \sum_{j\notin\Theta} \left|h_{0,j}\right|^2 - \eta_{R-|\Theta|} \\ &= \sum_{j=0}^{R} \alpha_j \left|\tilde{h}_{j,R+1}\right|^2 + \alpha_0 \sum_{j\notin\Theta} \left|h_{0,j}\right|^2 - \eta_{R-|\Theta|} \sum_{j=0}^{R} \alpha_j \doteq \mathbf{D}_{\Theta}^{T} \boldsymbol{\alpha}\end{aligned}, \tag{5.31}$$

where $\mathbf{D}_{\Theta} = \left[D_{\Theta}^{(0)} \; D_{\Theta}^{(1)} \; \ldots D_{\Theta}^{(R)} \right]^T$ with

$$D_{\Theta}^{(j)} = \begin{cases} \left|h_{0,R+1}\right|^2 + \sum_{j_1 \notin \Theta} \left|h_{0,j_1}\right|^2 - \eta_{R-|\Theta|}, & \text{if } j = 0 \\ \left|\tilde{h}_{j,R+1}\right|^2 - \eta_{R-|\Theta|}, & \text{if } j \in \Theta \\ -\eta_{R-|\Theta|}, & \text{otherwise} \end{cases} . \quad (5.32)$$

Note that $\mathbf{D}_{\Theta}^{T}\boldsymbol{\alpha}$ is a linear combination of elements in $\boldsymbol{\alpha}$. Substituting (5.31) into (5.29) yields

$$\begin{aligned} &\arg\max_{\boldsymbol{\alpha}} \min_{\Theta \subseteq \{1,2,\ldots R\}} \mathbf{D}_{\Theta}^{T}\boldsymbol{\alpha} \\ &\text{s.t.} \quad \mathbf{1}^T\boldsymbol{\alpha} \le 1, \\ &\quad 0 \le \alpha_j \le 1,\ j = 0,1,\cdots,R \end{aligned} . \quad (5.33)$$

To solve (5.33), recast it as

$$\begin{aligned} &\underset{\boldsymbol{\alpha},\,\beta}{\text{maximize}} \quad \beta \\ &\text{s.t.} \quad \beta \le \mathbf{D}_{\Theta}^{T}\boldsymbol{\alpha},\ \ \Theta \subseteq \{1,2,\ldots R\} \\ &\quad \mathbf{1}^T\boldsymbol{\alpha} \le 1, \text{ and } 0 \le \alpha_j \le 1,\ j = 0,1,\cdots,R \end{aligned} . \quad (5.34)$$

Since the objective function and all the constraints are linear, (5.34) is a linear programming problem (though not in a standard form) and can be solved efficiently with the Simplex method [81].

S-DF/AF

For S-DF/AF, PA-MGEC is slightly more complicated than that in S-DF/RT. Firstly, bring $M_{\Theta}(\boldsymbol{\alpha})$ in (5.25) into (5.29) leads to

$$\begin{aligned} &M_{\Theta}(\boldsymbol{\alpha}) + \alpha_0 \sum_{j \notin \Theta} \left|h_{0,j}\right|^2 - \eta_{R-|\Theta|} \\ &= \sum_{j \in \tilde{\Theta}} \alpha_j \left|h_{j,R+1}\right|^2 + \sum_{j \notin \tilde{\Theta}} \left[\frac{\alpha_0 \left|h_{0,j}\right|^2 \alpha_j \left|h_{j,R+1}\right|^2}{\alpha_0 \left|h_{0,j}\right|^2 + \alpha_j \left|h_{j,R+1}\right|^2 + N_0/P_T} + \alpha_0 \left|h_{0,j}\right|^2 \right] - \eta_{R-|\Theta|} \end{aligned} . \quad (5.35)$$

Eq. (5.35) is evidently not a linear function of $\boldsymbol{\alpha}$. Fortunately, (5.35) is concave because the first term is linear and the second term is concave as proved in Appendix C. Now bringing (5.35) back to the optimization problem in (5.29) yields

$$\boldsymbol{\alpha}^{*}=\arg\max_{\boldsymbol{\alpha}}\min_{\Theta\subset\{1,2,\ldots R\}}\left\{\sum_{j\in\tilde{\Theta}}\alpha_j\left|h_{j,R+1}\right|^2+\sum_{j\notin\tilde{\Theta}}\left[\frac{\alpha_0\left|h_{0,j}\right|^2\alpha_j\left|h_{j,R+1}\right|^2}{\alpha_0\left|h_{0,j}\right|^2+\alpha_j\left|h_{j,R+1}\right|^2+N_0/P_T}+\alpha_0\left|h_{0,j}\right|^2\right]-\eta_{R-|\Theta|}\right\} \quad (5.36)$$

s.t. $\mathbf{1}^T\boldsymbol{\alpha}\le 1,\ 0\le\alpha_j\le 1,\ j=0,1,\cdots,R$

Since the minimum of concave functions is also concave [80], the problem in (5.36) is a convex optimization problem. Due to the fact that (5.36) could be non-differentiable, sub-gradient method [83] is employed to find the optimum.

5.3 Power Allocation Examples

This section provides examples of how power is allocated for AF with PA-EC and those for S-DF with PA-MGEC. Consider a simple 3-node network with only 1 relay and the channel gains $\left|h_{0,2}\right|^2=\left|h_{0,2}^{(1)}\right|^2=1$, $\left|h_{0,1}\right|^2=4$, $\left|h_{1,2}\right|^2=10$ (cf. Network-9 in Table IV). We use a half-rate convolutional codes CC(171,133) with $d_f=10$ and $W_I\left(d_f\right)=33$. The length of the information sequence is $K=506$ such that the length of the coded sequence is $N=1024$. Gray-mapped 16-QAM is used with $N_\chi=0.75$. Note that the total transmit power is calculated as $P_T=E_b\cdot R_C\cdot l$ where E_b is the bit energy, and $R_C=0.5$ is the channel code rate.

Table IV. Network setups used in Chapter 5

Networks	S-D link	S-R link	R-D link
Network-9	$\left\|h_{0,2}\right\|^2=\left\|h_{0,2}^{(1)}\right\|^2=1$	$\left\|h_{0,1}\right\|^2=4$	$\left\|h_{1,2}\right\|^2=10$
Network-10	$\left\|h_{0,3}\right\|^2=\left\|h_{0,3}^{(1)}\right\|^2=\left\|h_{0,3}^{(2)}\right\|^2=1$	$\left\|h_{0,1}\right\|^2=4,$ $\left\|h_{0,2}\right\|^2=2$	$\left\|h_{1,3}\right\|^2=10,$ $\left\|h_{2,3}\right\|^2=5$
Network-11	$\left\|h_{0,3}\right\|^2=\left\|h_{0,3}^{(1)}\right\|^2=\left\|h_{0,3}^{(2)}\right\|^2=1$	$\left\|h_{0,1}\right\|^2=4,$ $\left\|h_{0,2}\right\|^2=8$	$\left\|h_{1,3}\right\|^2=10,$ $\left\|h_{2,3}\right\|^2=5$
Network-12	$\left\|h_{0,4}\right\|^2=\left\|h_{0,4}^{(1)}\right\|^2=\left\|h_{0,4}^{(2)}\right\|^2=\left\|h_{0,4}^{(3)}\right\|^2=1$	$\left\|h_{0,1}\right\|^2=4,$ $\left\|h_{0,2}\right\|^2=8$ $\left\|h_{0,3}\right\|^2=2$	$\left\|h_{1,4}\right\|^2=10,$ $\left\|h_{2,4}\right\|^2=5$ $\left\|h_{3,4}\right\|^2=5$
Network-13	$\left\|h_{0,2}\right\|^2=1$	$\left\|h_{0,1}\right\|^2=10$	$\left\|h_{1,2}\right\|^2=5$

5.3.1 PA-EC on AF

In this example, the cost function $M_{AF}(\boldsymbol{\alpha})$ in (5.7) becomes

$$M_{AF}(\alpha_0)=\alpha_0\left|h_{0,2}\right|^2+\frac{\alpha_1\left|h_{1,2}\right|^2\left|h_{0,1}\right|^2\alpha_0}{\left|h_{1,2}\right|^2\alpha_1+\alpha_0\left|h_{0,1}\right|^2+N_0/P_T}. \qquad (5.37)$$
$$=\alpha_0+\frac{40\alpha_0(1-\alpha_0)}{10(1-\alpha_0)+\alpha_0 4+N_0/P_T}$$

The curves of $M_{AF}(\alpha_0)$ with different values of N_0/P_T are plotted in Fig. 5.1. As is observed, when SNR is very low, e.g., $E_b/N_0=-\infty$, The curve becomes an almost straight line with slope $\left|h_{0,2}\right|^2=1$. This is due to the fact that large N_0/P_T diminishes the effect of the second term at the

right hand side of (5.37), so that (5.37) can be approximated as $M_{AF}(\alpha_0) \approx \alpha_0 |h_{0,2}|^2$. In this case, the optimum (highest) point locates at $\alpha_0 = 1$, which means that all power will be allocated to the source. As the SNR increases, i.e., N_0/P_T decreases or E_b/N_0 increases, the curve bends to be concave (as proved in Appendix C), and the optimal α_0 decreases from 1 to the final point 0.68372 as $E_b/N_0 = \infty$, which means the SNR approaches infinity. In summary, when SNR is low, all power is allocated to source, as the SNR increases, the source decreases to a limit point. Note that the optimal α_0 does not always decline with SNR. In some channel realizations, the optimal α_0 may locate at 1 for all SNRs, e.g., when $|h_{1,2}|^2 \le |h_{0,2}|^2$. This case is drawn in Fig. 5.2 with $|h_{1,2}|^2 = 0.8$.

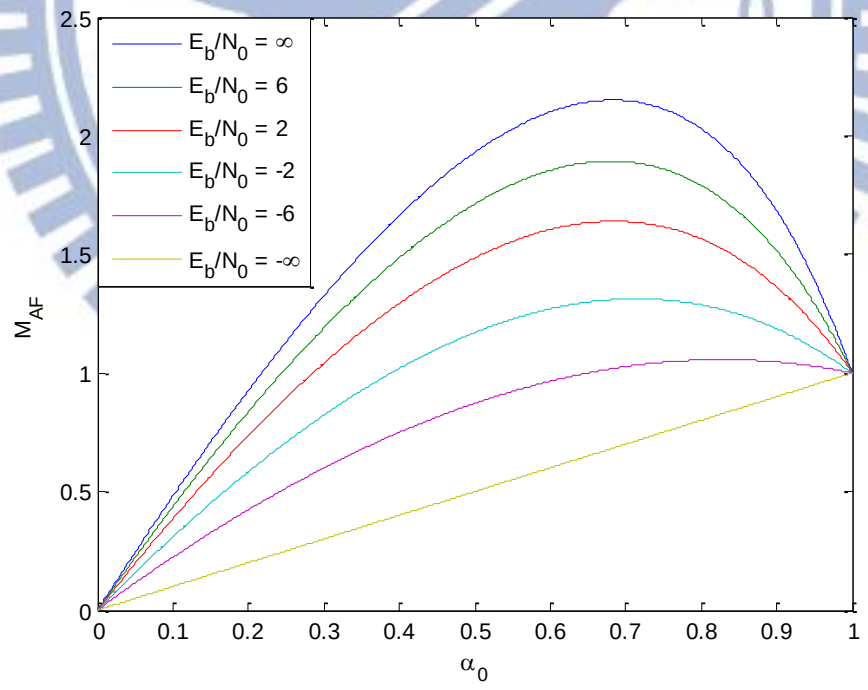

Fig. 5.1. The curves of $M_{AF}(\alpha_0)$ for Network-9 with different values of E_b/N_0.

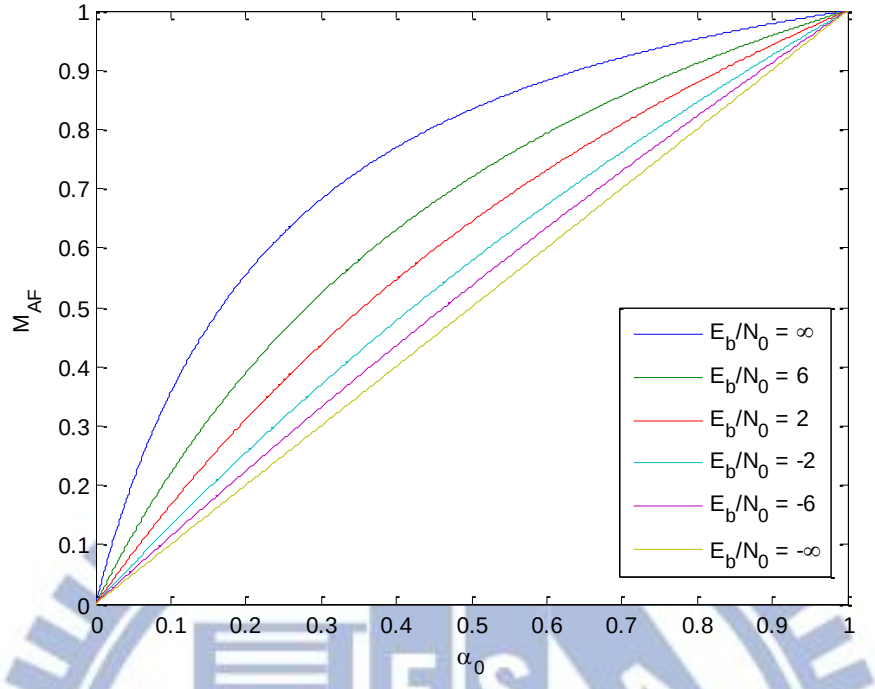

Fig. 5.2. Another example of curves of $M_{AF}(\alpha_0)$ with positive slopes for different values of E_b/N_0.

5.3.2 PA-MGEC on S-DF/RT

For S-DF/RT, $M_\Theta(\boldsymbol{\alpha})$ depends on the active relay set Θ, which could be $\varnothing$ or $\{1\}$ in this example. Specifically, (5.31) becomes

$$M_\Theta(\boldsymbol{\alpha})+\alpha_0\sum_{j\notin\Theta}\left|h_{0,j}\right|^2-\eta_1=\begin{cases}\alpha_0\left|h_{0,2}\right|^2+\alpha_1\left|h_{1,2}\right|^2, & \Theta=\{1\}\\ \alpha_0\left|h_{0,2}\right|^2+\alpha_1\left|h_{0,2}^{(1)}\right|^2+\alpha_0\left|h_{0,1}\right|^2-\eta_1, & \Theta=\varnothing\end{cases}=\begin{cases}10-9\alpha_0, & \Theta=\{1\}\\ 4\alpha_0+1-\eta_1, & \Theta=\varnothing\end{cases}. \tag{5.38}$$

According to (5.32), define

$$\begin{cases}L_1=10-9\alpha_0\\ L_0=4\alpha_0+1-\eta_1\end{cases}, \tag{5.39}$$

whose curves are plotted with different values of E_b/N_0 in Fig. 5.3. The curves of L_1 and L_0 for Network-9 with different values of E_b/N_0. (PA-MGEC on S-DF/RT).. Since $\eta_1 = 0$ when $|\Theta| = 1$, L_1 is invariant to the change of SNR. On the other hand, the curve of L_0 shifts up as SNR increases (η_1 decreases).

To determine the optimal power, according to (5.33), we need to maximize $\min\{L_1, L_0\}$. As is shown in Fig. 5.3, when the SNR is very low, e.g., $E_b/N_0 \le -1.68$ (which corresponds to $\eta_1 \ge 4$), the whole curve of L_0 is below L_1, so that $\min\{L_1, L_0\} = L_0$. Since L_0 has positive slope (in fact, L_0 always has positive slope for any channel realizations), the optimum occurs at $\alpha_0 = 1$. As the SNR increases such that $E_b/N_0 > -1.68$, these two curves begin to intersect. This intersection maximizes $\min\{L_1, L_0\}$ and is chosen as the optimal power allocation. As observed from Fig. 5.3, the optimal α_0 decreases with SNR, starting from 1 to about 0.69 when $E_b/N_0 \to \infty$ (or $\eta_1 \to 0$). In summary, somehow similar to that case of PA-EC on AF, when SNR is low, all power is allocated to source. As the SNR increases, the source power decreases to a final point. This result is intuitive because when SNR is too low, the probability of correct decoding at relay is also very low so that more power should be put on source to increase the probability of correct decoding at the relay.

Note that the optimal α_0 may be always at 1 for all SNRs if $|h_{1,2}|^2 \le |h_{0,2}^{(j)}|^2$. ($L_1$ will also have non-negative slope.) In this situation, no power is allocated on relay which attempts to transmit the packet through a link worse than the S-D link.

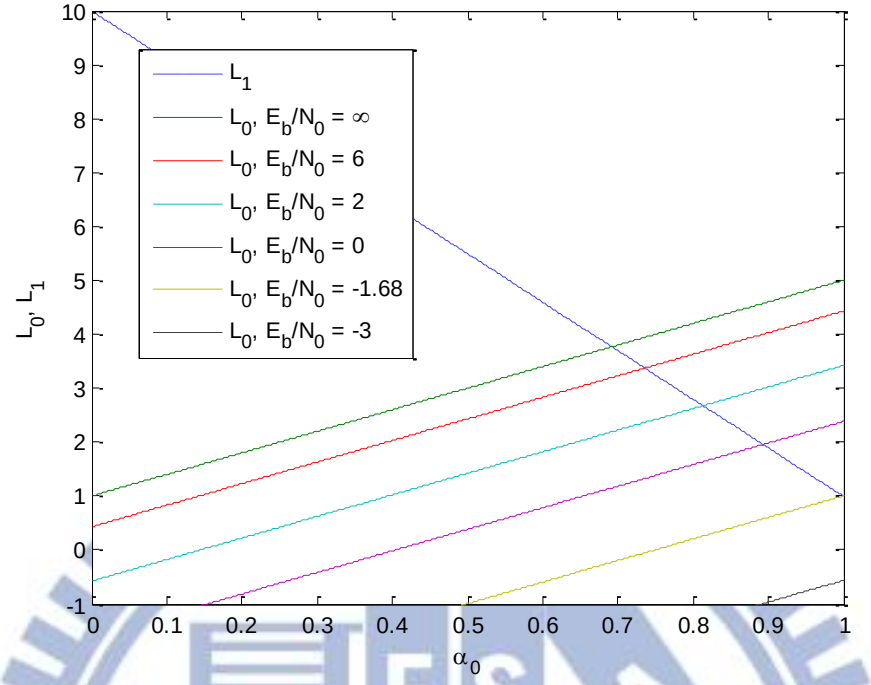

Fig. 5.3. The curves of L_1 and L_0 for Network-9 with different values of E_b/N_0. (PA-MGEC on S-DF/RT).

5.3.3 PA-MGEC on S-DF/Idle

PA-MGEC on S-DF/Idle is very similar to that on S-DF/RT. The main different is that $M_\Theta(\boldsymbol{\alpha})$ should be replaced by $\sum_{j\in\tilde{\Theta}}\alpha_j\left|h_{j,R+1}\right|^2$, which means that the orthogonal-channels of inactive relays will never contribute to $M_\Theta(\boldsymbol{\alpha})$. Specifically, (5.31) becomes

$$M_\Theta(\boldsymbol{\alpha})+\alpha_0\sum_{j\notin\Theta}\left|h_{0,j}\right|^2-\eta_1=\begin{cases}\alpha_0\left|h_{0,2}\right|^2+\alpha_1\left|h_{1,2}\right|^2, & \Theta=\{1\}\\ \alpha_0\left|h_{0,2}\right|^2+\alpha_0\left|h_{0,1}\right|^2-\eta_1, & \Theta=\varnothing\end{cases}=\begin{cases}10-9\alpha_0, & \Theta=\{1\}\\ 5\alpha_0-\eta_1, & \Theta=\varnothing\end{cases}, \tag{5.40}$$

and (5.32) as

$$\begin{cases} L_1 = 10 - 9\alpha_0 \\ L_0 = 5\alpha_0 - \eta_1 \end{cases}. \tag{5.41}$$

These curves are plotted in Fig. 5.4 with different values of E_b/N_0.

To determine the optimal power, according to (5.33), we need to maximize $\min\{L_1, L_0\}$. As is shown in Fig. 5.4, when $E_b/N_0 \le -1.68$, the optimum occurs at $\alpha_0 = 1$. As the SNR increases such that $E_b/N_0 > -1.68$, the optimal α_0 decreases with SNR, starting from 1 to about 0.715 when $E_b/N_0 \to \infty$ (or $\eta_1 \to 0$). Compared with the results for S-DF/RT, given a fixed SNR ($E_b/N_0 > -1.68$), the optimal α_0 in Fig. 5.4 is slightly greater than that in Fig. 5.3. This is due to the fact that the power allocated to the relay will be wasted if the relay fails to decode when S-DF/Idle relaying scheme is adopted. Therefore, more power (compared to S-DF/RT) should be allocated to source to avoid this power waste.

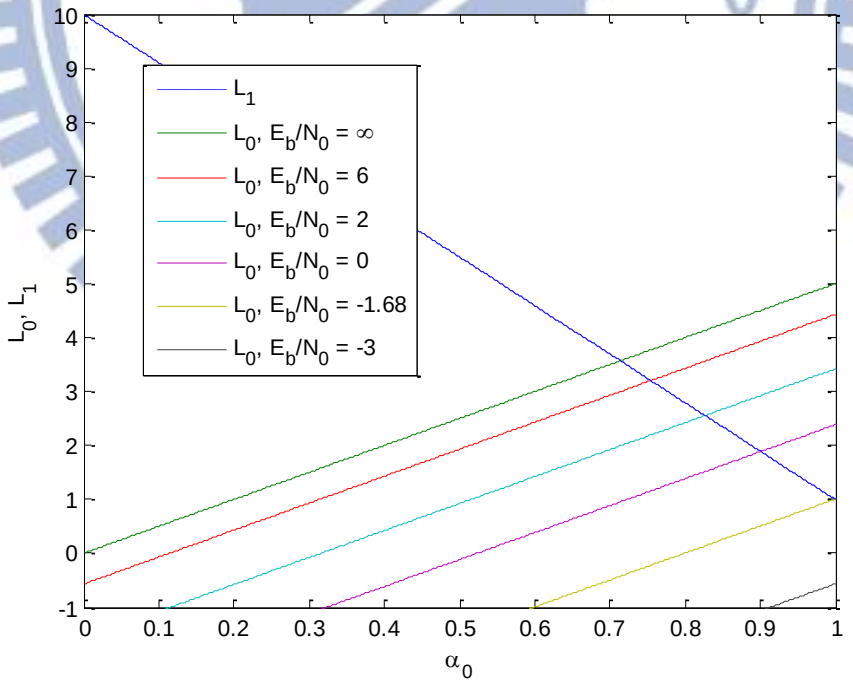

Fig. 5.4. The curves of L_1 and L_0 for Network-9 with different values of E_b/N_0. (PA-MGEC on S-DF/Idle)

5.3.4 PA-MGEC on S-DF/AF

For S-DF/AF, (5.31) becomes

$$
\begin{aligned}
& M_{\Theta}(\boldsymbol{\alpha}) + \alpha_0 \sum_{j \notin \Theta} \left| h_{0,j} \right|^2 - \eta_1 \\
&= \begin{cases} \alpha_0 \left| h_{0,2} \right|^2 + \alpha_1 \left| h_{1,2} \right|^2, & \Theta = \{1\} \\ \alpha_0 \left| h_{0,2} \right|^2 + \dfrac{\alpha_0 \left| h_{0,1} \right|^2 \alpha_1 \left| h_{1,2} \right|^2}{\alpha_1 \left| h_{1,2} \right|^2 + \alpha_0 \left| h_{0,1} \right|^2 + N_0 / P_T} + \alpha_0 \left| h_{0,1} \right|^2 - \eta_1, & \Theta = \varnothing \end{cases} \\
&= \begin{cases} 10 - 9\alpha_0, & \Theta = \{1\} \\ 5\alpha_0 + \dfrac{40\alpha_0 (1 - \alpha_0)}{10 - 6\alpha_0 + N_0 / P_T} - \eta_1, & \Theta = \varnothing \end{cases}
\end{aligned}
\tag{5.42}
$$

We have plot the two curves at the last row of (5.42), i.e.,

$$
L_1 = 10 - 9\alpha_0 \quad \text{and} \quad L_0 = 5\alpha_0 + \frac{40\alpha_0 (1 - \alpha_0)}{10 - 6\alpha_0 + N_0 / P_T} - \eta_1 \tag{5.43}
$$

with different values of E_b / N_0 in Fig. 5.5. Note that since what the relay forwards is the same for all these 3 S-DF relaying schemes, L_1 in Fig. 5.5 is no different from that for S-DF/RT and S-DF/Idle. The main difference is that the curve of L_0 now bends to be concave, though it still shifts up as SNR increases (η_1 decreases).

To determine the optimal power, according to (5.33), we need to maximize (5.36), i.e., $\min\{L_0, L_1\}$. As is shown in Fig. 5.5, when the SNR is very low, e.g., $E_b / N_0 \le -1.68$, the whole curve of L_0 is below that of L_1, so that $\min\{L_1, L_0\} = L_0$. The problem turns to optimize L_0 alone. In this case, L_0 is maximized at $\alpha_0 = 1$. (Note that the optimum could be somewhere else for different channel realizations.) As the SNR increases such that $E_b / N_0 > -1.68$, these two curves begin to intersect. This intersection is chosen as the optimal power allocation. As observed from Fig. 5.5, the optimal α_0 decreases with SNR, starting from 1 to about 0.607 when $E_b / N_0 \to \infty$ (or $\eta_1 \to 0$).

Not surprisingly, when SNR is low, all power is allocated to source. As the SNR increases, the source power decreases to a final point. This final point $\alpha_0 = 0.607$ is even lower than that

for S-DF/RT or S-DF/Idle. This is because, in Network-9, the relay uses AF can provide a better equivalent channel than re-transmission through the S-D link. Therefore, more power is allocated to the relay.

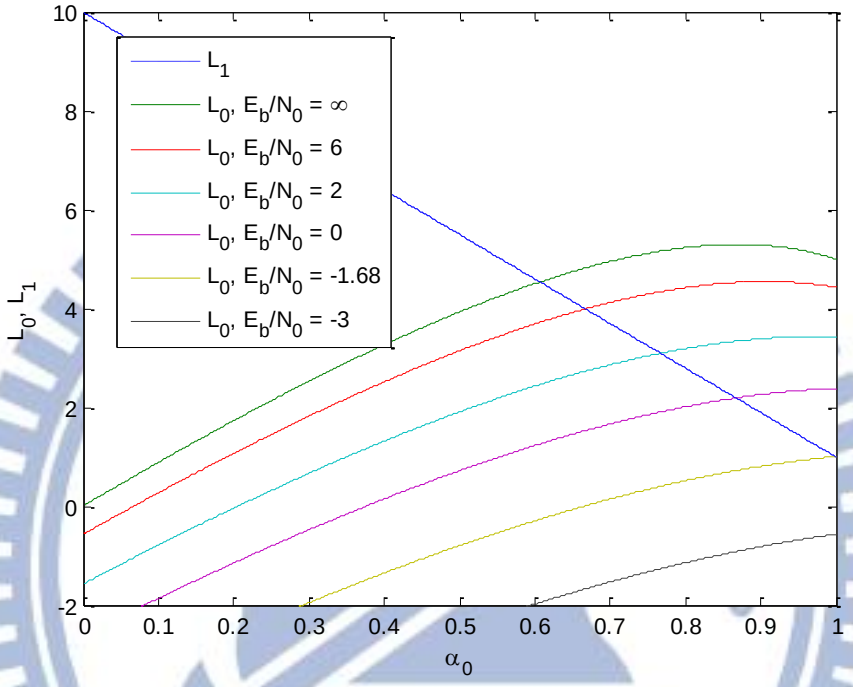

Fig. 5.5. The curves of L_0 and L_1 for Network-9 with different values of E_b/N_0. (PA-MGEC on S-DF/AF)

5.4 Numerical Results

This section verifies the proposed methods (PA-EC, PA-ABER and PA-MGEC) through BER simulation and compares them with the equal gain power allocation (PA-EG). In all the following numerical results, we use a half-rate convolutional codes with generator matrix $\left(1+D+D^2+D^3+D^6, 1+D^2+D^3+D^5+D^6\right)$, $d_f = 10$ and $W_I\left(d_f\right) = 33$. The length of the information sequence is $K = 506$ such that the length of the coded sequence is $N = 1024$.

Gray-mapped 16-QAM is used with $N_\chi = 0.75$. Note that the total transmit power is calculated as $P_T = E_b \cdot R_C \cdot l$ where E_b is the bit energy, and $R_C = 0.5$ is the channel code rate.

As first, the power allocation and simulation results for examples in Section 5.3 with Network-9 are provided. For PA-EC on the AF relaying scheme, the optimal α_0 is plotted in Fig. 5.6 ($\alpha_1 = 1 - \alpha_0$) as well as that for PA-EG, which always give half power to source and half to relay. As was predicted in Section 5.3.1, when at low SNRs, e.g., $E_b/N_0 \le -9$, PA-EC allocates all power to source. As the SNR increases, the source power declines and finally converges to about $\alpha_0 = 0.68$. In fact α_0 begin to be very close to 0.68 after $E_b/N_0 \ge 2$. The corresponding BER is given in Fig. 5.7, wherein PA-EC outperforms PA-EG with about 0.5 dB gain at BER of 10^{-5}.

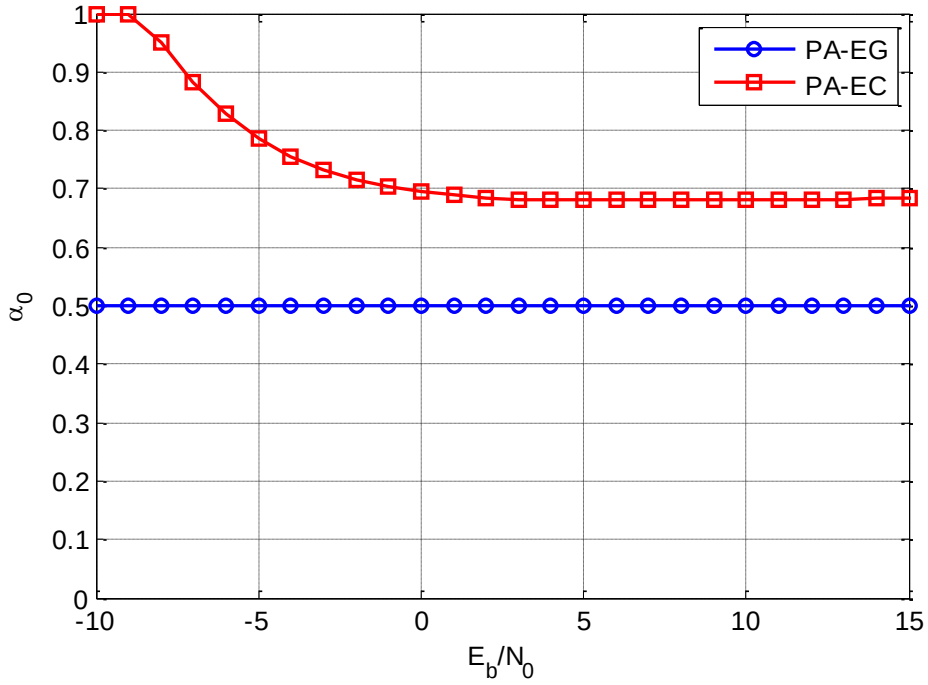

Fig. 5.6. Power allocation results for PA-EG and PA-EC on Network-9 with AF relaying scheme.

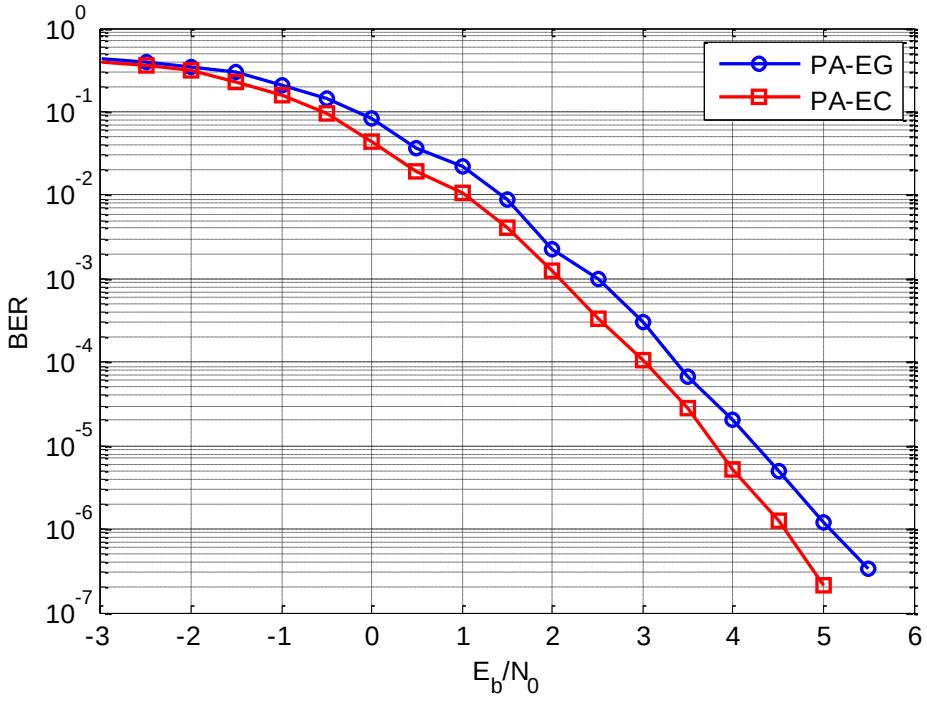

Fig. 5.7. BER simulation results for PA-EG and PA-EC on Network-9 with AF relaying scheme.

For S-DF/RT relaying scheme, the optimal α_0's for both PA-ABER and PA-MGEC are plotted in Fig. 5.8 as well as that for PA-EG. As was predicted in Section 5.3.2, when at low SNRs, e.g., $E_b/N_0 \le -2$, PA-MGEC allocates all power to source, and PA-ABER does when $E_b/N_0 \le -1$. As the SNR increases, the source power of both methods decline and finally converge to about $\alpha_0 = 0.69$, as $E_b/N_0 \ge 16$. Generally, PA-ABER tends to allocate less power to source, but, however, the difference is not large. The corresponding BER is given in Fig. 5.9, wherein PA-ABER and PA-MGEC outperform PA-EG with about 1.2 dB gain at BER of 10^{-5}. PA-ABER is slightly better than PA-MGEC at low-to-moderate SNRs. (Note that PA-ABER has higher computation complexity than PA-MGEC.) At high SNRs, they perform almost the same.

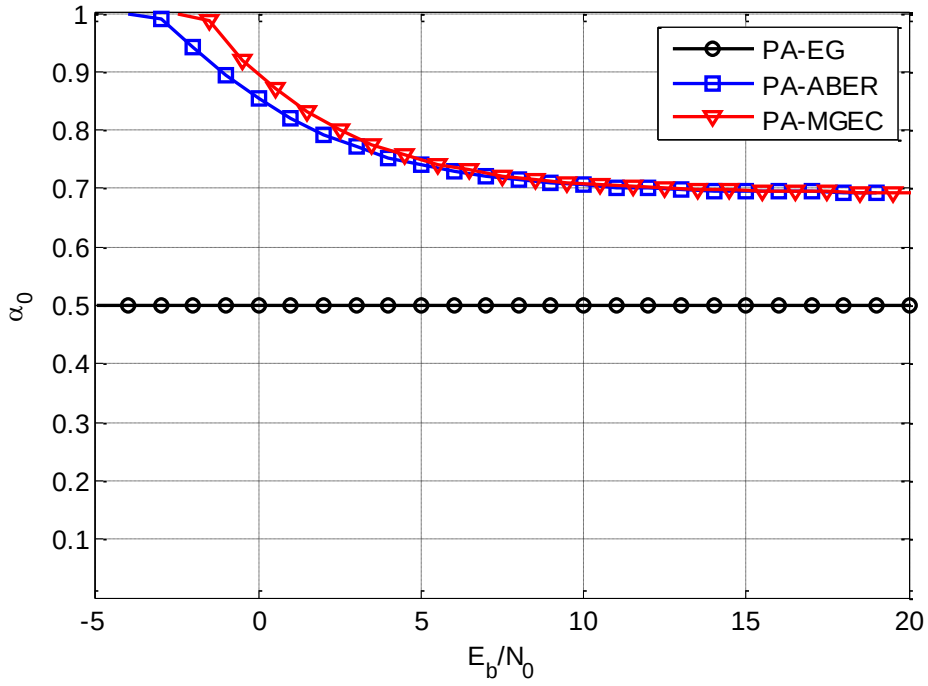

Fig. 5.8. Power allocation results for PA-EG, PA-ABER and PA-MGEC on Network-9 with S-DF/RT relaying scheme.

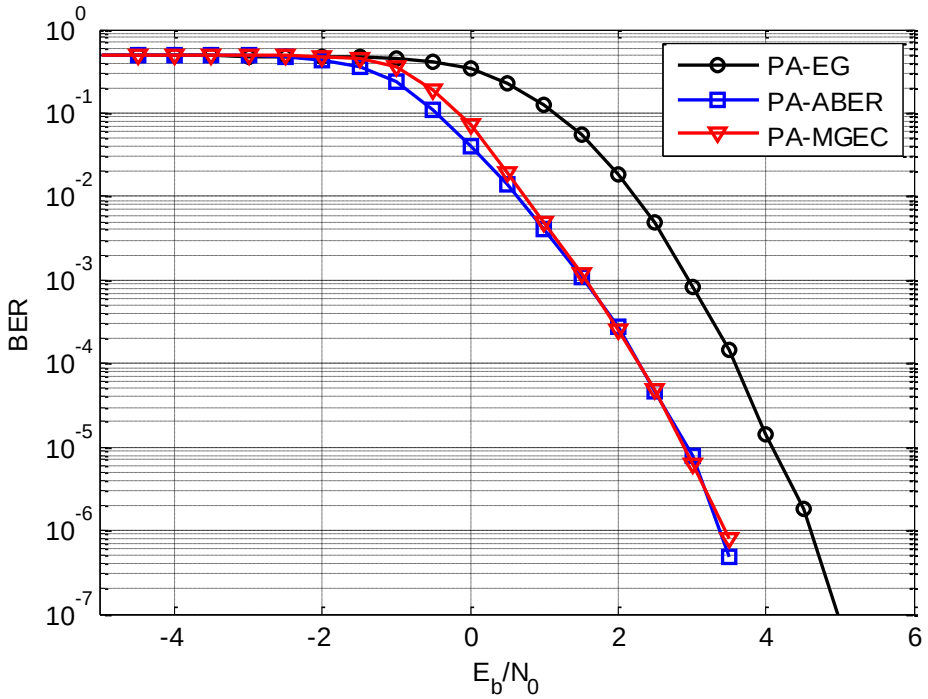

Fig. 5.9. BER simulation results for PA-EG, PA-ABER and PA-MGEC on Network-9 with S-DF/RT relaying scheme.

For S-DF/Idle relaying scheme, the optimal α_0's for both PA-ABER and PA-MGEC are plotted in Fig. 5.10 as well as that for PA-EG. As was predicted in Section 5.3.3, when $E_b/N_0 \le -2$, PA-MGEC allocates all power to source, and so does PA-ABER. As the SNR increases, the source power of both methods decline and finally converge to about $\alpha_0 = 0.715$, as $E_b/N_0 \ge 16$. Similarly, PA-ABER tends to allocate slightly less power to source than PA-MGEC. Compared with Fig. 5.8 for S-DF/RT, the α_0's in Fig. 5.10 are higher than those in Fig. 5.8 for all $E_b/N_0 > -2$. This is because, in S-DF/Idle, power allocated to relay will be wasted if the relay cannot decode correctly. Thus, power allocation tends to be more conservative and put more power on source. The corresponding BER is given in Fig. 5.11, wherein PA-ABER slightly outperforms PA-MGEC. This is intuitive because their power allocation results are rather close. Both the proposed method significantly outperform PA-EG with about 2 dB gain at BER of 10^{-5}, which is larger than the gain for S-DF/RT.

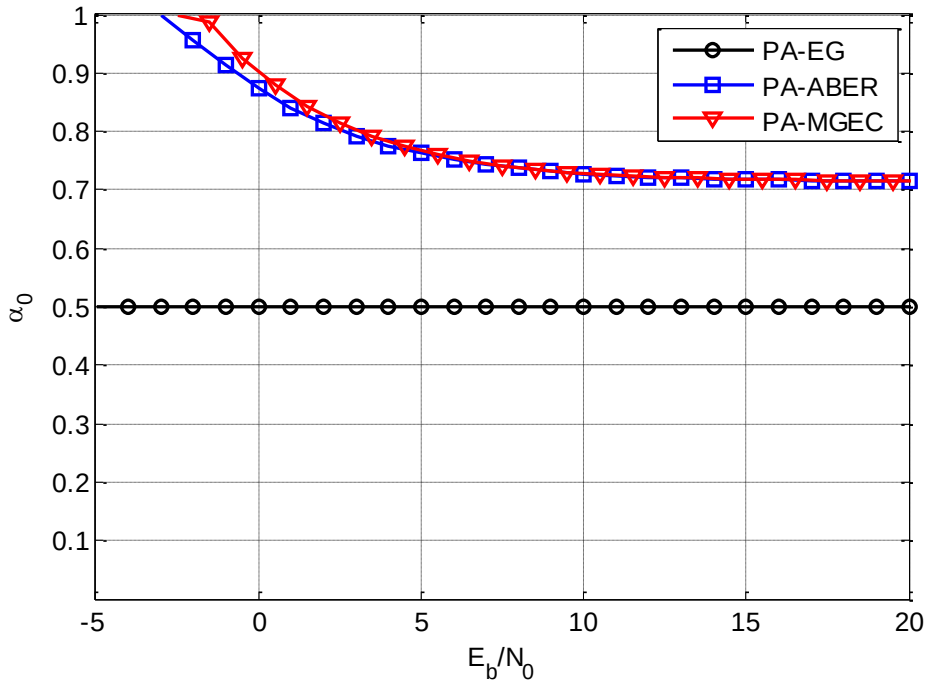

Fig. 5.10. Power allocation results for PA-EG, PA-ABER and PA-MGEC on Network-9 with S-DF/Idle relaying scheme.

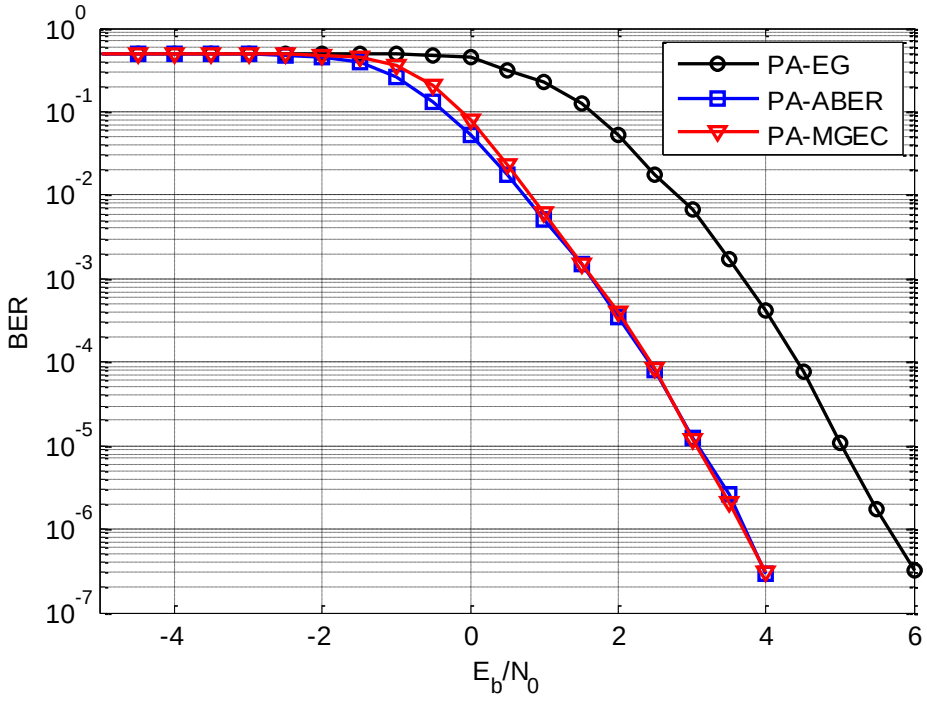

Fig. 5.11. BER simulation results for PA-EG, PA-ABER and PA-MGEC on Network-9 with S-DF/Idle relaying scheme.

For S-DF/AF relaying scheme, the power allocation results are plotted in Fig. 5.12. As was predicted in Section 5.3.4, when $E_b/N_0 \le -2$, both method allocate all power to source. As the SNR increases, the source power declines and finally converge to about $\alpha_0 = 0.607$, as $E_b/N_0 \ge 16$. PA-ABER tends to allocate slightly less power to source than PA-MGEC. Compared with S-DF/RT and S-DF/Idle, the α_0's in Fig. 5.12 are lower than those in Fig. 5.8 and Fig. 5.10. This is because S-DF/AF is less sensitive to decoding failure at relay. Thus, power allocation tends to put more power on relay for transmitting the packet through the R-D link, which is better than the S-D link. The corresponding BER is given in Fig. 5.13, wherein PA-ABER outperforms PA-MGEC with 0.2 dB at BER of 10^{-5} and outperforms PA-EG with about 1.2 dB gain at BER of 10^{-5}.

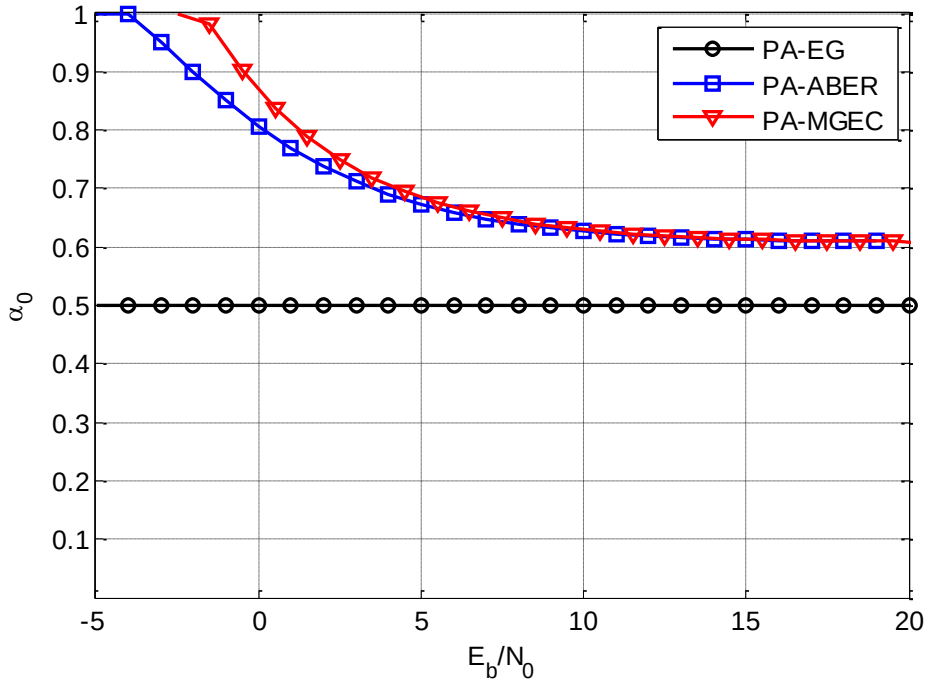

Fig. 5.12. Power allocation results for PA-EG, PA-ABER and PA-MGEC on Network-9 with S-DF/AF relaying scheme.

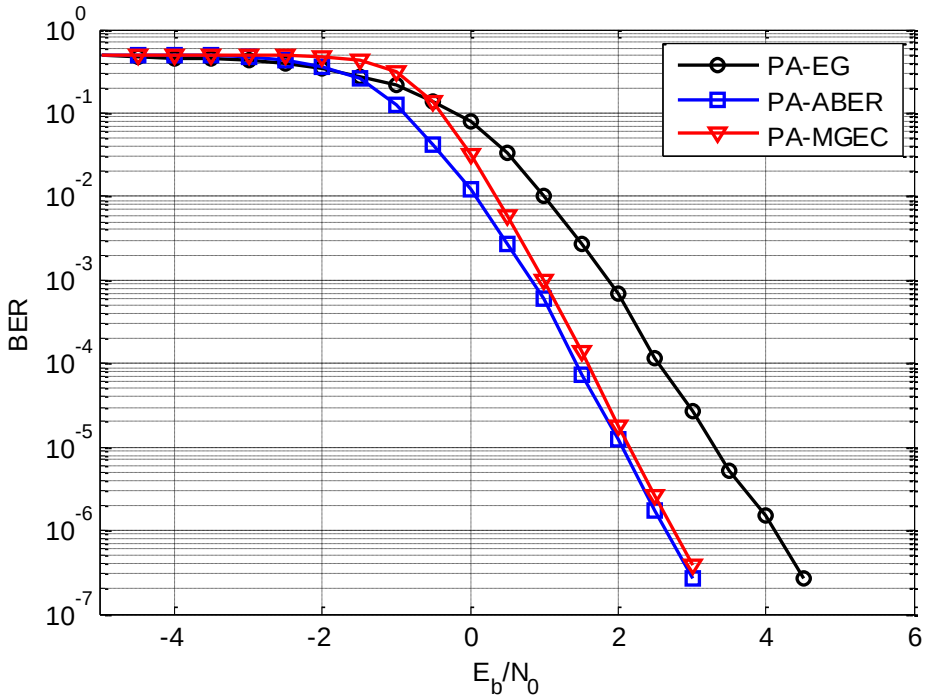

Fig. 5.13. BER simulation results for PA-EG, PA-ABER and PA-MGEC on Network-9 with S-DF/AF relaying scheme.

Numerical results for 2 relays are also provided by considering Network-10 in Table IV, where relay 1 has the same S-R and R-D link is those in Network-9, but relay 2 has worse S-R link and worse R-D link than relay 1. For AF relaying scheme, there is no decoding issue. The power allocation result for PA-EC (which allocates $\alpha_0 = \alpha_1 = \alpha_2 = 0.333$) and PA-EG are plotted in Fig. 5.14 and the corresponding BER performance in Fig. 5.15. As is observed, at low E_b/N_0, all power is allocated to source. After $E_b/N_0 \geq -8$, α_1 becomes non-zero, though the difference on BER performance between PAEC and PA-EG is trivial before $E_b/N_0 \leq -2$. PA-EC starts to allocate power to relay 2 when $E_b/N_0 \geq 4$. A gain of 1 dB is observed at BER of 10^{-5} for PA-EC over PA-EG.

For S-DF schemes, it is reasonable to predict that relay 1 is more likely to achieve correct decoding than relay 2. Therefore, we might start to allocate non-zero power to relay 1 at the SNR smaller than that for relay 2. Similar results are observed for S-DF/RT on Network-10.The power allocation results are provided in Fig. 5.16 and the corresponding BER performance in Fig. 5.17. In spite of the observations mentioned in AF, in Fig. 5.16, the results of the two power allocation methods are quite similar, which leads to that, as is shown in Fig. 5.17, PA-ABER and PA-MGEC perform almost the same. They both have a more than 2 dB gain over PA-EG. Such a gain becomes more significant for S-DF/Idle, whose corresponding results are provided in Fig. 5.18 and Fig. 5.19 for the power allocation and BER performance, respectively. In Fig. 5.19, an about 3.4 dB gain achieved for both methods over PA-EG. This is because, as mentioned before, our proposed power allocations tend to allocate more power to source (compared to PA-EG) so as to increases the probability of correct decoding at relay and to avoid power waste due to inactive relays. The results for S-DF/AF are provided in Fig. 5.20 and Fig. 5.21. Although PA-EG benefits significantly from S-DF/AF over S-DF/Idle because the relays now always use their power on forwarding, our proposed method still provide an almost 2 dB gain over PA-EG.

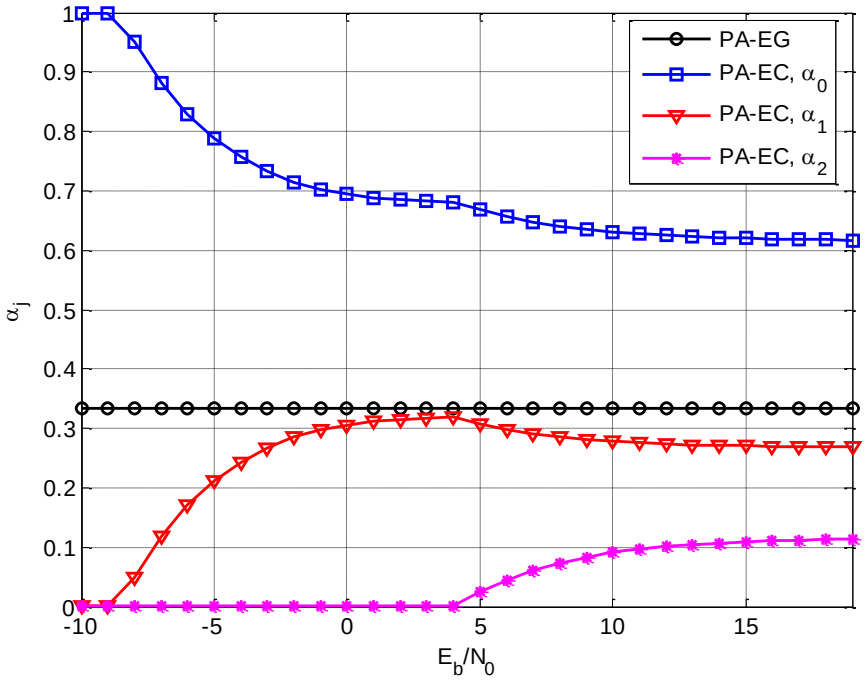

Fig. 5.14. Power allocation results for PA-EG and PA-EC on Network-10 with AF relaying scheme.

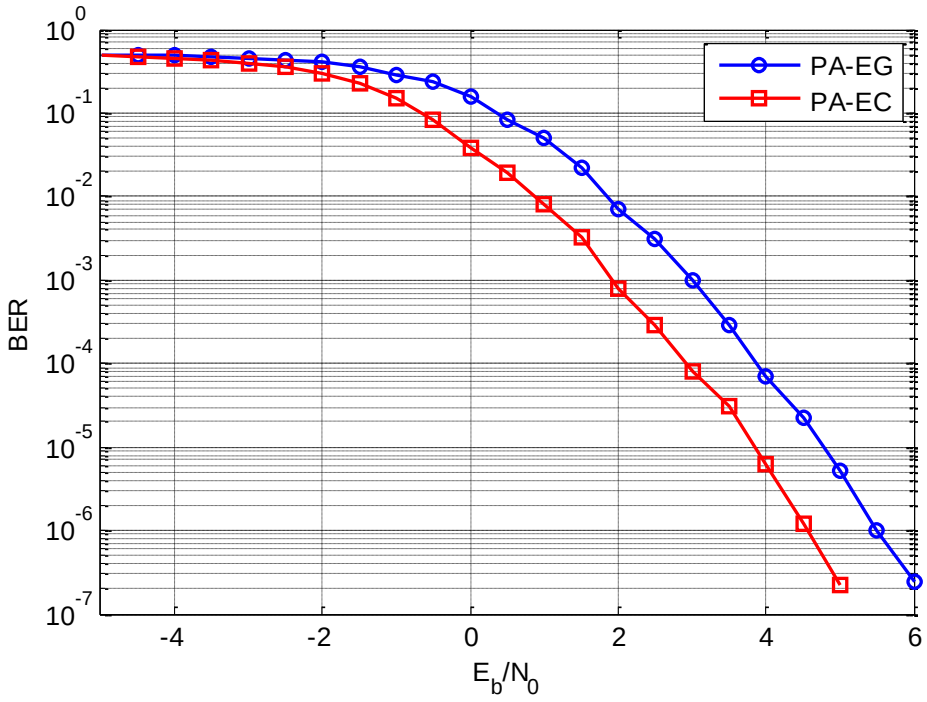

Fig. 5.15. BER simulation results for PA-EG and PA-EC on Network-10 with AF relaying scheme.

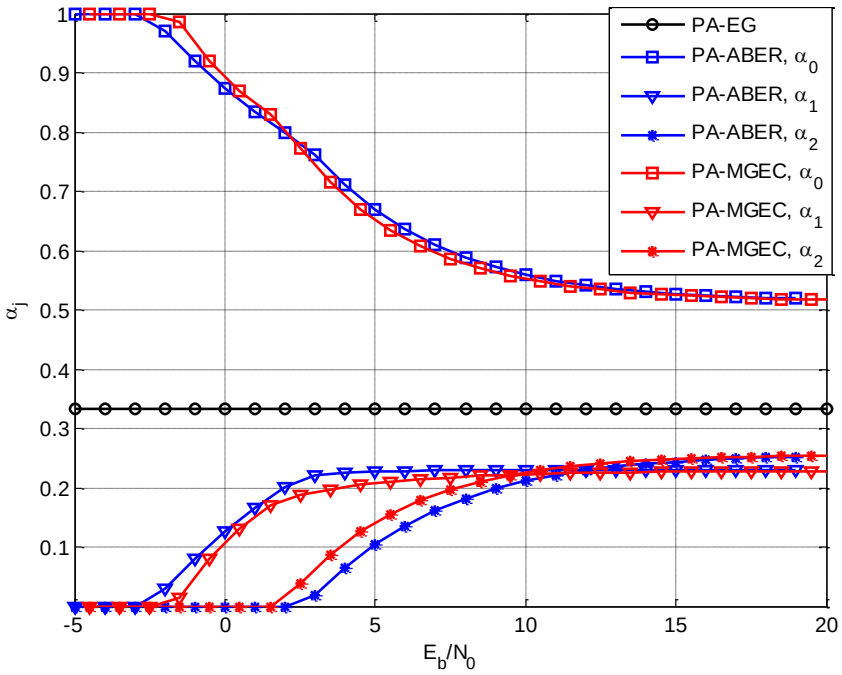

Fig. 5.16. Power allocation results on Network-10 with S-DF/RT relaying scheme.

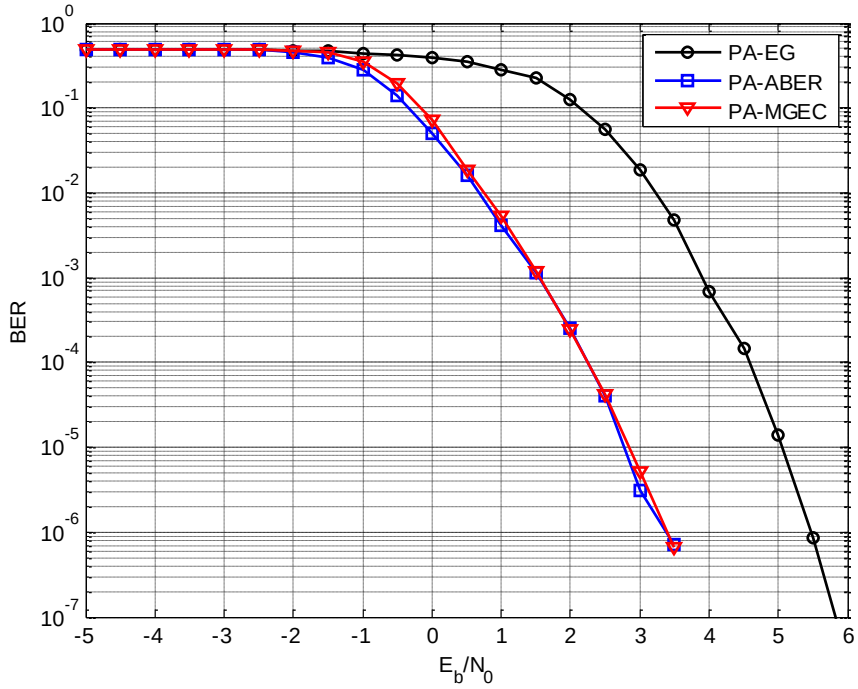

Fig. 5.17. BER simulation results on Network-10 with S-DF/RT relaying scheme.

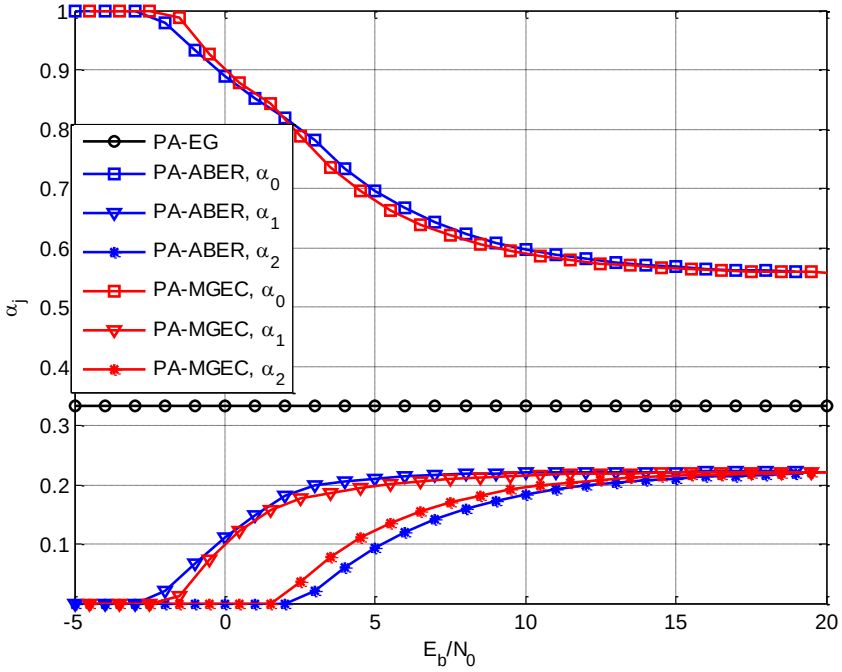

Fig. 5.18. Power allocation results on Network-10 with S-DF/Idle relaying scheme.

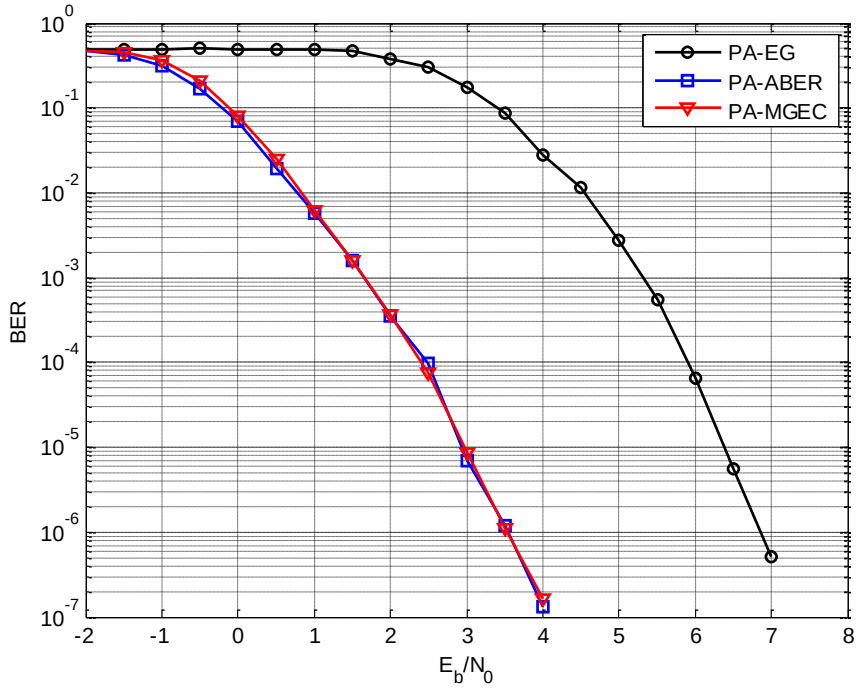

Fig. 5.19. BER simulation results on Network-10 with S-DF/Idle relaying scheme.

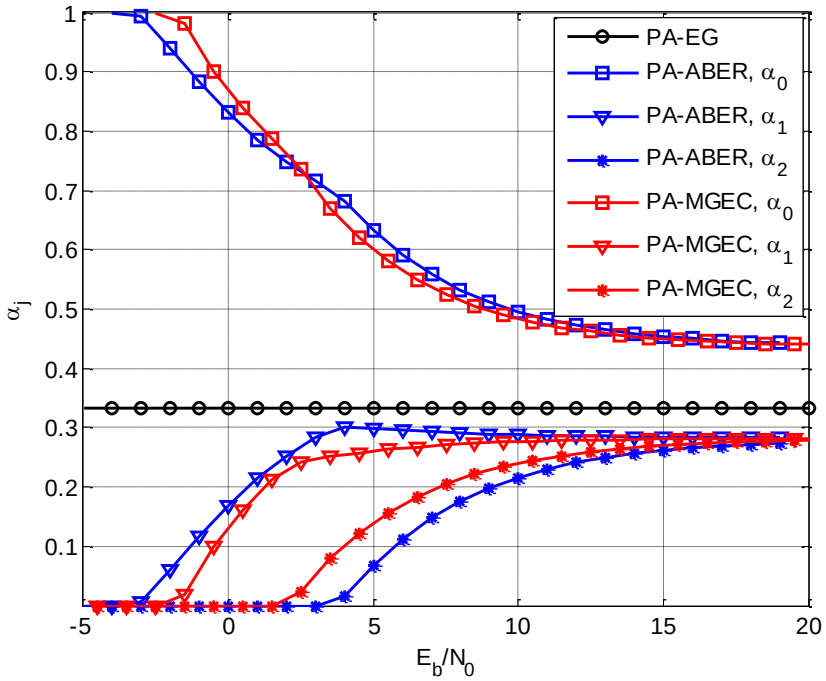

Fig. 5.20. Power allocation results on Network-10 with S-DF/AF relaying scheme.

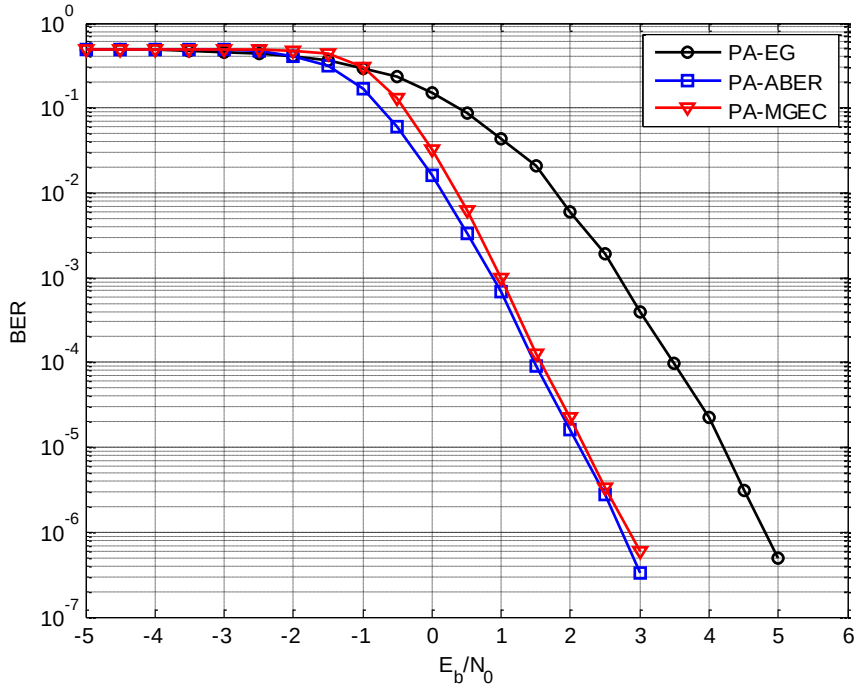

Fig. 5.21. BER simulation results on Network-10 with S-DF/AF relaying scheme.

Another interesting example is on Network-11, in which the S-R and R-D links of relay 1 remains the same, but the S-R link of relay 2 is better than that of relay 1. For AF relaying scheme, PA-EC still prefers to allocate non-zero power to relay 1 earlier than relay 2 as the SNR increases, as shown in Fig. 5.22 with the BER performance given in Fig. 5.23. But, for S-DF relaying schemes, both PA-ABER and PA-MGEC prefer to allocate power to relay 2 earlier than relay 1, as the SNR increases. The power allocation results and BER performance are shown in Fig. 5.24 and Fig. 5.25 for S-DF/RT, while those for S-DF/Idle and S-DF/AF are similar. In Network-11, all methods allocate more power on relay 2 when SNR approaches infinity. The reason could be that, for AF, relay 2 provides a better equivalent channel than relay 1 and that, for S-DF, relay 2 is more likely to decode erroneously under the condition that both relay have the same R-D link quality.

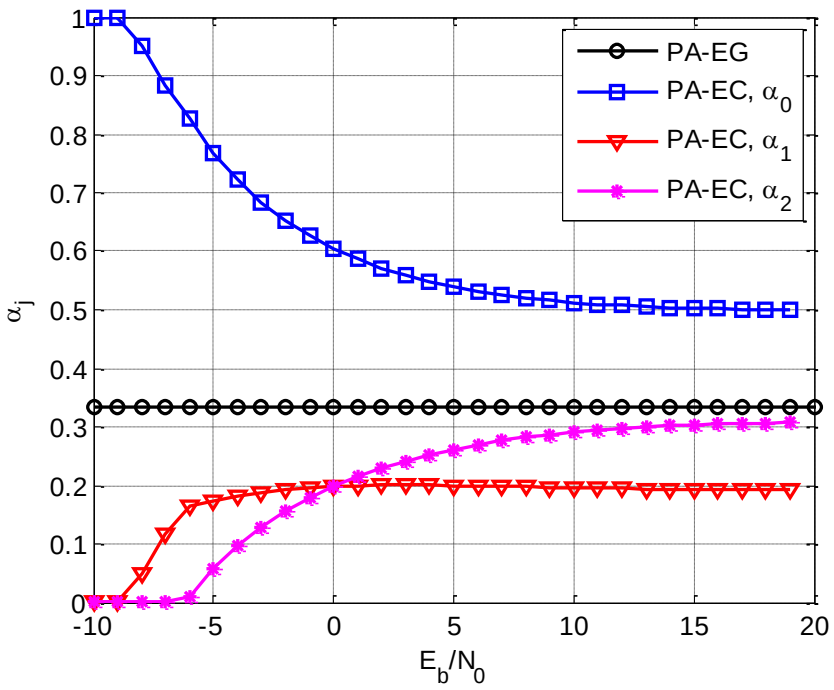

Fig. 5.22. Power allocation results on Network-11 with AF relaying scheme.

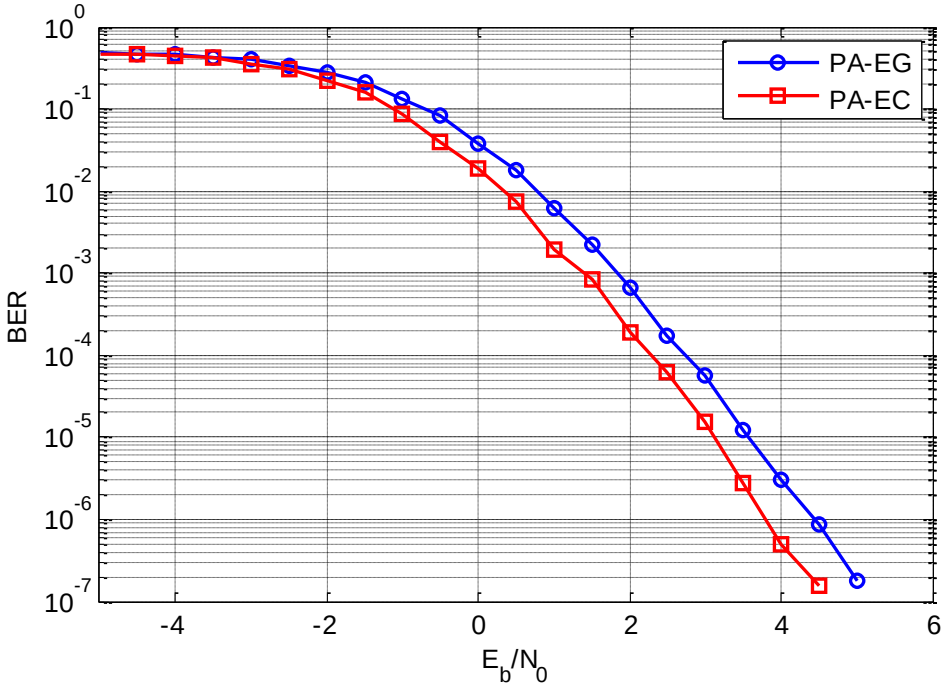

Fig. 5.23. BER simulation results on Network-11 with AF relaying scheme.

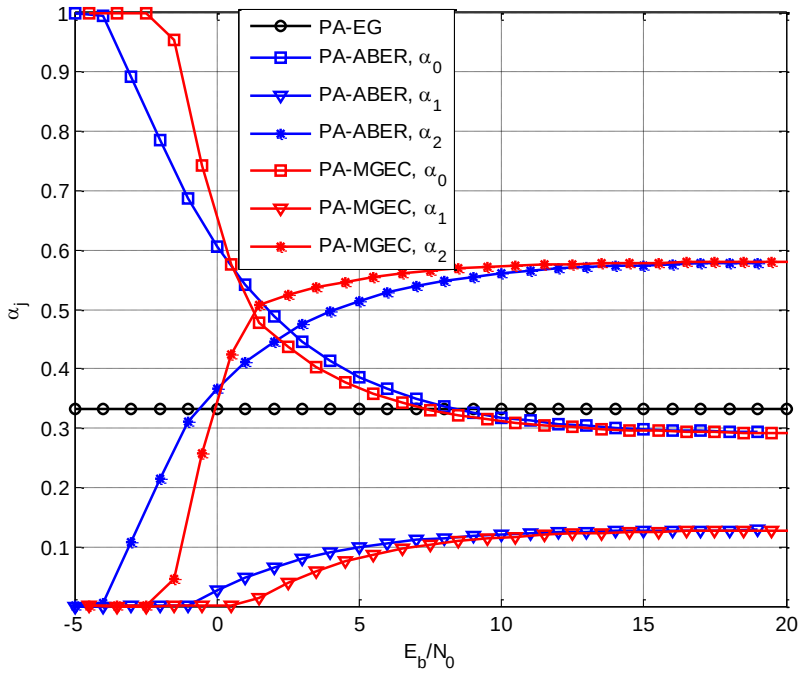

Fig. 5.24. Power allocation results on Network-11 with S-DF/RT relaying scheme.

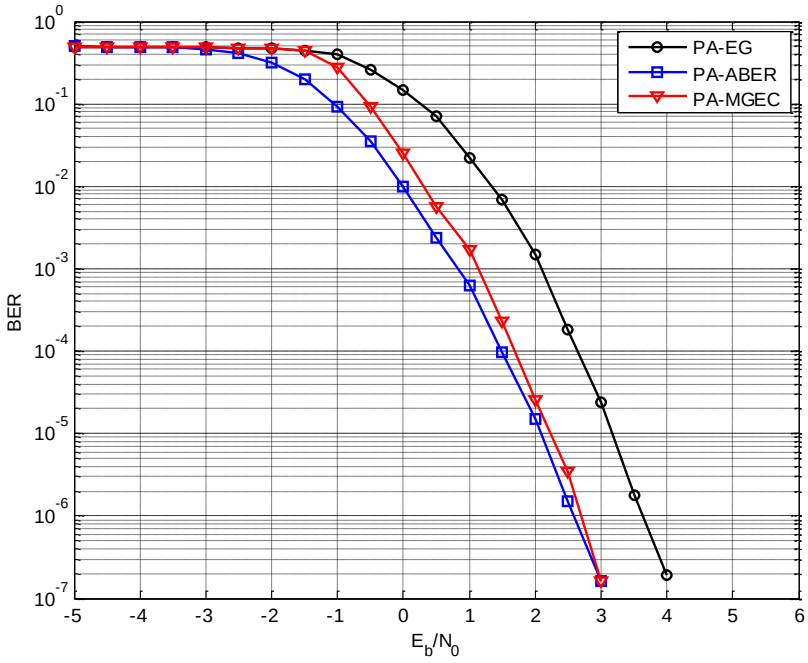

Fig. 5.25. BER simulation results on Network-11 with S-DF/RT relaying scheme.

The proposed power allocation methods (PA-EC, PA-ABER and PA-MGEC) straightforwardly applied to Network with 3 or more relays. In fact, it is important to know that the gain of these methods over PA-EG generally increases with the number of relays. The reason is simply that as the relay increases, less power is expected to be allocated to source for PA-EG, e.g., $P_T/(R+1)$. Therefore, a high SNR is required for the source to activate relays. Oppositely, for PA-ABER and PA-MGEC, the source usually takes full power at low SNRs. This implies that PA-ABER and PA-MGEC can start to benefit from active relays at a lower SNR than PA-EG. Thus, a gain can be expected. As an example, another example is conducted on Network-12 with 3 relays and the channel gains given in Table VI. The proposed power allocation results and the corresponding BER performance of AF are shown in Fig. 5.26 and Fig. 5.27, S-DF/RT in Fig. 5.28 and Fig. 5.29, S-DF/Idle in Fig. 5.30 and Fig. 5.31, as well as S-DF/AF in Fig. 5.32 and Fig. 5.33, respectively.

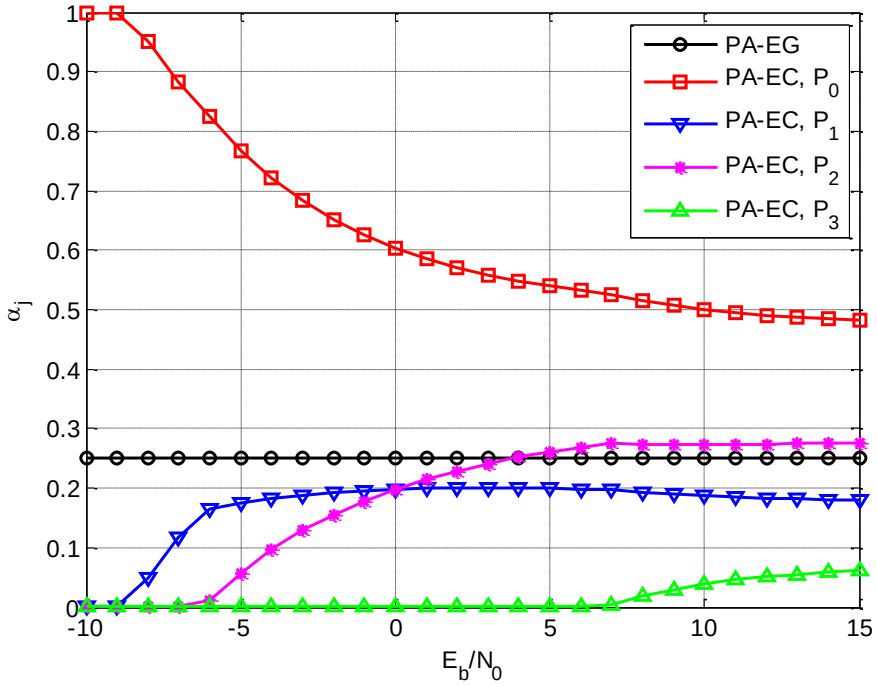

Fig. 5.26. Power allocation results on Network-12 with AF relaying scheme.

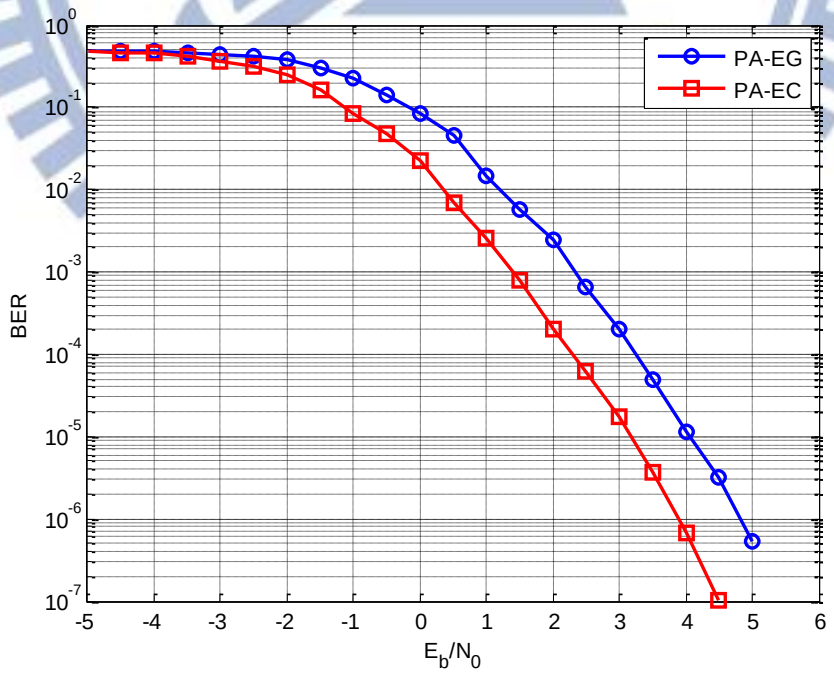

Fig. 5.27. BER simulation resultss on Network-12 with AF relaying scheme.

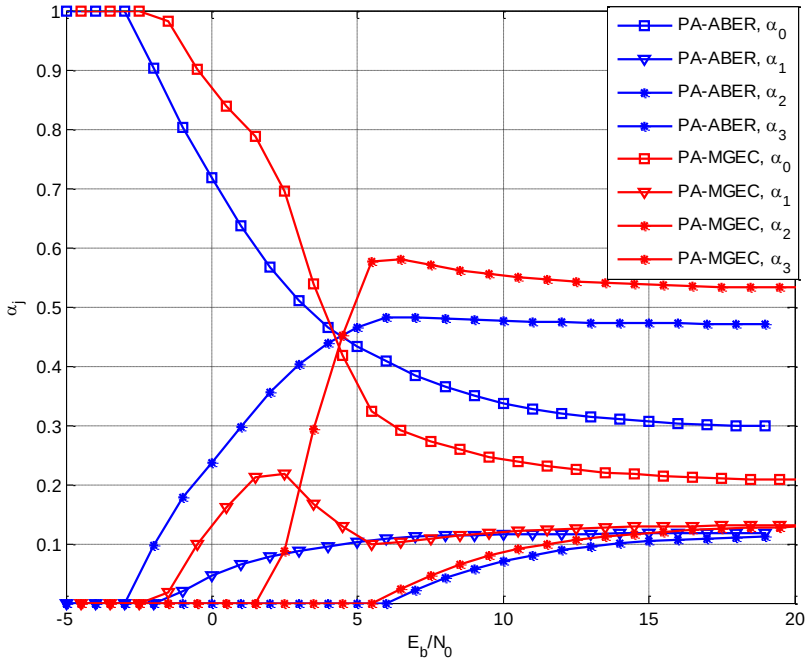

Fig. 5.28. Power allocation results on Network-12 with S-DF/RT relaying scheme.

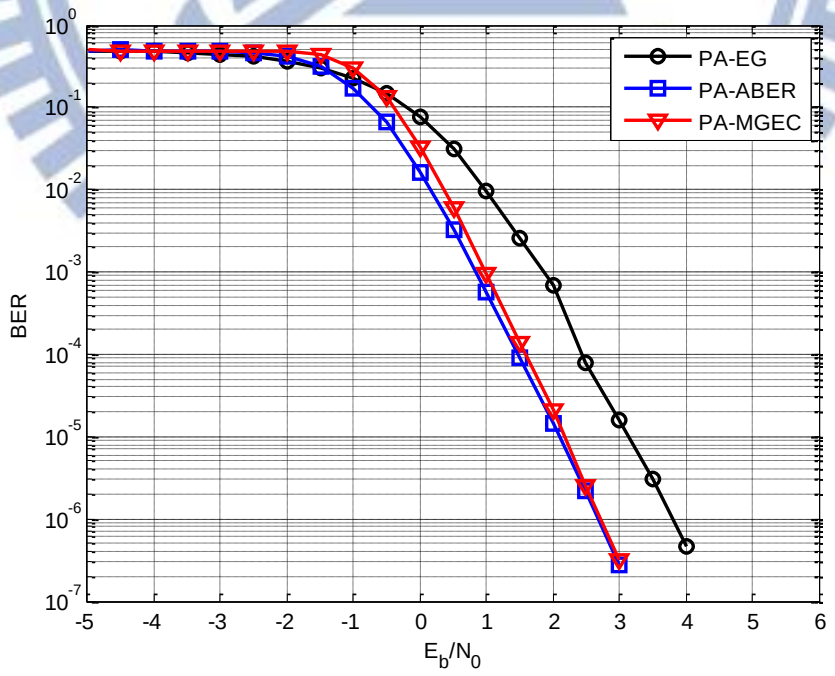

Fig. 5.29. BER simulation results on Network-12 with S-DF/RT relaying scheme.

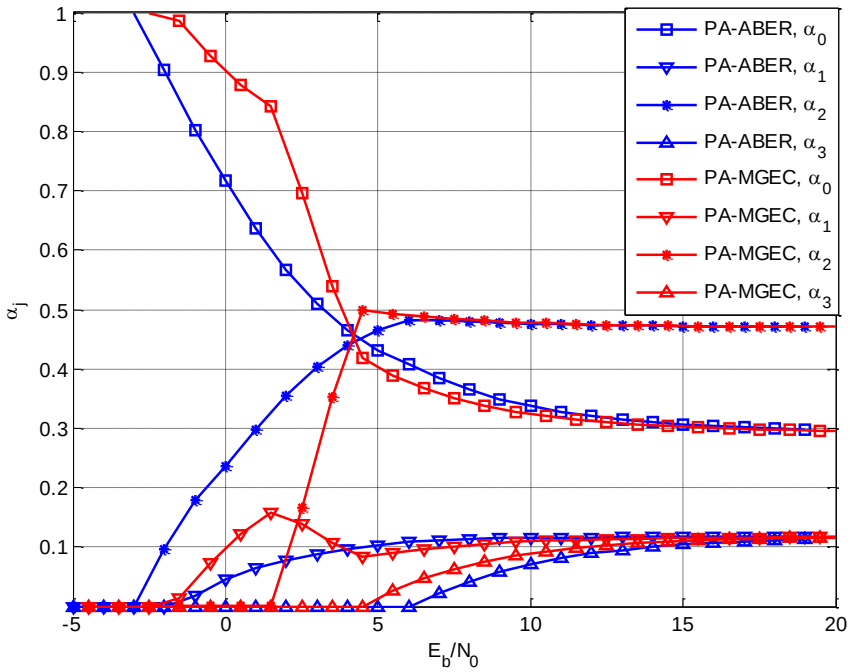

Fig. 5.30. Power allocation results on Network-12 with S-DF/Idle relaying scheme.

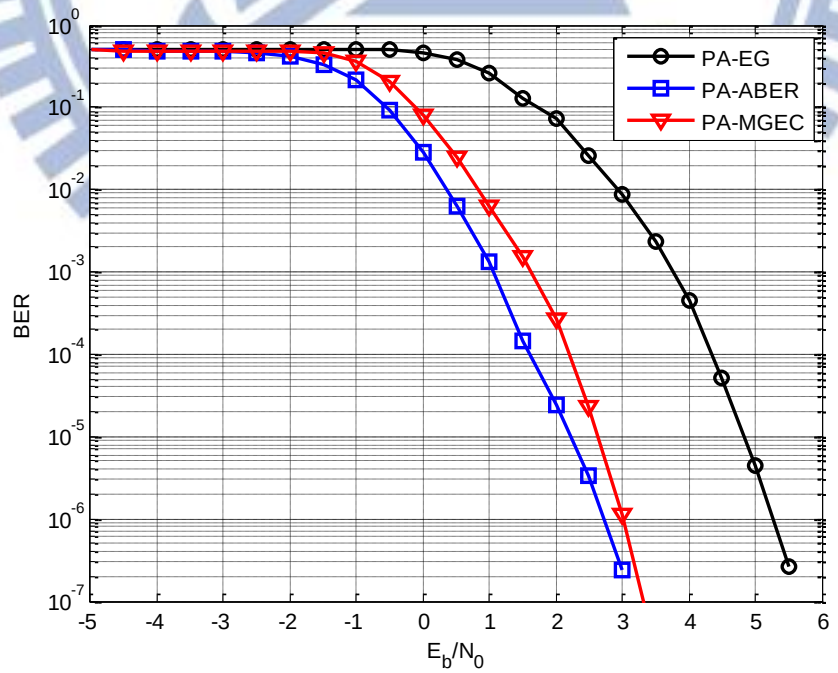

Fig. 5.31. BER simulation results on Network-12 with S-DF/Idle relaying scheme.

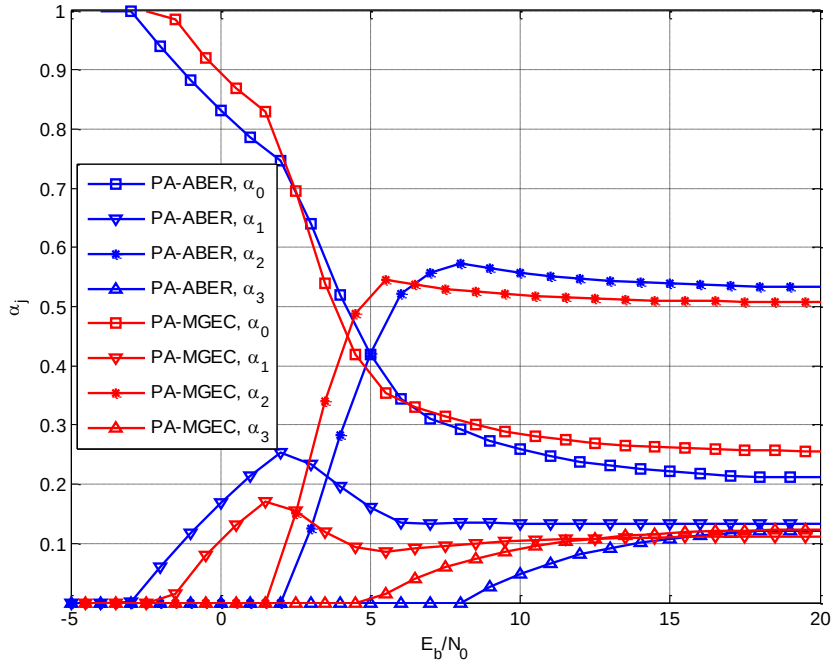

Fig. 5.32. Power allocation results on Network-12 with S-DF/AF relaying scheme.

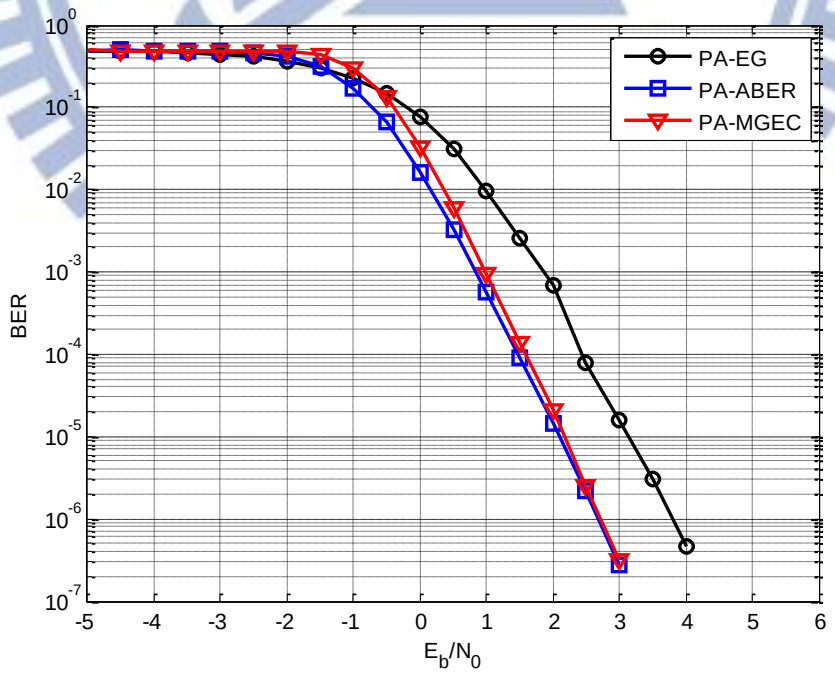

Fig. 5.33. BER simulation results on Network-12 with S-DF/AF relaying scheme.

In the last example of this chapter, we compare our proposed method with the power allocation in [84] which maximized the capacity of a 3-node cooperative repaying network (denoted by PA-MC). We consider Network-13 in Table IV with S-DF/Idle and plot the power allocation results of our methods and PA-MC in Fig. 5.34. As is seen in Fig. 5.34, the optimal α_0 of PA-MC is invariant to the change E_b/N_0 ($\alpha_0 = 0.357$). It can be expected that, at low SNRs, the insufficient source power is not able to active the relay so that the power allocated to the relay is wasted. In this case, the BER at destination will be high because destination could only decode the packet based on the signal transmitted from source with a low power ratio $\alpha_0 = 0.357$ .At high SNRs, the power allocation of the three methods are very similar. The BER performance is plotted in Fig. 5.35. As is expected, PA-MC is outperformed by our methods with about 0.8 dB gain at BER of 10^{-5}. Such a gap is expected to diminish, as the SNR further increases. However, the corresponding BER is too low to be obtained through computer simulation.

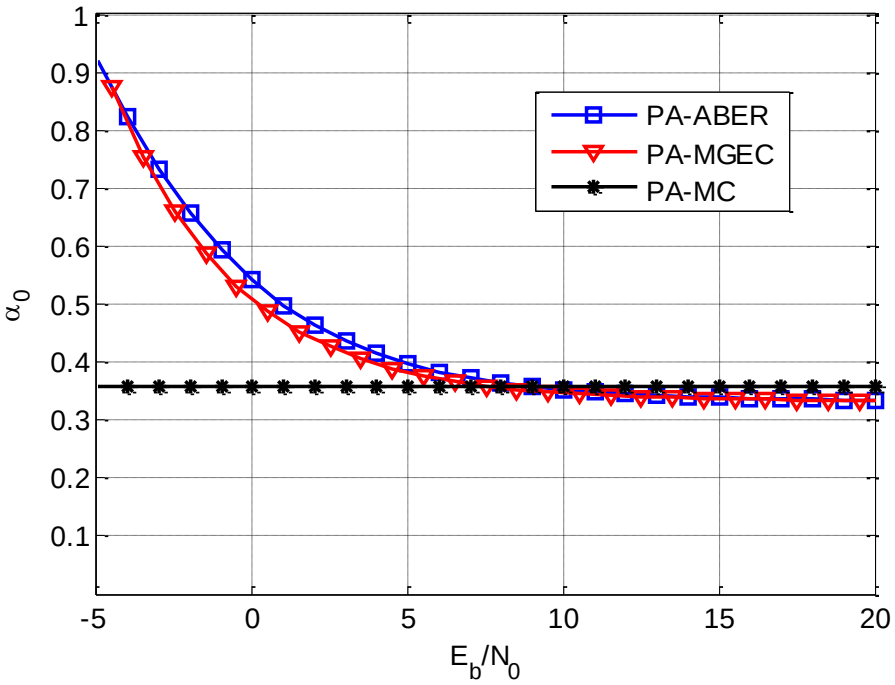

Fig. 5.34. Power allocation results on Network-13 with S-DF/Idle relaying scheme.

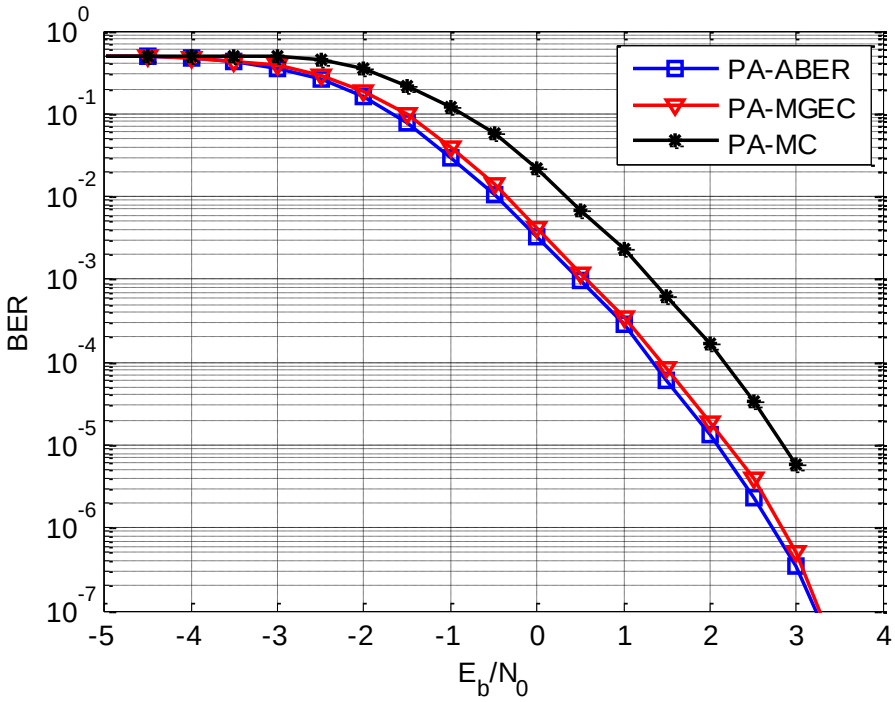

Fig. 5.35. BER simulation results on Network-13 with S-DF/Idle relaying scheme.

5.5 Summary

Chapter 5 investigates the power allocation of the BICM-coded cooperative network. Four relaying schemes are considered: AF, S-DF/RT, S-DF/Idle and S-DF/AF with the general formulation in Section 2.4. For AF, the union bound of the BER proposed in [47] is simplified by considering only the worst-case error event and the shortest Euclidean between constellation points. An approximate BER is obtained and is shown to be monotonically decreasing with an equivalent channel gain, which is then taken as the cost function of PA-EC. For S-DF relaying schemes, two power allocation methods, named PA-ABER and PA-MGEC, are proposed. In PA-ABER, by following similar steps in deriving PA-EC, an approximate BER is obtained as the cost function and is shown to be a convex function for S-DF/RT, S-DF/Idle and S-DF/AF. Therefore, gradient method can be adopted to find the solution. Then, PA-MGEC transforms the approximate BER to a max-min problem, which can be optimized with even lower complexity, e.g., Simplex algorithm

can be used for S-DF/RT and S-DF/Idle. Examples are given to demonstrate how power is allocated as the SNR increases for PA-EC and PA-MGEC on the AF and S-DF relaying schemes, respectively. In general, our methods tend to allocate full power to source at low SNR to avoid power waste on inactive relays. Simulation results are provided to confirm that our proposed methods outperform PA-EG with large margins for different network setups.

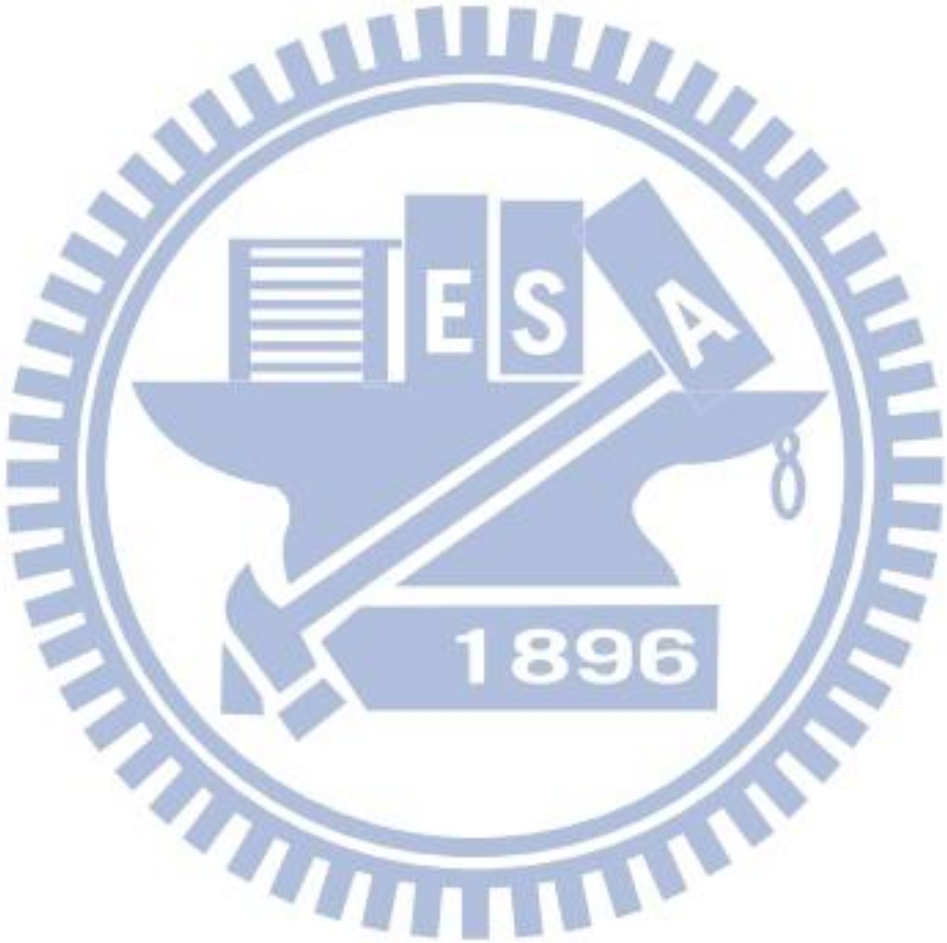

Chapter 6

Power Allocation on De-code-Remap-and-Forward

This chapter extends the results of the previous chapter to S-DRF, which allows active relays to change the constellation mapping used in modulation before forwarding. S-DRF has been proved to provide significant remapping gain over conventional S-DF [47]-[49]. In spite of it importance, this section shows how PA-ABER and PA-MGEC are applied work on S-DRF[3].

For notation clarity, denote $x^{(j)} = \mu^{(j)}(v)$ the operation that a label v is mapped by a mapper $\mu^{(j)}$ to a complex symbol $x^{(j)}$, where $\mu^{(j)}$ is the mapper used at relay j. (Note that $\mu^{(0)}$ is used for the mapper at source.) With this notation, the general form representation in Section 2.4 is modified as

$$\tilde{y}_{j,R+1} = \tilde{h}_{j,R+1}\sqrt{P_j}\tilde{\mu}_j(v) + \tilde{\omega}_{j,R+1},\ \ j = 1,2,\cdots,R+1, \tag{6.1}$$

where

[3] In our previous work [50], the power allocation for S-DRF/Idle had been presented. In this dissertation, the derivation is provided in the general form so that S-DRF/Idle will also be covered.

$$\tilde{\mu}_j = \begin{cases} \mu^{(j)}, & \text{if } j \in \Theta \\ \mu^{(0)}, & \text{if } j \notin \Theta \end{cases} \tag{6.2}$$

Note that the time index k has be dropped for simplicity in a slowly-fading environment in which the channel gains remain constant during a frame. In (6.2), relay j is assumed to use $\mu^{(j)}$ on forwarding when decoding correctly. Upon decoding failure, 1) for S-DF/Idle, nothing is going to be transmitted, 2) for S-DF/RT, the source remains its original mapper $\mu^{(0)}$ (Or, in other words, send $x^{(0)}$ again through the orthogonal-channel.[4]), and 3) for S-DF/AF, relay forwards without neither decoding nor re-mapping. Consequently, the LLR for the i-th bit of the label v at the destination is evaluated by

$$\min_{v\in\Gamma_0^i} \sum_{j=0}^{R} \frac{\left|\tilde{y}_{j,R+1} - \tilde{h}_{j,R+1}\sqrt{P_j}\tilde{\mu}_j(v)\right|^2}{\tilde{N}_0^{(j)}} - \min_{v\in\Gamma_1^i} \sum_{j=0}^{R} \frac{\left|\tilde{y}_{j,R+1} - \tilde{h}_{j,R+1}\sqrt{P_j}\tilde{\mu}_j(v)\right|^2}{\tilde{N}_0^{(j)}}, \tag{6.3}$$

where Γ_b^i is the set of labels with the binary value b on its i-th position. Note that for S-DF/Idle, the summations $\sum_{j=0}^{R}(\cdot)$ should be replaced by $\sum_{j\in\tilde{\Theta}}(\cdot)$.

6.1 PA-ABER

Although new notations are used, the BER analysis is not much different. In fact, one can follow (5.13)-(5.14) and modify (5.15) as (or refer to our work [50])

$$f_{ub}^{\text{S-DRF}}\left(d_f, \Theta, \boldsymbol{\alpha}\right) = \frac{1}{2\pi \boldsymbol{j}} \int_{s_0-\boldsymbol{j}\infty}^{s_0+\boldsymbol{j}\infty} \left[\frac{1}{l2^l} \sum_{i=1}^{l} \sum_{b=0}^{1} \sum_{v\in\Gamma_b^i} \sum_{w\in\Gamma_{\tilde{b}}^i} \prod_{j=0}^{R} \Phi_{\Delta_{\tilde{h}_{j,R+1}}(v,w)}(s) \right]^{d_f} \frac{ds}{s} \tag{6.4}$$

with the MGF

[4] An option is to allow remapping on source's re-transmissions in S-DRF/RT. Although this dissertation does not consider the re-mapping at source in this work, the corresponding power allocation can be easily extended based on our derivations.

$$\Phi_{\Delta_{\tilde{h}_{j,R+1}}(v,w)}(s)=\exp\left[\left(-s+s^2\right)P_T\left|x^{(j)}-z^{(j)}\right|^2\frac{\alpha_j\left|\tilde{h}_{j,R+1}\right|^2}{\tilde{N}_0^{(j)}}\right], \tag{6.5}$$

where $x^{(j)}=\tilde{\mu}_j(v)$ and $z^{(j)}=\tilde{\mu}_j(w)$ are the symbols mapped by $\tilde{\mu}_j$ from the label v and the erroneous label w, respectively. Bringing (6.5) and the saddle point $s=0.5+\boldsymbol{j}t$ into (6.4) yields

$$\begin{aligned}&f_{ub}^{\text{S-DRF}}\left(d_f,\Theta,\boldsymbol{\alpha}\right)\\&=\frac{1}{4\pi}\int_{-\infty}^{\infty}\left[\frac{1}{l2^l}\sum_{i=1}^{l}\sum_{b=0}^{1}\sum_{v\in\Gamma_b^i}\sum_{w\in\Gamma_{\bar{b}}^i}\exp\left[-\left(t^2+\frac{1}{4}\right)P_T\sum_{j=0}^{R}D^{(j)}\frac{\alpha_j\left|\tilde{h}_{j,R+1}\right|^2}{\tilde{N}_0^{(j)}}\right]\right]^{d_f}\frac{dt}{t^2+\frac{1}{4}},\end{aligned} \tag{6.6}$$

where $D^{(j)}=\left|x^{(j)}-z^{(j)}\right|^2$ is the squared Euclidean distance between $x^{(j)}$ and $z^{(j)}$.

Since the summation (6.6) contains only real exponential functions, at high SNRs, such a summation is dominated by the terms with the largest exponent, i.e.,

$$f_{ub}^{\text{S-DF}}\left(d_f,\Theta,\boldsymbol{\alpha}\right)=\frac{1}{4\pi}\int_{-\infty}^{\infty}\left[\frac{N_\Theta(\boldsymbol{\alpha})}{l2^l}\exp\left[-\left(t^2+\frac{1}{4}\right)\frac{P_T}{N_0}\hat{M}_\Theta(\boldsymbol{\alpha})\right]\right]^{d_f}\frac{dt}{t^2+\frac{1}{4}}, \tag{6.7}$$

where

$$\hat{M}_\Theta(\boldsymbol{\alpha})=\min_{v\in\Gamma_b^i,\ w\in\Gamma_{\bar{b}}^i,\ i=1,\cdots l,\ b=0,1}N_0\sum_{j=0}^{R}D^{(j)}\frac{\alpha_j\left|\tilde{h}_{j,R+1}\right|^2}{\tilde{N}_0^{(j)}}, \tag{6.8}$$

and N_Θ is the number of (v,w) pairs that achieve $\hat{M}_\Theta(\boldsymbol{\alpha})$. Compared to $M_\Theta(\boldsymbol{\alpha})$, each term in the summation of (5.17) is now further weighted by $D^{(j)}$ in (6.8). When Remapping is considered, for one label pair (v,w), their resulting symbol distance $D^{(j)}=\left|x^{(j)}-z^{(j)}\right|^2$ may not be the same for all j because the mappers are now different. Thus, the channel gains are further weighted by the distance $D^{(j)}$. As a special case, when all mappers are the same, i.e., $D^{(0)}=D^{(1)}=\cdots=D^{(R)}$, $\hat{M}_\Theta(\boldsymbol{\alpha})$ degenerates to

$$\hat{M}_{\Theta}(\boldsymbol{\alpha}) = \left(\min_{v\in\Gamma_b^i,\, w\in\Gamma_{\bar{b}}^i,\, i=1,\cdots l,\, b=0,1} D^{(0)} \right) \cdot \left(N_0 \sum_{j=0}^{R} \frac{\alpha_j \left|\tilde{h}_{j,R+1}\right|^2}{\tilde{N}_0^{(j)}} \right)$$
$$= D_{\chi} N_0 \sum_{j=0}^{R} \frac{\alpha_j \left|\tilde{h}_{j,R+1}\right|^2}{\tilde{N}_0^{(j)}} \quad . \tag{6.9}$$
$$= D_{\chi} M_{\Theta}(\boldsymbol{\alpha})$$

Eq. (6.9) clearly shows the relation between $\hat{M}_{\Theta}(\boldsymbol{\alpha})$ and $M_{\Theta}(\boldsymbol{\alpha})$.

An alternative representation of (6.8) is

$$\hat{M}_{\Theta}(\boldsymbol{\alpha}) = \min_{\mathbf{D}\in\Psi} N_0 \sum_{j=0}^{R} D^{(j)} \frac{\alpha_j \left|\tilde{h}_{j,R+1}\right|^2}{\tilde{N}_0^{(j)}}, \tag{6.10}$$

where Ψ is the set of all distinct $\mathbf{D} = \left[D^{(0)}\ D^{(1)}\ \ldots D^{(R)} \right]^T$ obtained by exhausting all possible (v, w) pairs. Note that the numbers of (v, w) pairs for different $\mathbf{D}$'s in Ψ are usually not the same so that $N_{\Theta}(\boldsymbol{\alpha})$ in (6.7) may not be a continuous function of $\boldsymbol{\alpha}$. Table V enumerates Ψ for the following setups.

Setup-1: $R = 1$, 16QAM, and $\mu^{(0)} = \mu^{(1)} = \mu_G$ (the Gray mapping) in Fig. 6.1. (Note that all elements in $\mathbf{D}$ are the same if $\mu^{(j)} = \mu^{(0)}$ for all j.)

Setup-2: $R = 1$, 16QAM, $\mu^{(0)} = \mu_G$ and $\mu^{(1)} = \mu_A$ in Fig. 6.1.

Setup-3: $R = 2$, 16QAM, $\mu^{(0)} = \mu_G$, $\mu^{(1)} = \mu_A$ and $\mu^{(2)} = \mu_B$ in Fig. 6.1.

Table V. Ψ for Setup-1, Setup-2 and Setup-3

Setup	Ψ
Setup-1	$\left\{\begin{bmatrix}4\\4\end{bmatrix},\begin{bmatrix}8\\8\end{bmatrix},\begin{bmatrix}16\\16\end{bmatrix},\begin{bmatrix}20\\20\end{bmatrix},\begin{bmatrix}32\\32\end{bmatrix},\begin{bmatrix}36\\36\end{bmatrix},\begin{bmatrix}40\\40\end{bmatrix},\begin{bmatrix}52\\52\end{bmatrix},\begin{bmatrix}72\\72\end{bmatrix}\right\}$
Setup-2	$\left\{\begin{bmatrix}4\\16\end{bmatrix},\begin{bmatrix}4\\20\end{bmatrix},\begin{bmatrix}4\\36\end{bmatrix},\begin{bmatrix}4\\52\end{bmatrix},\begin{bmatrix}8\\16\end{bmatrix},\begin{bmatrix}8\\20\end{bmatrix},\begin{bmatrix}8\\52\end{bmatrix},\begin{bmatrix}8\\72\end{bmatrix},\begin{bmatrix}16\\4\end{bmatrix},\begin{bmatrix}16\\8\end{bmatrix},\begin{bmatrix}16\\40\end{bmatrix},\begin{bmatrix}20\\4\end{bmatrix},\begin{bmatrix}20\\8\end{bmatrix},\begin{bmatrix}20\\32\end{bmatrix},\begin{bmatrix}20\\40\end{bmatrix},\begin{bmatrix}32\\20\end{bmatrix},\begin{bmatrix}36\\4\end{bmatrix},\begin{bmatrix}40\\16\end{bmatrix},\begin{bmatrix}40\\20\end{bmatrix},\begin{bmatrix}40\\40\end{bmatrix},\begin{bmatrix}52\\4\end{bmatrix},\begin{bmatrix}52\\8\end{bmatrix},\begin{bmatrix}72\\8\end{bmatrix}\right\}$
Setup-3	$\left\{\begin{bmatrix}4\\16\\20\end{bmatrix},\begin{bmatrix}4\\20\\20\end{bmatrix},\begin{bmatrix}4\\20\\40\end{bmatrix},\begin{bmatrix}4\\36\\8\end{bmatrix},\begin{bmatrix}4\\36\\40\end{bmatrix},\begin{bmatrix}4\\36\\72\end{bmatrix},\begin{bmatrix}4\\52\\4\end{bmatrix},\begin{bmatrix}4\\52\\8\end{bmatrix},\begin{bmatrix}8\\16\\16\end{bmatrix},\begin{bmatrix}8\\16\\52\end{bmatrix},\begin{bmatrix}8\\20\\16\end{bmatrix},\begin{bmatrix}8\\20\\20\end{bmatrix},\begin{bmatrix}8\\20\\40\end{bmatrix},\begin{bmatrix}8\\20\\52\end{bmatrix},\begin{bmatrix}8\\52\\4\end{bmatrix},\begin{bmatrix}8\\52\\36\end{bmatrix},\begin{bmatrix}8\\72\\32\end{bmatrix},\begin{bmatrix}16\\4\\20\end{bmatrix},\begin{bmatrix}16\\8\\16\end{bmatrix},\begin{bmatrix}16\\8\\52\end{bmatrix},\begin{bmatrix}16\\40\\4\end{bmatrix},\begin{bmatrix}16\\40\\16\end{bmatrix},\begin{bmatrix}20\\4\\20\end{bmatrix},\begin{bmatrix}20\\4\\40\end{bmatrix},\begin{bmatrix}20\\8\\16\end{bmatrix},\begin{bmatrix}20\\8\\20\end{bmatrix},\begin{bmatrix}20\\8\\40\end{bmatrix},\begin{bmatrix}20\\8\\52\end{bmatrix},\begin{bmatrix}20\\32\\4\end{bmatrix},\begin{bmatrix}20\\32\\8\end{bmatrix},\begin{bmatrix}20\\32\\16\end{bmatrix},\begin{bmatrix}20\\40\\4\end{bmatrix},\begin{bmatrix}20\\40\\36\end{bmatrix},\begin{bmatrix}32\\20\\4\end{bmatrix},\begin{bmatrix}32\\20\\8\end{bmatrix},\begin{bmatrix}32\\20\\16\end{bmatrix},\begin{bmatrix}36\\4\\4\end{bmatrix},\begin{bmatrix}36\\4\\8\end{bmatrix},\begin{bmatrix}36\\4\\40\end{bmatrix},\begin{bmatrix}36\\4\\72\end{bmatrix},\begin{bmatrix}40\\16\\4\end{bmatrix},\begin{bmatrix}40\\16\\16\end{bmatrix},\begin{bmatrix}40\\20\\8\end{bmatrix},\begin{bmatrix}40\\20\\32\end{bmatrix},\begin{bmatrix}40\\40\\32\end{bmatrix},\begin{bmatrix}40\\40\\36\end{bmatrix},\begin{bmatrix}52\\4\\4\end{bmatrix},\begin{bmatrix}52\\4\\8\end{bmatrix},\begin{bmatrix}52\\8\\8\end{bmatrix},\begin{bmatrix}52\\8\\32\end{bmatrix}\right\}$

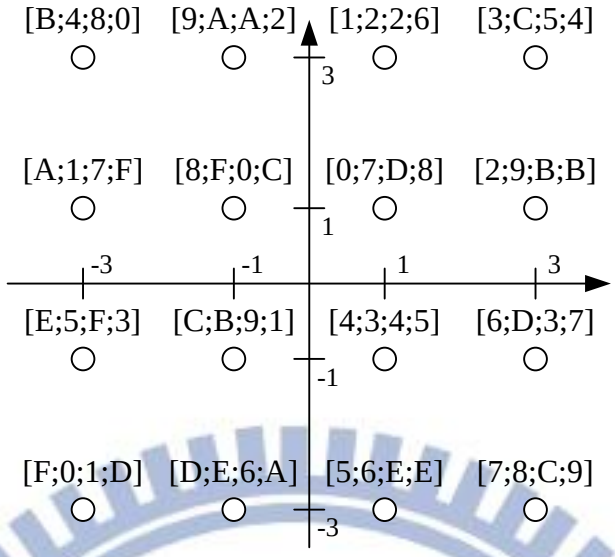

Fig. 6.1. Four example mappers $(\mu_G, \mu_A, \mu_B, \mu_C)$ for the 16-QAM constellation. The signal point labels $[v_G; v_A; v_B; v_C]$ are in hexadecimal format, where v_G, v_A, v_B and v_C are to denote the label of μ_G, μ_A, μ_B and μ_C, respectively. (The μ_A, μ_B and μ_C mappers are the MBER mappings which maximize the minimum Euclidean distance between transmit symbols for the second, third and fourth transmissions of the hybrid automatic repeat-request system in [82], respectively.)

In fact, there are irrelevant $\mathbf{D}$'s in Ψ which can be removed without changing $\hat{M}_{\Theta}(\boldsymbol{\alpha})$. To determine these irrelevant $\mathbf{D}$'s, the following Lemma is introduced with its proof given in Appendix E .

Lemma-3: For a $\mathbf{D}_2 \in \Psi$, if there exist a $\mathbf{D}_1 \in \Psi$ with $D_1^{(j)} \le D_2^{(j)}$ for all j, then $\mathbf{D}_2$ can be removed from Ψ without changing $\hat{M}_{\Theta}(\boldsymbol{\alpha})$.

Let $\hat{\Psi}$ be the set after removing all irrelevant elements in Ψ. In Table VI, the sets $\hat{\Psi}$ are listed for Setup-1, 2 and 3. After applying Lemma-3, the number of elements in Ψ is reduced dramatically from 9, 23 and 50 to 1, 2 and 10 in $\hat{\Psi}$ for Setup-1, 2 and 3, respectively.

Table VI. $\hat{\Psi}$ for Setup-1, Setup-2 and Setup-3

Setup	$\hat{\Psi}$
Setup-1	$\left\{\begin{bmatrix}4\\4\end{bmatrix}\right\}$
Setup-2	$\left\{\begin{bmatrix}4\\16\end{bmatrix},\begin{bmatrix}16\\4\end{bmatrix}\right\}$
Setup-3	$\left\{\begin{bmatrix}4\\16\\20\end{bmatrix},\begin{bmatrix}4\\36\\8\end{bmatrix},\begin{bmatrix}4\\52\\4\end{bmatrix},\begin{bmatrix}8\\16\\16\end{bmatrix},\begin{bmatrix}16\\4\\20\end{bmatrix},\begin{bmatrix}16\\8\\16\end{bmatrix},\begin{bmatrix}16\\40\\4\end{bmatrix},\begin{bmatrix}20\\32\\4\end{bmatrix},\begin{bmatrix}32\\20\\4\end{bmatrix},\begin{bmatrix}36\\4\\4\end{bmatrix}\right\}$

Now, (6.7) becomes

$$f_{ub}^{\text{S-DRF}}\left(d_f,\Theta,\boldsymbol{\alpha}\right)=\left(\frac{N_\Theta\left(\boldsymbol{\alpha}\right)}{l2^l}\right)^{d_f}\frac{1}{4\pi}\int_{-\infty}^{\infty}\exp\left[-\left(t^2+\frac{1}{4}\right)\frac{d_f P_T}{N_0}\hat{M}_\Theta\left(\boldsymbol{\alpha}\right)\right]\frac{dt}{t^2+\frac{1}{4}}. \tag{6.11}$$

Following the same steps from (5.6) to (5.10), the conditional BER at the destination is approximated by

$$p_{b,R+1}^{\text{S-DRF}}\left(\Theta\right)\approx w_I\left(d_f\right)\left(\frac{N_\Theta\left(\boldsymbol{\alpha}\right)}{l2^l}\right)^{d_f}\sqrt{\frac{N_0}{\pi d_f P_T\hat{M}_\Theta\left(\boldsymbol{\alpha}\right)}}\exp\left[-\frac{d_f P_T}{4N_0}\hat{M}_\Theta\left(\boldsymbol{\alpha}\right)\right], \tag{6.12}$$

and, similarly,

$$p_{b,j}\approx w_I\left(d_f\right)\left(\frac{N_\varnothing\left(\boldsymbol{\alpha}\right)}{l2^l}\right)^{d_f}\sqrt{\frac{N_0}{\pi d_f P_T\alpha_0\left|h_{0,j}\right|^2 D_\chi}}\exp\left[-\frac{d_f P_T}{4N_0}\alpha_0\left|h_{0,j}\right|^2 D_\chi\right]. \tag{6.13}$$

Note that $\frac{N_\varnothing\left(\boldsymbol{\alpha}\right)}{l2^l}=N_\chi$. Now, (5.13) can be approximated by using (6.12) and (6.13).

As to power allocation, note that (i) $N_\Theta\left(\boldsymbol{\alpha}\right)$'s may not be continuous functions of $\boldsymbol{\alpha}$ and (ii) at high SNRs $N_\Theta\left(\boldsymbol{\alpha}\right)$ and $N_\varnothing\left(\boldsymbol{\alpha}\right)$ (the numbers of pairs) are less dominant than $\hat{M}_\Theta\left(\boldsymbol{\alpha}\right)$ and

$\alpha_0 \left|h_{0,j}\right|^2 D_\chi$ in (6.12) and (6.13), respectively. Therefore, for simplicity, the effects of $N_\Theta(\boldsymbol{\alpha})$ and $N_\varnothing(\boldsymbol{\alpha})$ are neglected by replacing them with $l2^l$, and (5.13) is simplified further to

$$w_I\left(d_f\right)\hat{G}(\boldsymbol{\alpha}), \tag{6.14}$$

where

$$\hat{G}(\boldsymbol{\alpha}) = \sum_{\Theta \subset \{1,2,\ldots R\}} \hat{g}_\Omega \prod_{j \notin \Theta} K w_I\left(d_f\right)\tilde{g}_j, \tag{6.15}$$

$$\hat{g}_\Theta = \sqrt{\frac{N_0}{\pi d_f P_T \hat{M}_\Theta(\boldsymbol{\alpha})}} \exp\left[-\frac{d_f P_T}{4N_0}\hat{M}_\Theta(\boldsymbol{\alpha})\right] \tag{6.16}$$

and $\tilde{g}_j$ is the same as that defined in (5.23). As a result, PA-ABER for S-DRF is modified as

$$\boldsymbol{\alpha} = \arg\min_{\boldsymbol{\alpha}} \hat{G}(\boldsymbol{\alpha}),\ \text{s.t.}\ \mathbf{1}^T\boldsymbol{\alpha} \le 1,\ 0 \le \alpha_j \le 1,\ j = 0,1,\cdots,R. \tag{6.17}$$

Following the same steps in Appendix D, $\hat{G}(\boldsymbol{\alpha})$ can be proved to be a convex function (for S-DRF/RT, S-DRF/Idle and S-DRF/AF). Here, we provide point out the differences during the proof.

a) S-DRF/RT and S-DRF/Idle: Firstly, following Appendix D, the problem turns to prove the concavity of $\hat{M}_\Theta(\boldsymbol{\alpha})$, which is (for S-DRF/RT)

$$\hat{M}_\Theta(\boldsymbol{\alpha}) = \min_{\mathbf{D}\in\hat{\Psi}} \sum_{j=0}^{R} D^{(j)} \alpha_j \left|\tilde{h}_{j,R+1}\right|^2. \tag{6.18}$$

The summation in (6.18) is a linear function of $\boldsymbol{\alpha}$, which is both convex and concave. Since the minimum of concave functions is still concave [80], (6.18) is a concave function of $\boldsymbol{\alpha}$. With this property, we can continue the steps in Appendix D and finally prove the convexity of $\hat{G}(\boldsymbol{\alpha})$.

b) S-DRF/AF: In this case, $\hat{M}_\Theta(\boldsymbol{\alpha})$ becomes

$$\hat{M}_\Theta(\boldsymbol{\alpha}) = \min_{\mathbf{D}\in\hat{\Psi}} \left\{ \sum_{j\in\tilde{\Theta}} D^{(j)} \alpha_j \left|h_{j,R+1}\right|^2 + \sum_{j\notin\tilde{\Theta}} D^{(j)} \frac{\alpha_0 \left|h_{0,j}\right|^2 \alpha_j \left|h_{j,R+1}\right|^2}{\alpha_0 \left|h_{0,j}\right|^2 + \alpha_j \left|h_{j,R+1}\right|^2 + N_0/P_T} \right\}. \tag{6.19}$$

Similarly, the first summation is linear and the second is concave (as is proved in Appendix C).

Their sum is still concave, and (6.19), which is the minimum of concave functions, remains concave.

However, $\hat{G}(\boldsymbol{\alpha})$ may not be differentiable because $\hat{M}_{\Theta}(\boldsymbol{\alpha})$ is the minimum of concave functions of $\boldsymbol{\alpha}$ and may not be differentiable. Such a constrained convex optimization problem with a non-differentiable cost function can be solved by applying the projected sub-gradient method [83].

6.2 PA-MGEC

PA-MGEC can also be applied for S-DRF. Following the same steps from (5.26) to (5.29) yields

$$\begin{aligned}\boldsymbol{\alpha}^{*} &= \arg\min_{\boldsymbol{\alpha}} \max_{\Theta\subset\{1,2,\ldots R\}} \ln B_{\Theta}(\boldsymbol{\alpha}) \\ &= \arg\max_{\boldsymbol{\alpha}} \min_{\Theta\subset\{1,2,\ldots R\}} \left\{ \hat{M}_{\Theta}(\boldsymbol{\alpha}) + \alpha_0 D_{\chi} \sum_{j\notin\Theta} \left|h_{0,j}\right|^2 - \hat{\eta}_{R-|\Theta|} \right\},\end{aligned} \tag{6.20}$$

where

$$\hat{\eta}_{R-|\Theta|} = \frac{4N_0}{d_f P_T} \ln\left(KW_I\left(d_f\right) \sqrt{\frac{N_0}{\pi d_f P_T}} \right)^{R-|\Theta|}. \tag{6.21}$$

Here, some detail about solving (6.20) is provided for different schemes.

a) S-DRF/RT: We have

$$\hat{M}_{\Theta}(\boldsymbol{\alpha}) = \min_{\mathbf{D}\in\hat{\Psi}} \sum_{j=0}^{R} D^{(j)} \alpha_j \left|\tilde{h}_{j,R+1}\right|^2. \tag{6.22}$$

Bringing (6.20) into (6.20) yields

$$\boldsymbol{\alpha}^{*} = \arg\max_{\boldsymbol{\alpha}} \min_{\Theta\subset\{1,2,\ldots R\}} \left\{ \min_{\mathbf{D}\in\hat{\Psi}} \sum_{j=0}^{R} D^{(j)} \alpha_j \left|\tilde{h}_{j,R+1}\right|^2 + \alpha_0 D_{\chi} \sum_{j\notin\Theta} \left|h_{0,j}\right|^2 - \hat{\eta}_{R-|\Theta|} \sum_{j=0}^{R} \alpha_j \right\}. \tag{6.23}$$

Since (6.23) is also a linear programming problem which can be solved through Simplex algorithm. For the case of S-DRF/Idle, simply replacing the summation $\sum_{j=0}^{R}(\cdot)$ by $\sum_{j\in\tilde{\Theta}}(\cdot)$.

b) S-DRF/AF: Bringing (6.19) into (6.20) yields

$$\hat{M}_{\Theta}(\boldsymbol{\alpha})+\alpha_0 D_{\chi}\sum_{j\notin\Theta}\left|h_{0,j}\right|^2-\hat{\eta}_{R-|\Theta|}$$
$$=\min_{\mathbf{D}\in\hat{\Psi}}\left\{\sum_{j\in\tilde{\Theta}}D^{(j)}\alpha_j\left|h_{j,R+1}\right|^2+\sum_{j\notin\tilde{\Theta}}D^{(j)}\frac{\alpha_0\left|h_{0,j}\right|^2\alpha_j\left|h_{j,R+1}\right|^2}{\alpha_0\left|h_{0,j}\right|^2+\alpha_j\left|h_{j,R+1}\right|^2+N_0/P_T}\right\}+\alpha_0 D_{\chi}\sum_{j\notin\Theta}\left|h_{0,j}\right|^2-\hat{\eta}_{R-|\Theta|} \quad , \quad (6.24)$$

which is not linear and not differentiable. Fortunately, it is still concave so that (6.20) is convex, and its optimum can be obtained through the sub-gradient method.

6.3 Power Allocation Example

Similar to what in Section 5.3, this section provides an example of how power is allocated by PA-MGEC on S-DRF modes. Consider again Network-9 in Table IV. As will be also employed in the simulation results, we use a half-rate convolutional codes CC(171,133) with $d_f=10$ and $W_I\left(d_f\right)=33$. The length of the information sequence is $K=506$ such that the length of the coded sequence is $N=1024$. The mappers μ_G and μ_A are used on a 16-QAM constellation at source and relay, respectively. Note that the total transmit power is calculated as $P_T=E_b\cdot R_C\cdot l$ where E_b is the bit energy, and $R_C=0.5$ is the channel code rate.

6.3.1 PA-MGEC on S-DRF/RT

For S-DF/RT, $\hat{M}_{\Theta}(\boldsymbol{\alpha})$ depends on the active relay set Θ, which could be $\varnothing$ or {1} in this example. Specifically, (6.23) becomes

$$
\begin{aligned}
&\min_{\mathbf{D}\in\hat{\Psi}} \sum_{j=0}^{R} D^{(j)}\alpha_j \left|\tilde{h}_{j,R+1}\right|^2 + \alpha_0 D_\chi \sum_{j\notin\Theta} \left|h_{0,j}\right|^2 - \hat{\eta}_{R-|\Theta|} \\
&= \min_{\mathbf{D}\in\hat{\Psi}} \left\{ D^{(0)}\alpha_0 \left|\tilde{h}_{0,2}\right|^2 + D^{(1)}\alpha_1 \left|\tilde{h}_{1,2}\right|^2 \right\} + \alpha_0 D_\chi \sum_{j\notin\Theta} \left|h_{0,j}\right|^2 - \hat{\eta}_{R-|\Theta|} \\
&= \begin{cases} \min\left\{4\cdot\alpha_0\cdot 1+16\cdot\alpha_1\cdot 10, 16\cdot\alpha_0\cdot 1+4\cdot\alpha_1\cdot 10\right\}, & \Theta=\{1\} \\ 4\cdot\alpha_0\cdot 1+4\cdot\alpha_1\cdot 1+\alpha_0\cdot 4\cdot 4-\hat{\eta}_1, & \Theta=\varnothing \end{cases} \\
&= \begin{cases} \min\left\{160-156\alpha_0, 40-24\alpha_0\right\}, & \Theta=\{1\} \\ 4+16\alpha_0-\hat{\eta}_1, & \Theta=\varnothing \end{cases}
\end{aligned}
\tag{6.25}
$$

Note that when $\Theta=\varnothing$, $D^{(1)}=D^{(0)}$, and $\min_{\mathbf{D}\in\hat{\Psi}}\left\{D^{(0)}\right\}=D_\chi$, which is 4 in this example. Using (6.25) leads to

$$
\begin{aligned}
\boldsymbol{\alpha}^* &= \arg\max_{\boldsymbol{\alpha}} \min_{\Theta\subset\{1,2,\ldots R\}} \left\{ \min_{\mathbf{D}\in\hat{\Psi}} \sum_{j=0}^{R} D^{(j)}\alpha_j \left|\tilde{h}_{j,R+1}\right|^2 + \alpha_0 D_\chi \sum_{j\notin\Theta} \left|h_{0,j}\right|^2 - \hat{\eta}_{R-|\Theta|} \sum_{j=0}^{R}\alpha_j \right\}. \\
&= \arg\max_{\boldsymbol{\alpha}} \min\left\{160-156\alpha_0, 40-24\alpha_0, 4+16\alpha_0-\hat{\eta}_1\right\}
\end{aligned}
\tag{6.26}
$$

The problem becomes to determine the optimum of the minimum of three linear functions of α_0. Define

$$
\begin{cases} L_1 = 160-156\alpha_0 \\ L_2 = 40-24\alpha_0 \\ L_0 = 4+16\alpha_0-\hat{\eta}_1 \end{cases},
\tag{6.27}
$$

whose curves are plotted with different values of E_b/N_0 in Fig. 6.2,. Since $\eta_1=0$ as $|\Theta|=1$, L_1 and L_2 are invariant to the change of SNR. On the other hand, the curve of L_0 shifts up as SNR increases (η_1 decreases).

To determine the optimal power, according to (6.26), we need to maximize $\min\{L_0, L_1, L_2\}$. As is shown in Fig. 6.2, when the SNR is very low, e.g., $E_b/N_0 \le -1.2$ (which corresponds to $\hat{\eta}_1=16$), the whole curve of L_0 is below both L_1 and L_2, so that $\min\{L_0, L_1, L_2\}=L_0$. Since L_0 has positive slope (in fact, L_0 always has positive slope for any channel realizations), the optimum occurs at $\alpha_0=1$. As the SNR increases such that $E_b/N_0 > -1.2$, L_0 and L_1 begin to intersect. This intersection maximizes $\min\{L_0, L_1, L_2\}$ and is chosen as the optimal power allo-

cation. As the SNR further increases, the optimum point changes to the intersection between L_0 and L_2. Observing from Fig. 6.2, the optimal α_0 decreases with SNR, starting from 1 to about 0.9 when $E_b/N_0 \to \infty$ (or $\hat{\eta}_1 \to 0$). In summary, when SNR is low, all power is allocated to source. As the SNR increases, the source power decreases to a final point. This result is intuitive because when SNR is too low, more power should be allocated to source to increase the probability of correct decoding at the relay.

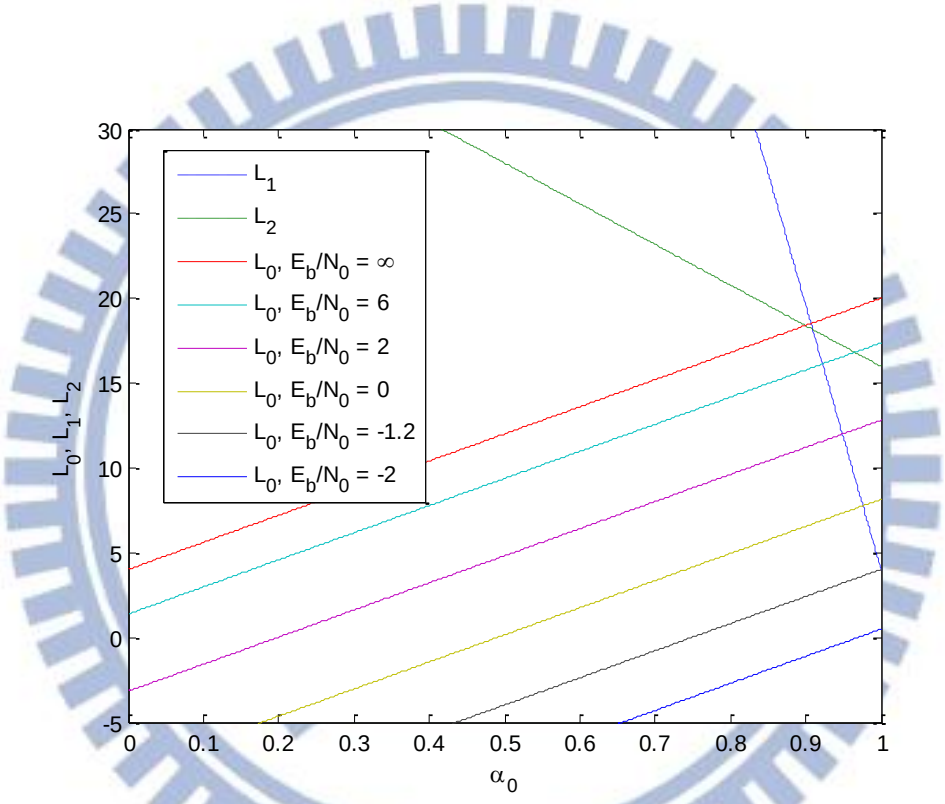

Fig. 6.2. The curves of L_0, L_1 and L_2 for Network-9 with different values of E_b/N_0. (PA-MGEC on S-DRF/RT)

6.3.2 PA-MGEC on S-DRF/Idle

PA-MGEC on S-DRF/Idle is very similar to that on S-DRF/RT. The main different is that $\hat{M}_\Theta(\boldsymbol{\alpha})$ now becomes $\sum_{j\in\tilde{\Theta}} D^{(j)}\alpha_j \left|h_{j,R+1}\right|^2$, which means that the orthogonal-channels of inactive relays will never contribute to $\hat{M}_\Theta(\boldsymbol{\alpha})$. Specifically, (6.23) becomes

$$\begin{aligned}
&\min_{\mathbf{D}\in\hat{\Psi}} \sum_{j\in\tilde{\Theta}}^{R} D^{(j)}\alpha_j \left|\tilde{h}_{j,R+1}\right|^2 + \alpha_0 D_\chi \sum_{j\notin\Theta} \left|h_{0,j}\right|^2 - \hat{\eta}_{R-|\Theta|} \\
&= \begin{cases} \min\left\{4\cdot\alpha_0\cdot 1+16\cdot\alpha_1\cdot 10, 16\cdot\alpha_0\cdot 1+4\cdot\alpha_1\cdot 10\right\}, & \Theta=\{1\} \\ 4\cdot\alpha_0\cdot 1+\alpha_0\cdot 4\cdot 4-\hat{\eta}_1, & \Theta=\varnothing \end{cases}, \\
&= \begin{cases} \min\left\{160-156\alpha_0, 40-24\alpha_0\right\}, & \Theta=\{1\} \\ 20\alpha_0-\hat{\eta}_1, & \Theta=\varnothing \end{cases}
\end{aligned} \tag{6.28}$$

and

$$\begin{aligned}
\boldsymbol{\alpha}^* &= \arg\max_{\boldsymbol{\alpha}} \min_{\Theta\subset\{1,2,\ldots R\}} \left\{ \min_{\mathbf{D}\in\hat{\Psi}} \sum_{j=0}^{R} D^{(j)}\alpha_j \left|\tilde{h}_{j,R+1}\right|^2 + \alpha_0 D_\chi \sum_{j\notin\Theta} \left|h_{0,j}\right|^2 - \hat{\eta}_{R-|\Theta|} \sum_{j=0}^{R}\alpha_j \right\}. \\
&= \arg\max_{\boldsymbol{\alpha}} \min\left\{160-156\alpha_0, 40-24\alpha_0, 20\alpha_0-\hat{\eta}_1\right\}
\end{aligned} \tag{6.29}$$

Define

$$\begin{cases} L_1 = 160-156\alpha_0 \\ L_2 = 40-24\alpha_0 \\ L_0 = 20\alpha_0-\hat{\eta}_1 \end{cases}, \tag{6.30}$$

which are plotted in Fig. 6.3 with different values of E_b/N_0.

To determine the optimal power, according to (6.29), we need to maximize $\min\{L_2, L_1, L_0\}$. As is shown in Fig. 6.3, when $E_b/N_0 \le -1.2$, the optimum occurs at $\alpha_0 = 1$. As the SNR increases such that $E_b/N_0 > -1.2$, the optimal α_0 decreases with SNR, starting from 1 to about 0.91 when $E_b/N_0 \to \infty$ (or $\hat{\eta}_1 \to 0$). Compared with the results for S-DRF/RT, given a fixed $E_b/N_0 > -1.2$, the optimal α_0 in Fig. 6.3 is slightly greater than that in Fig. 6.2. This is due to the fact that the power allocated to the relay will be wasted if the relay fails to decode when S-DF/Idle relaying scheme is adopted. Therefore, more power (compared to S-DRF/RT) should be allocated to source to avoid this power waste.

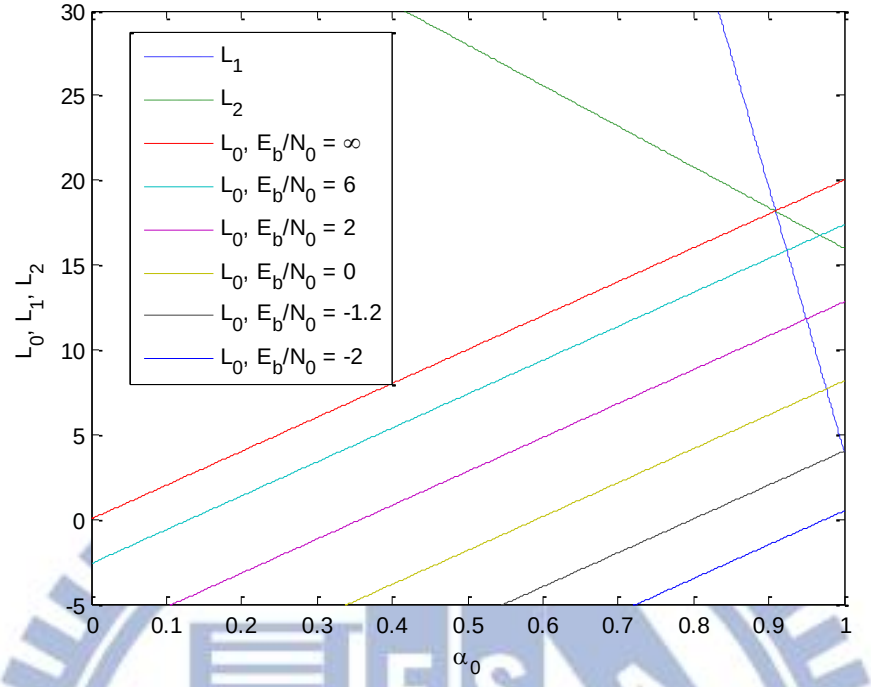

Fig. 6.3. The curves of L_0, L_1 and L_2 for Network-9 with different values of E_b/N_0.

(PA-MGEC on S-DRF/Idle)

6.3.3 PA-MGEC on S-DRF/AF

For S-DRF/AF, (6.24) becomes

$$\hat{M}_{\Theta}(\boldsymbol{\alpha}) + \alpha_0 D_{\chi} \sum_{j \notin \Theta} \left|h_{0,j}\right|^2 - \hat{\eta}_{R-|\Theta|}$$

$$= \min_{\mathbf{D} \in \hat{\Psi}} \left\{ \sum_{j \in \vec{\Theta}} D^{(j)} \alpha_j \left|h_{j,R+1}\right|^2 + \sum_{j \notin \vec{\Theta}} D^{(j)} \frac{\alpha_0 \left|h_{0,j}\right|^2 \alpha_j \left|h_{j,R+1}\right|^2}{\alpha_0 \left|h_{0,j}\right|^2 + \alpha_j \left|h_{j,R+1}\right|^2 + N_0/P_T} \right\}$$

$$+ \alpha_0 D_{\chi} \sum_{j \notin \Theta} \left|h_{0,j}\right|^2 - \hat{\eta}_{R-|\Theta|}$$

$$= \begin{cases} \min\left\{4 \cdot \alpha_0 \cdot 1 + 16 \cdot \alpha_1 \cdot 10, 16 \cdot \alpha_0 \cdot 1 + 4 \cdot \alpha_1 \cdot 10\right\}, & \Theta = \{1\} \\ 4 \cdot \alpha_0 \cdot 1 + 4 \cdot \dfrac{\alpha_0 \cdot 4 \cdot \alpha_1 \cdot 10}{\alpha_0 \cdot 4 + \alpha_1 \cdot 10 + N_0/P_T} + \alpha_0 \cdot 4 \cdot 4 - \hat{\eta}_1, & \Theta = \varnothing \end{cases}$$

$$= \begin{cases} \min\left\{160 - 156\alpha_0, 40 - 24\alpha_0\right\}, & \Theta = \{1\} \\ 20\alpha_0 + \dfrac{160\alpha_0(1-\alpha_0)}{10 - 6\alpha_0 + N_0/P_T} - \hat{\eta}_1, & \Theta = \varnothing \end{cases} . \qquad (6.31)$$

Define

$$\begin{cases} L_1 = 160 - 156\alpha_0 \\ L_2 = 40 - 24\alpha_0 \\ L_0 = 20\alpha_0 + \dfrac{160\alpha_0(1-\alpha_0)}{10 - 6\alpha_0 + N_0/P_T} - \hat{\eta}_1 \end{cases}, \tag{6.32}$$

which are plotted with different values of E_b/N_0 in Fig. 6.4. Note that since what the relay forwards is the same for all these 3 S-DF relaying schemes, L_1 and L_2 in Fig. 6.4 are the same as those for S-DRF/RT and S-DRF/Idle. The main difference is that the curve of L_0 now bends to be concave, though it still shifts up as SNR increases ($\hat{\eta}_1$ decreases).

To determine the optimal power, we need to maximize $\min\{L_0, L_1, L_2\}$. As is shown in Fig. 6.4, when the SNR is very low, e.g., $E_b/N_0 \le -1.2$, the whole curve of L_0 is below both L_1 and L_2, so that $\min\{L_0, L_1, L_2\} = L_0$. The problem turns to optimize L_0 alone. In this case, L_0 is maximized at $\alpha_0 = 1$. (Note that the optimum could be somewhere else for different channel realizations.) As the SNR increases such that $E_b/N_0 > -1.2$, L_0 and L_1 begin to intersect. This intersection is chosen as the optimal power allocation. As the SNR further increases, the optimum moves to the intersection between L_0 and L_2. Observing from Fig. 6.4, the optimal α_0 decreases with SNR, starting from 1 to about 0.8 when $E_b/N_0 \to \infty$ (or $\eta_1 \to 0$).

Not surprisingly, when SNR is low, all power is allocated to source. As the SNR increases, the source power decreases to a final point. This final point $\alpha_0 = 0.8$ is even lower than that for S-DRF/RT or S-DRF/Idle. This is because, in Network-9, the relay uses AF can provide a better equivalent channel than re-transmission through the S-D link.

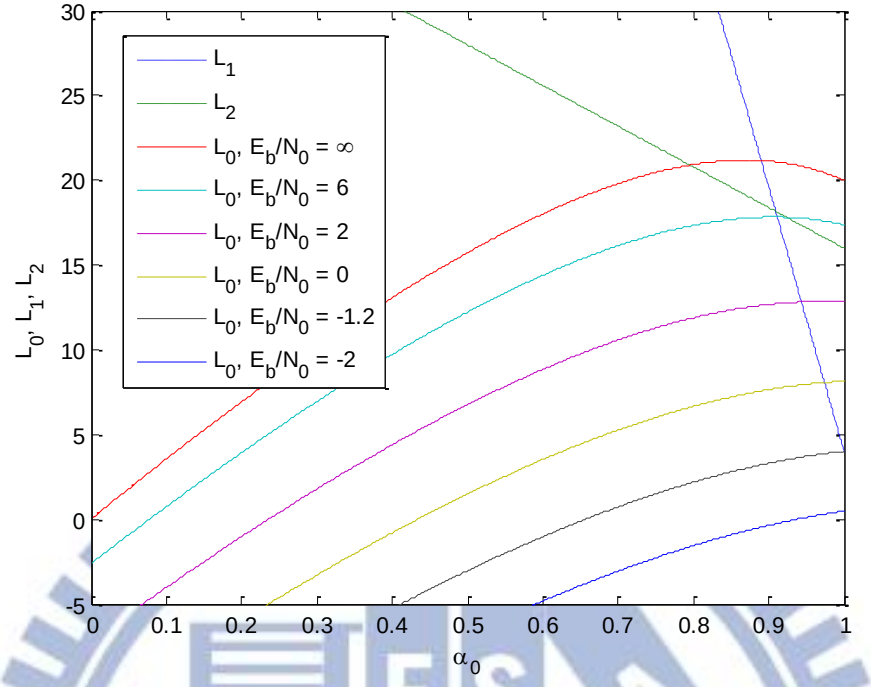

Fig. 6.4. The curves of L_0, L_1 and L_2 for Network-9 with different values of E_b/N_0. (PA-MGEC on S-DRF/AF)

6.4 Numerical Results

This section verifies PA-ABER and PA-MGEC on S-DRF through BER simulation and compares them with PA-EG. In all the following numerical results, we use a half-rate convolutional codes CC(171,133) with $d_f = 10$ and $W_I(d_f) = 33$. The length of the information sequence is $K = 506$ such that the length of the codeword is $N = 1024$. The constellation 16-QAM is used. Note that the total transmit power is calculated as $P_T = E_b \cdot R_C \cdot l$ where E_b is the bit energy, and $R_C = 0.5$ is the channel code rate.

As first, the power allocation and simulation results for examples in Section 6.3 with Network-9 are provided. For S-DRF/RT, the optimal α_0's for both PA-ABER and PA-MGEC are plotted in Fig. 6.5 as well as that for PA-EG. As was predicted in Section 6.3.1, when at low

SNRs, e.g., $E_b/N_0 \le -1.5$, PA-MGEC allocates all power to source, and PA-ABER does so when $E_b/N_0 \le -5$. As the SNR increases, the source power of both methods decline and finally converge to about $\alpha_0 = 0.9$, as $E_b/N_0 \ge 10$. Generally, PA-ABER tends to allocate slightly less power to source. The corresponding BER is given in Fig. 6.6, wherein PA-ABER outperforms PA-MGEC by 0.4 dB at BER of 10^{-5} and PA-EG by 1.1 dB. At high SNRs, PA-ABER and PA-MGEC are expected to have the same performance, although the corresponding BER is too low to be simulated.

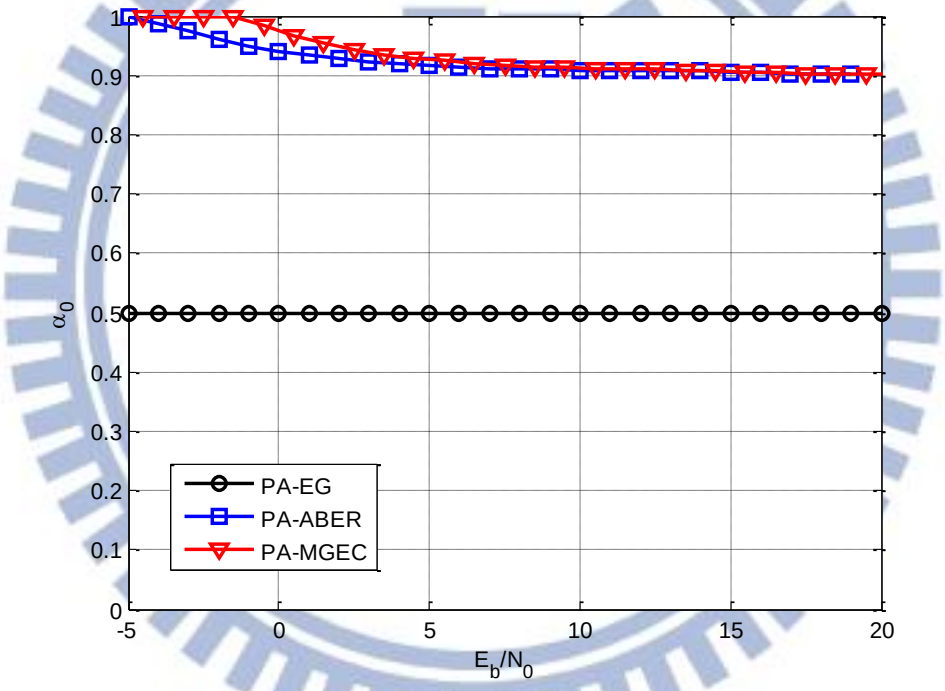

Fig. 6.5. Power allocation results for PA-EG, PA-ABER and PA-MGEC on Network-9 with S-DRF/RT relaying scheme.

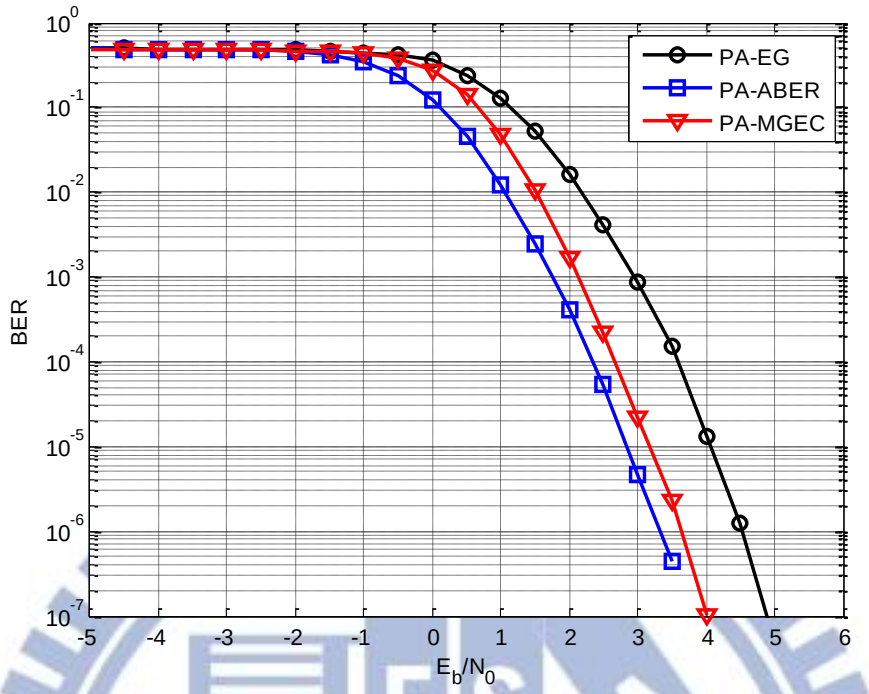

Fig. 6.6. BER simulation results for PA-EG, PA-ABER and PA-MGEC on Network-9 with S-DRF/RT relaying scheme.

For S-DRF/Idle, the optimal α_0's for both PA-ABER and PA-MGEC are plotted in Fig. 6.7 as well as that for PA-EG. As was predicted in Section 6.3.2, when $E_b/N_0 \le -1.5$, PA-MGEC allocates all power to source, and so does PA-ABER. As the SNR increases, the source power of both methods decline and finally converge to about $\alpha_0 = 0.91$, as $E_b/N_0 \ge 10$. Similarly, PA-ABER tends to allocate slightly less power to source than PA-MGEC. Compared with S-DRF/RT, the α_0's in Fig. 6.7 are higher than those in Fig. 6.5 for all $E_b/N_0 > -1.5$. The corresponding BER is given in Fig. 6.8, wherein PA-ABER outperforms PA-MGEC by 0.3 dB and significantly outperform PA-EG with about 2.2 dB gain at BER of 10^{-5}, which is larger than the gain for S-DRF/RT.

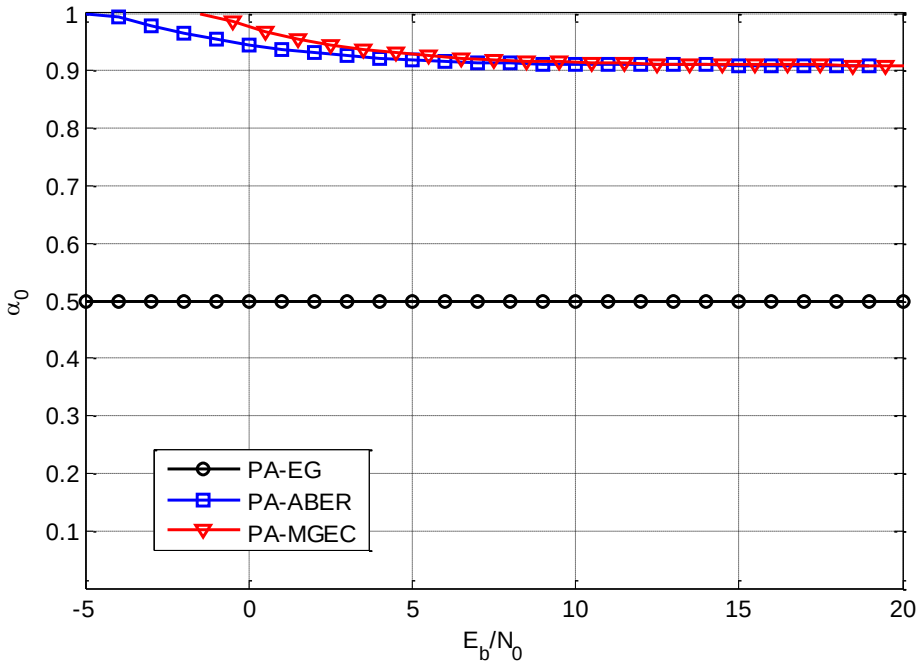

Fig. 6.7. Power allocation results for PA-EG, PA-ABER and PA-MGEC on Network-9 with S-DRF/Idle relaying scheme.

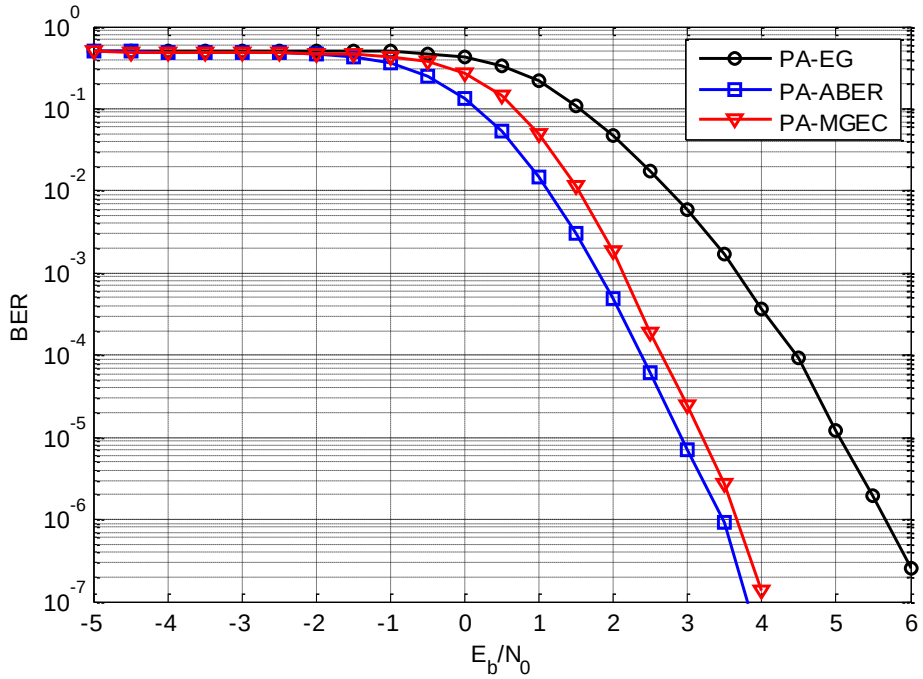

Fig. 6.8. BER simulation results for PA-EG, PA-ABER and PA-MGEC on Network-9 with S-DRF/Idle relaying scheme.

For S-DRF/AF, the power allocation results are plotted in Fig. 6.9. As was predicted in Section 5.3.4, when $E_b/N_0 \le -2$, both method allocate all power to source. As the SNR increases, the source power declines and finally converge to about $\alpha_0 = 0.607$, as $E_b/N_0 \ge 16$. PA-ABER tends to allocate slightly less power to source than PA-MGEC. Compared with S-DRF/RT and S-DF/Idle, the α_0's in Fig. 6.9 are lower than those in Fig. 6.5 and Fig. 6.7. This is because S-DF/AF is even less sensitive to decoding failure at relay. Thus, power allocation tends to put more power on relay for transmitting the packet through the R-D link, which is better than the S-D link. The corresponding BER is given in Fig. 6.10, wherein PA-ABER outperforms PA-MGEC with 0.5 dB at BER of 10^{-5} and outperforms PA-EG with about 0.7 dB gain at BER of 10^{-5}.

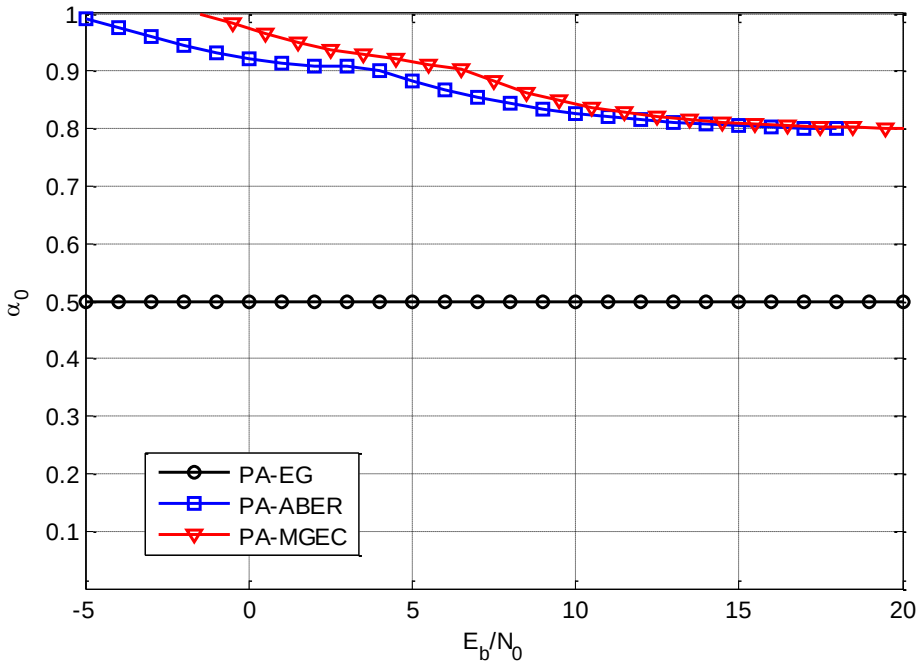

Fig. 6.9. Power allocation results for PA-EG, PA-ABER and PA-MGEC on Network-9 with S-DRF/AF relaying scheme.

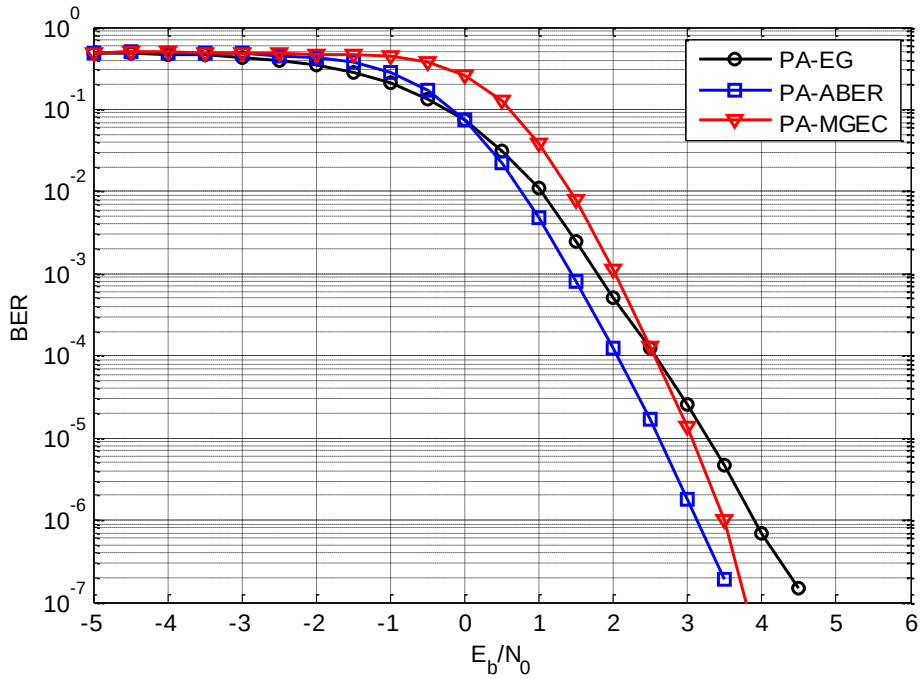

Fig. 6.10. BER simulation results for PA-EG, PA-ABER and PA-MGEC on Network-9 with S-DRF/AF relaying scheme.

For more relays, Network-14 with 2 relays and setup in Table VII with $\mu^{(0)} = \mu_G$, $\mu^{(1)} = \mu_A$ and $\mu^{(2)} = \mu_B$ (see Fig. 6.1) is considered. For S-DRF/RT, the power allocation results are plotted in Fig. 6.11. In Fig. 6.11, the source power ratio is 1 when $E_b/N_0 \le -2$ for both schemes, and then decays as the SNR increase. The power allocation results of PA-ABER and PA-MGEC are rather close. Note that in this example, relay 1 is less preferable than relay 2 so that only little power is allocated to relay 1. The reason is simply that the S-R link to relay 1 is not as good as that to relay 2, which leads to a higher probability of decoding failure at relay 1 (compared to relay 2). The BER performance is provided in Fig. 6.12, where PA-ABER performs best, closely followed by PA-MGEC. PA-ABER and PA-MGEC outperform PA-EG by 1 and 0.8 dB at BER of 10^{-5}, respectively.

For S-DRF/Idle, the power allocation results and the BER performance are provided in Fig. 6.13 and Fig. 6.14, respectively. Similarly, both methods tend to be more conservative on allocating power to relays than those for S-DRF/RT, and the gains in BER are larger than those for SDRF/RT because the proposed methods suffer from less power waste. For S-DF/AF, the results are provided in Fig. 6.15 and Fig. 6.16.

Table VII. Network setup for Chapter 6

Networks	S-D link	S-R link	R-D link
Network-14	$\left\|h_{0,3}\right\|^2 = \left\|h_{0,3}^{(1)}\right\|^2 = \left\|h_{0,3}^{(2)}\right\|^2 = 1$	$\left\|h_{0,1}\right\|^2 = 2$, $\left\|h_{0,2}\right\|^2 = 4$	$\left\|h_{1,3}\right\|^2 = 10$, $\left\|h_{2,3}\right\|^2 = 5$
Network-15	$\left\|h_{0,3}\right\|^2 = \left\|h_{0,3}^{(1)}\right\|^2 = \left\|h_{0,3}^{(2)}\right\|^2 = 1$	$\left\|h_{0,1}\right\|^2 = 4$, $\left\|h_{0,2}\right\|^2 = 4$	$\left\|h_{1,3}\right\|^2 = 2$, $\left\|h_{2,3}\right\|^2 = 2$

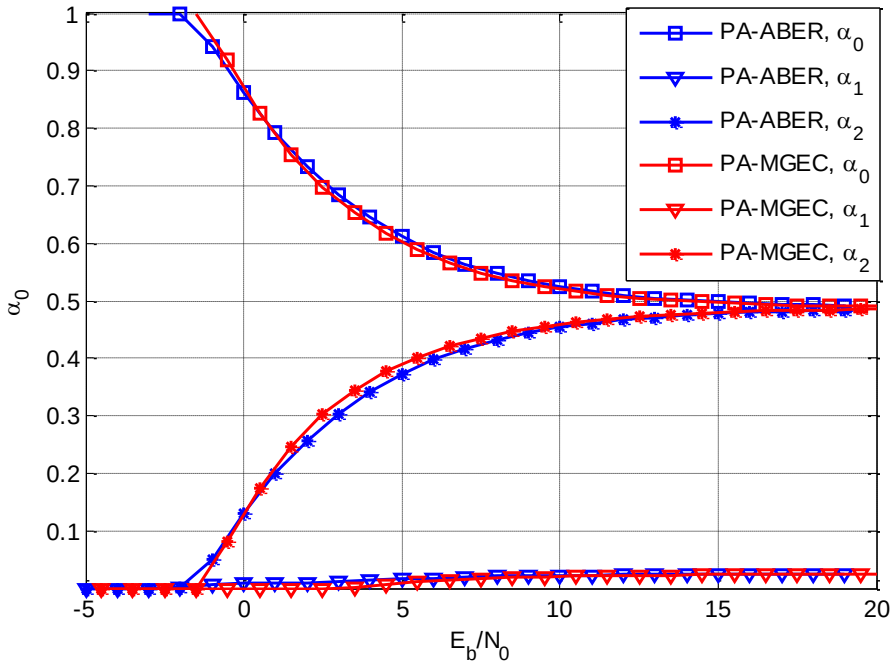

Fig. 6.11. Power allocation results on Network-14 with S-DRF/RT relaying scheme.

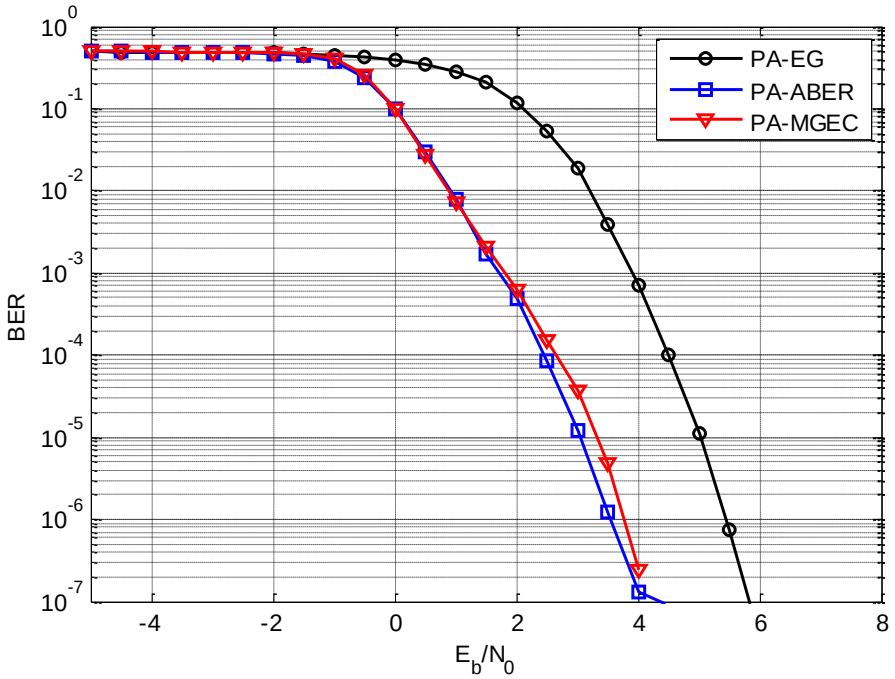

Fig. 6.12. BER simulation results on Network-14 with S-DRF/RT relaying scheme.

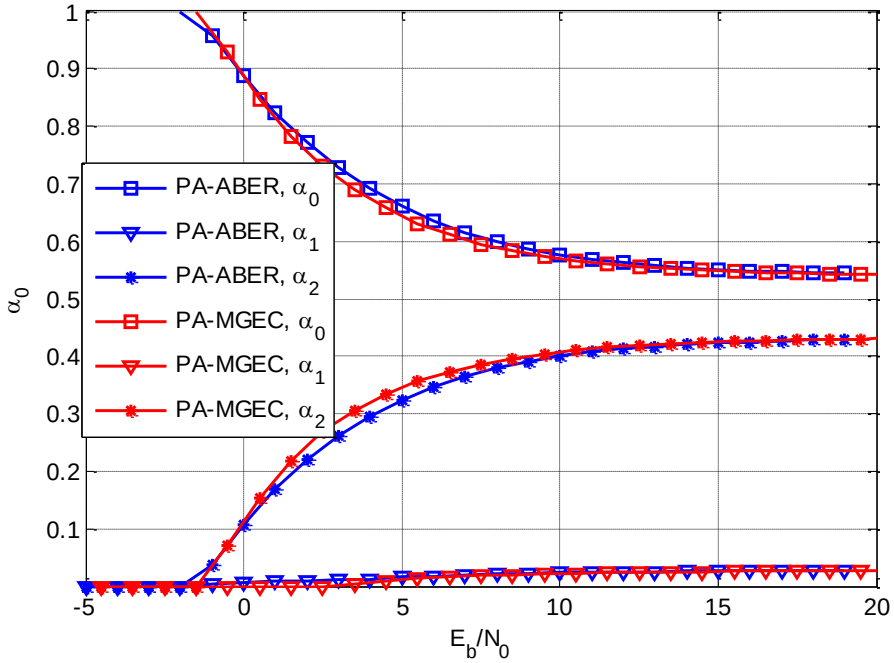

Fig. 6.13. Power allocation results on Network-14 with S-DRF/Idle relaying scheme.

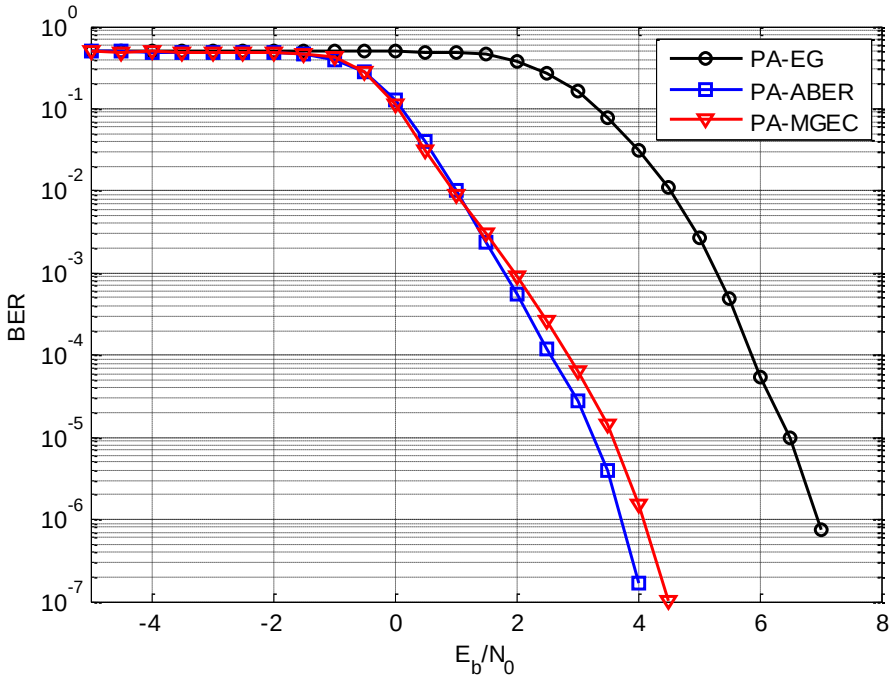

Fig. 6.14. BER simulation results on Network-14 with S-DRF/Idle relaying scheme.

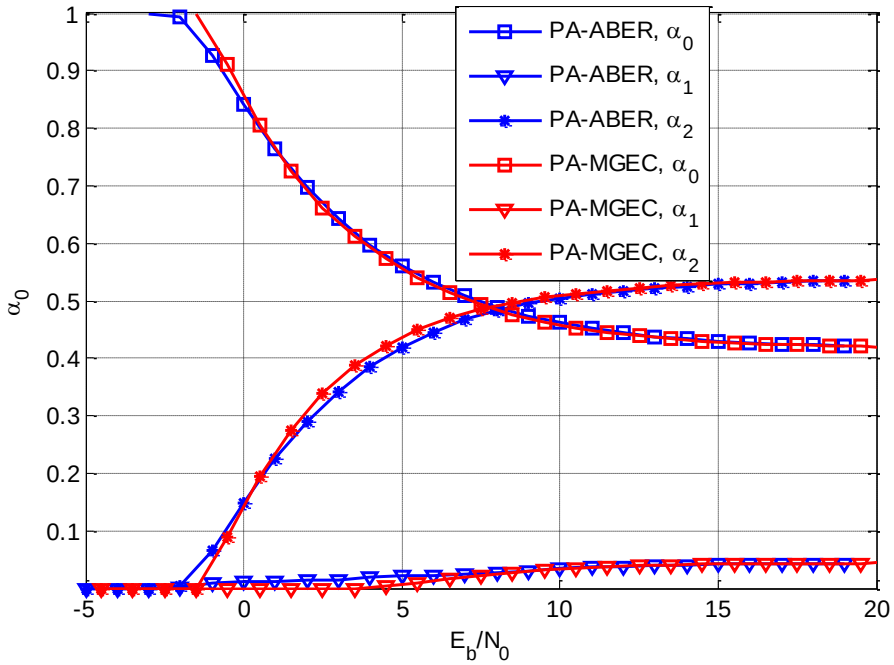

Fig. 6.15. Power allocation results on Network-14 with S-DRF/AF relaying scheme.

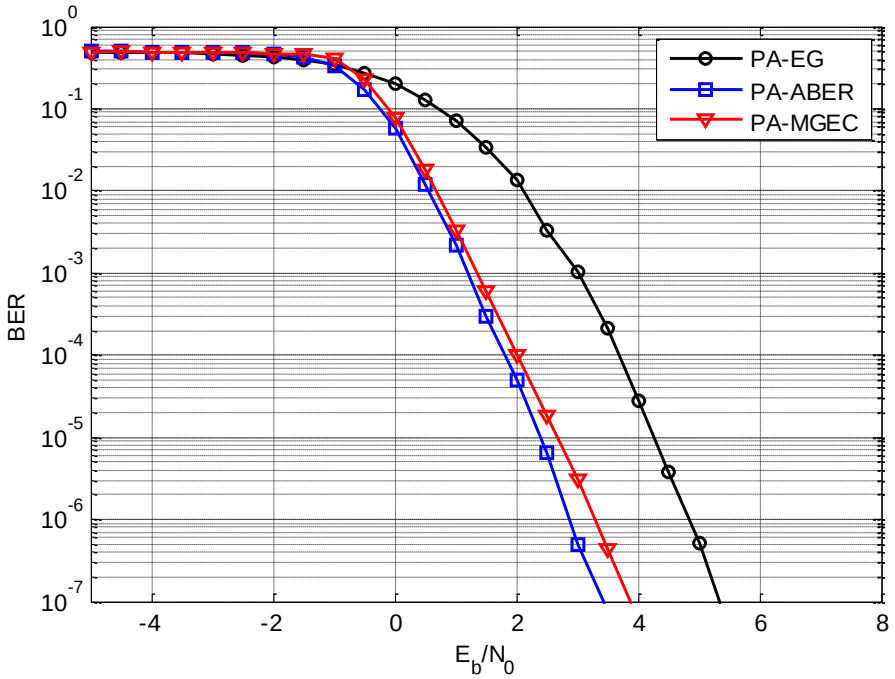

Fig. 6.16. BER simulation results on Network-14 with S-DRF/AF relaying scheme.

Another results for the 2-relay network is provided with setup of Network-15 in Table VII. In Network-15, the two relays have the same power gain on S-R links, and so are their R-D links. The mappers used are the same as those in Network-14. The power allocation results and BER performance are given in Fig. 6.17 and Fig. 6.18 for S-DF/AF. Observing from these figures, PA-ABER is still the best, and our proposed methods still provide non-trivial gain to PA-EG. Note that, although power gains of the S-R and R-D links of relay 1 and relay 2 are the same, the mappers used are different. Therefore, the resulting α_1 and α_2 are not the same. (For more power allocation examples, please refer to [50].)

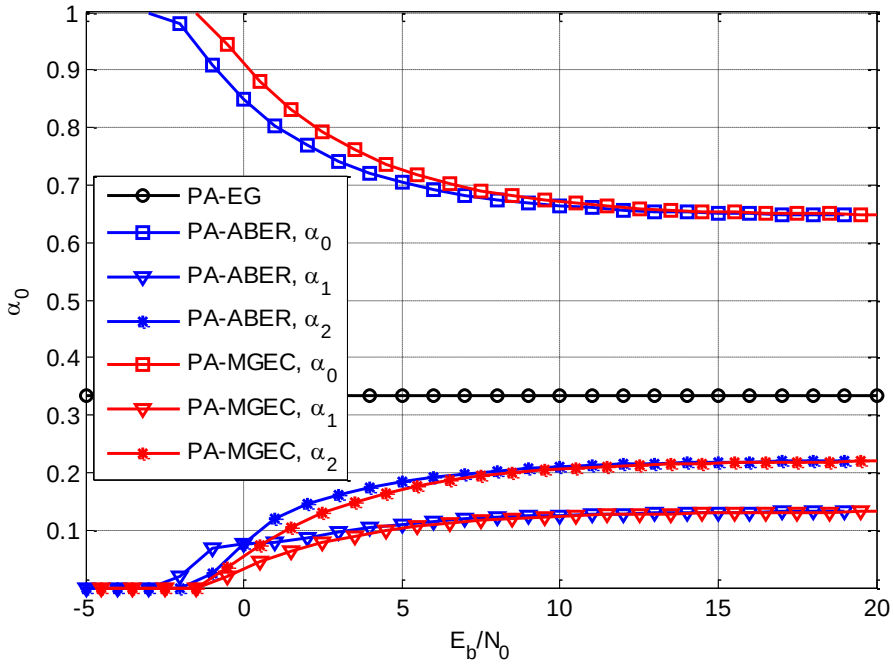

Fig. 6.17. Power allocation results on Network-15 with S-DRF/AF relaying scheme.

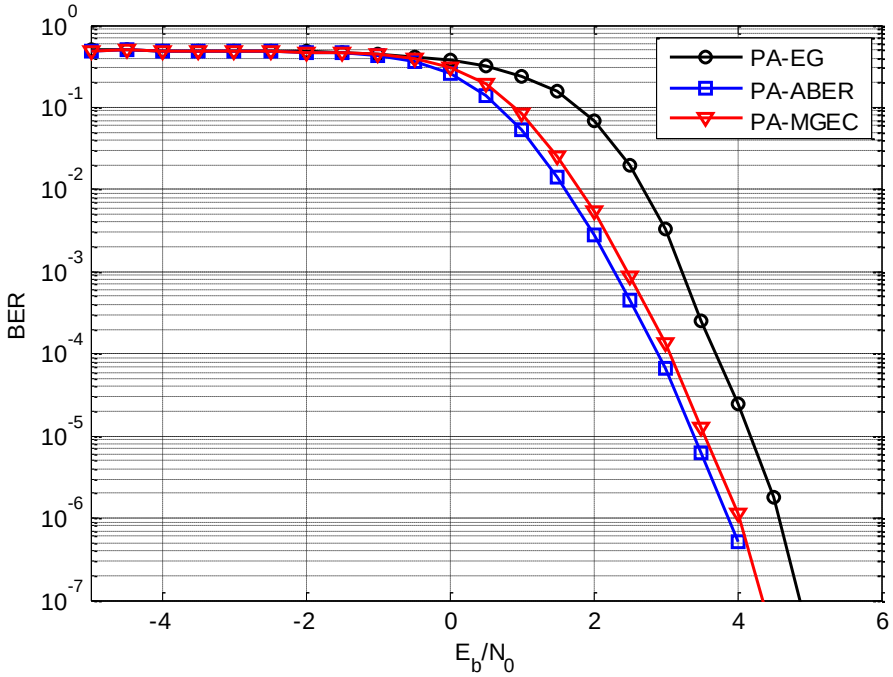

Fig. 6.18. BER simulation results on Network-15 with S-DRF/AF relaying scheme.

6.5 Summary

This Chapter extends the results in Chapter 5 to BICM-coded cooperative networks with S-DRF relays. The DRF relays are allowed to change the mappers before forwarding so as to obtain an addition remapping gain. We discuss how PA-ABER and PA-MGEC are applied with remapping. Examples are provided to demonstrate how power is allocated, and numerical results confirm that the proposed method outperform PA-EG with large margins for different network setups.

Chapter 7

Conclusions

This dissertation investigates the performance analysis and power allocation for BICM-coded cooperative network.

For the performance analysis, this dissertation considers S-DF relaying over Nakagami-*m* fading channels. Unlike the existing works which adopt an un-coded, symbol-by-symbol forwarding strategy. This dissertation considers the BICM-coded cooperative relaying network with packet-by-packet forwarding strategy. Two types of S-DF schemes are investigated: S-DF/RT and S-DF/Idle. The analysis of BER at the destination is proposed and the diversity orders of the network is derived for both fast-fading and block-fading channels. Simulation results are given to show the effectiveness of our results in different modulations, number of relays and channel conditions.

For the power allocation, 4 relaying modes are considered: AF, S-DF/Idle, S-DF/RT and S-DF/AF. Based on perfect channel state information, power is allocated to minimize the BER at the destination. For AF, the equivalent channel is adopted as the cost function for optimization. For S-DF, two power allocation methods are proposed. PA-ABER employs an approximate BER as a cost function, which is then proved to be convex for each relaying mode and then optimized

through the gradient method. PA-MGEC transforms PA-ABER to a max-min problem and then adopts MGEC as the cost function. Specific solutions are proposed for optimizing the MGEC of the 3 relaying schemes. Furthermore, PA-ABER and PAMGEC are shown to be applicable to DRF relays, which are allowed to choose different constellation mappings from that of source so as to obtain a remapping gain. Numerical results show that both of the proposed methods outperform the equal gain power allocation by large margins with or without remapping.

Some possible extensions and future research topics are addressed in the following. The performance analysis can be further extended to different relaying schemes (S-DF/AF, cooperative H-ARQ), multi-carrier systems (OFDM), different network topologies (multi-hops, inter-relay links). The methodology used in the power allocation can be applied to relay selections, cooperative H-ARQ, or mapping design for DRF relays.

Appendixes

Appendix A: Proof of Lemma-1

Starting from the expectation in (3.6), we have

$$E_h\left[\exp\left[\left(-s+s^2\right)ah^2\right]\right]=\int_0^\infty p(h)e^{\left(-s+s^2\right)ah^2}dh$$
$$=\int_0^\infty \frac{2}{\Gamma(m)}\left(\frac{m}{\Omega}\right)^m h^{2m-1}e^{-\frac{mh^2}{\Omega}}e^{\left(-s+s^2\right)ah^2}dh. \quad (1)$$
$$=\frac{2}{\Gamma(m)}\left(\frac{m}{\Omega}\right)^m\int_0^\infty h^{2m-1}e^{-\left(\frac{m}{\Omega}-\left(-s+s^2\right)a\right)h^2}dh$$

According to [47] (pp. 337), the remaining integral can be exactly evaluated by using the formula

$$\int_0^\infty x^m\exp\left[-\beta x^n\right]dx=\frac{\Gamma(\gamma)}{n\beta^\gamma} \quad (2)$$

with $\gamma=(m+1)/n$, providing that $\beta>0$. Therefore, (1) becomes

$$\left(1-\left(-s+s^2\right)\frac{\Omega}{m}a\right)^{-m} \quad (3)$$

with the ROC determined by the necessary condition $\beta>0$, which leads to

$$s^2-s<\frac{m}{\Omega a}. \quad (4)$$

Using the method of competing the square, the ROC is

$$\frac{1}{2}-\sqrt{\frac{m}{\Omega a}+\frac{1}{4}}<s<\frac{1}{2}+\sqrt{\frac{m}{\Omega a}+\frac{1}{4}}. \quad (5)$$

Q.E.D.

Appendix B: Proof of Lemma-2

As $x \to \infty$, we first ignore the '1' in the product of (3.33) so that

$$\lim_{x\to\infty} \int_{-\infty}^{\infty} \prod_{j=0}^{R} \left(1 + a_j x\left(t^2 + \frac{1}{4}\right)\right)^{-b_j} \frac{dt}{t^2 + \frac{1}{4}}$$

$$= \int_{-\infty}^{\infty} \prod_{j=0}^{R} \left(a_j x\left(t^2 + \frac{1}{4}\right)\right)^{-b_j} \frac{dt}{t^2 + \frac{1}{4}} \quad . \tag{6}$$

$$= \prod_{j=0}^{R} a_j^{-b_j} \cdot \int_{-\infty}^{\infty} \left(t^2 + \frac{1}{4}\right)^{-\left(\sum_{j=0}^{R} b_j + 1\right)} dt \cdot x^{-\sum_{j=0}^{R} b_j}$$

Using (3.20) to evaluate the remaining integration in (6) yields

$$\lim_{x\to\infty} \int_{-\infty}^{\infty} \prod_{j=0}^{R} \left(1 + a_j x\left(t^2 + \frac{1}{4}\right)\right)^{-b_j} \frac{dt}{t^2 + \frac{1}{4}} = 4\pi \prod_{j=0}^{R} a_j^{-b_j} \cdot \frac{\left(\sum_{j=0}^{R} b_j - 1\right)!!}{\left(\sum_{j=0}^{R} b_j\right)!!} 2^{2\sum_{j=0}^{R} b_j - 1} \cdot x^{-\sum_{j=0}^{R} b_j} . \tag{7}$$

Appendix C: Concavity of $M_{AF}(\boldsymbol{\alpha})$

The concavity of $M_{AF}(\boldsymbol{\alpha})$ can be directly proved through Hessian matrix []. However, the Hessian matrix of $M_{AF}(\boldsymbol{\alpha})$ could be large and cumbersome, especially when R is large. This appendix provides an alternative method.

We would like to show that each term in the summation of (5.7) is concave so that the sum of concave functions remains concave. Since the first term $\alpha_0 \left|h_{0,R+1}\right|^2$ is linear to $\boldsymbol{\alpha}$, it is also concave to $\boldsymbol{\alpha}$. Thus, the problem becomes to show that each term in the summation of (5.7) is concave. It is equivalent to prove a sub-problem: Prove the concavity of

$$\frac{\alpha_j \left|h_{j,R+1}(k)\right|^2 \alpha_0 \left|h_{0,j}(k)\right|^2}{\left|h_{j,R+1}(k)\right|^2 \alpha_j + \alpha_0 \left|h_{0,j}(k)\right|^2 + N_0/P_T} \tag{8}$$

under the constraint $\alpha_0 + \alpha_j = 1$ [5]. For simplicity, re-write (8) as

$$h(\alpha) = \left[a\alpha^{-1} + b(1-\alpha)^{-1} + \varepsilon ab\alpha^{-1}(1-\alpha)^{-1} \right]^{-1}, \tag{9}$$

where $\alpha = \alpha_0$, $a = \left| h_{0,j}(k) \right|^{-2}$, $b = \left| h_{j,R+1}(k) \right|^{-2}$ and $\varepsilon = N_0 / P_T$. Taking the first derivative of h yields

$$\begin{aligned} \frac{\partial h}{\partial \alpha} = & \left[a\alpha^{-1} + b(1-\alpha)^{-1} + \varepsilon ab\alpha^{-1}(1-\alpha)^{-1} \right]^{-2} \\ & \cdot \left[+a\alpha^{-2} - b(1-\alpha)^{-2} + \varepsilon ab\alpha^{-2}(1-\alpha)^{-1} - \varepsilon ab\alpha^{-1}(1-\alpha)^{-2} \right] \end{aligned}, \tag{10}$$

and the second derivative is

$$\begin{aligned} \frac{\partial^2 h}{\partial \alpha^2} = & \frac{\partial}{\partial \alpha} \left[a\alpha^{-1} + b(1-\alpha)^{-1} + \varepsilon ab\alpha^{-1}(1-\alpha)^{-1} \right]^{-2} \\ & \cdot \left[a\alpha^{-2} - b(1-\alpha)^{-2} + \varepsilon ab\alpha^{-2}(1-\alpha)^{-1} - \varepsilon ab\alpha^{-1}(1-\alpha)^{-2} \right] \\ = & 2\left[a\alpha^{-1} + b(1-\alpha)^{-1} + \varepsilon ab\alpha^{-1}(1-\alpha)^{-1} \right]^{-3} \\ & \cdot \left[a\alpha^{-2} - b(1-\alpha)^{-2} + \varepsilon ab\alpha^{-2}(1-\alpha)^{-1} - \varepsilon ab\alpha^{-1}(1-\alpha)^{-2} \right]^2 \\ & - 2\left[a\alpha^{-1} + b(1-\alpha)^{-1} + \varepsilon ab\alpha^{-1}(1-\alpha)^{-1} \right]^{-2} \\ & \cdot \left[a\alpha^{-3} + b(1-\alpha)^{-3} + \varepsilon ab\alpha^{-3}(1-\alpha)^{-1} + \varepsilon ab\alpha^{-1}(1-\alpha)^{-3} - \varepsilon ab\alpha^{-2}(1-\alpha)^{-2} \right] \\ = & 2\left[a\alpha^{-1} + b(1-\alpha)^{-1} + \varepsilon ab\alpha^{-1}(1-\alpha)^{-1} \right]^{-2} \\ & \cdot \left\{ \begin{array}{l} \left[a\alpha^{-1} + b(1-\alpha)^{-1} + \varepsilon ab\alpha^{-1}(1-\alpha)^{-1} \right]^{-1} \\ \cdot \left[a\alpha^{-2} - b(1-\alpha)^{-2} + \varepsilon ab\alpha^{-2}(1-\alpha)^{-1} - \varepsilon ab\alpha^{-1}(1-\alpha)^{-2} \right]^2 \\ - \left[a\alpha^{-3} + b(1-\alpha)^{-3} + \varepsilon ab\alpha^{-3}(1-\alpha)^{-1} + \varepsilon ab\alpha^{-1}(1-\alpha)^{-3} - \varepsilon ab\alpha^{-2}(1-\alpha)^{-2} \right] \end{array} \right\}. \end{aligned} \tag{11}$$

Since $2\left[a\alpha^{-1} + b(1-\alpha)^{-1} + \varepsilon ab\alpha^{-1}(1-\alpha)^{-1} \right]^{-2}$ is always positive, the problem becomes to determine the sign of the other term. With some arrangement, it becomes

[5] Note that if h is concave in the region $\alpha_0 + \alpha_j = 1$, h is also concave in $\alpha_0 + \alpha_j = \varepsilon$ for any $0 < \varepsilon < 1$.

$$\frac{\alpha(1-\alpha)}{a(1-\alpha)+b\alpha+\varepsilon ab}\left[\frac{a}{\alpha^2}-\frac{b}{(1-\alpha)^2}+\frac{\varepsilon ab}{\alpha^2(1-\alpha)}-\frac{\varepsilon ab}{\alpha(1-\alpha)^2}\right]^2$$
$$-\frac{a}{\alpha^3}-\frac{b}{(1-\alpha)^3}-\frac{\varepsilon ab}{\alpha^3(1-\alpha)}-\frac{\varepsilon ab}{\alpha(1-\alpha)^3}+\frac{\varepsilon ab}{\alpha^2(1-\alpha)^2}$$
$$=\frac{\alpha(1-\alpha)}{a(1-\alpha)+b\alpha+\varepsilon ab}\left[\frac{a(1-\alpha)^2-b\alpha^2+\varepsilon ab(1-\alpha)-\varepsilon ab\alpha}{\alpha^2(1-\alpha)^2}\right]^2$$
$$-\frac{a(1-\alpha)^3+b\alpha^3+\varepsilon ab(1-\alpha)^2+\varepsilon ab\alpha^2-\varepsilon ab\alpha(1-\alpha)}{\alpha^3(1-\alpha)^3}$$
$$=\frac{1}{a(1-\alpha)+b\alpha+\varepsilon ab}\frac{\left[a(1-\alpha)^2-b\alpha^2+\varepsilon ab(1-\alpha)-\varepsilon ab\alpha\right]^2}{\alpha^3(1-\alpha)^3}$$
$$-\frac{a(1-\alpha)^3+b\alpha^3+\varepsilon ab(1-\alpha)^2+\varepsilon ab\alpha^2-\varepsilon ab\alpha(1-\alpha)}{\alpha^3(1-\alpha)^3}$$
$$=\frac{1}{a(1-\alpha)+b\alpha+\varepsilon ab}\frac{1}{\alpha^3(1-\alpha)^3}$$
$$\left\{\begin{array}{l}\left[a(1-\alpha)^2-b\alpha^2+\varepsilon ab(1-\alpha)-\varepsilon ab\alpha\right]^2\\ -\left[a(1-\alpha)^3+b\alpha^3+\varepsilon ab(1-\alpha)^2+\varepsilon ab\alpha^2-\varepsilon ab\alpha(1-\alpha)\right]\cdot\left[a(1-\alpha)+b\alpha+\varepsilon ab\right]\end{array}\right\}. \qquad (12)$$

Again, because both $\alpha^3(1-\alpha)^3$ and $a(1-\alpha)+b\alpha+\varepsilon ab$ are always non-negative in the region $0\le\alpha\le1$, the problem further reduced to the determination of the sign of the other term, which is

$$\left[a(1-\alpha)^2-b\alpha^2+\varepsilon ab(1-\alpha)-\varepsilon ab\alpha\right]^2$$
$$-\left[a(1-\alpha)^3+b\alpha^3+\varepsilon ab(1-\alpha)^2+\varepsilon ab\alpha^2-\varepsilon ab\alpha(1-\alpha)\right]\cdot\left[a(1-\alpha)+b\alpha+\varepsilon ab\right]$$
$$=a^2(1-\alpha)^4+b^2\alpha^4+\varepsilon^2a^2b^2(1-\alpha)^2+\varepsilon^2a^2b^2\alpha^2-2ab\alpha^2(1-\alpha)^2+2\varepsilon a^2b(1-\alpha)^3$$
$$-2\varepsilon a^2b\alpha(1-\alpha)^2-2\varepsilon ab^2\alpha^2(1-\alpha)+2\varepsilon ab^2\alpha^3-2\varepsilon^2a^2b^2\alpha(1-\alpha)$$
$$-\left[\begin{array}{l}a^2(1-\alpha)^4+ab\alpha(1-\alpha)^3+\varepsilon a^2b(1-\alpha)^3+ab\alpha^3(1-\alpha)+b^2\alpha^4+\varepsilon ab^2\alpha^3\\ +\varepsilon a^2b(1-\alpha)^3+\varepsilon ab^2\alpha(1-\alpha)^2+\varepsilon^2a^2b^2(1-\alpha)^2+\varepsilon a^2b\alpha^2(1-\alpha)+\varepsilon ab^2\alpha^3\\ +\varepsilon^2a^2b^2\alpha^2-\varepsilon a^2b\alpha(1-\alpha)^2-\varepsilon ab^2\alpha^2(1-\alpha)-\varepsilon^2a^2b^2\alpha(1-\alpha)\end{array}\right]$$
$$=-2ab\alpha^2(1-\alpha)^2-\varepsilon a^2b\alpha(1-\alpha)^2-\varepsilon ab^2\alpha^2(1-\alpha)-\varepsilon^2a^2b^2\alpha(1-\alpha)$$
$$-ab\alpha(1-\alpha)^3-ab\alpha^3(1-\alpha)-\varepsilon ab^2\alpha(1-\alpha)^2-\varepsilon a^2b\alpha^2(1-\alpha). \qquad (13)$$

Since $0\le\alpha\le1$, all terms in the last row of (13) are non-positive, implying that the second de-

rivative of h is non-positive. Thus, (8) is a concave function of α_0. (Note that with exchanging the roles between α_0 and α_j, e.g., $\alpha_j = \alpha$ and $\alpha_0 = 1-\alpha$, the same result for α_j can also be proved.) Therefore, $M_{AF}(\boldsymbol{\alpha})$, which is the sum of concave functions, is also concave. Q.E.D.

Appendix D: Convexity of $G(\boldsymbol{\alpha})$

To show the convexity, first re-write $G(\boldsymbol{\alpha}) = \sum_{\Theta \subset \{1,2,\ldots,R\}} F_\Theta(\boldsymbol{\alpha})$ and $F_\Theta(\boldsymbol{\alpha}) = h(q_1, q_2) = q_1 \cdot q_2$, where $q_1 = g_\Theta$ and $q_2 = \prod_{j=0}^{R} KW_I(d_f) N_\chi^{d_f} g_j$. We aim to show that $F_\Theta(\boldsymbol{\alpha})$ is convex for any Θ, and so is $G(\boldsymbol{\alpha})$ which is a sum of convex functions. According to [80], $F_\Theta(\boldsymbol{\alpha})$ is convex if (a) h is convex in each argument, (b) h is non-decreasing in each argument and (c) both q_1 and q_2 are convex. Firstly, (a) and (b) can be proved to be true by evaluating the first and second derivatives of h w.r.t. q_1 and q_2. Now consider the convexity of q_1 and q_2. According to [80], a function $S(T(\boldsymbol{\alpha}))$ is convex if S is convex non-increasing and T is concave. Define $S(x) = a_1 x^{-a_2/2} e^{-a_3 x}$. By evaluating the first and second derivatives of S, it can be shown that S is convex non-increasing in the region $x > 0$ for any $a_1 > 0$, $a_3 > 0$ and any positive integer a_2. Let $T(\boldsymbol{\alpha}) = M_\Theta(\boldsymbol{\alpha})$. In S-DF/RT, we have

$$M_\Theta(\boldsymbol{\alpha}) = \sum_{j=0}^{R} \alpha_j \left| \tilde{h}_{j,R+1} \right|^2, \tag{14}$$

which is the minimum of linear functions of $\boldsymbol{\alpha}$, is positive and convex. Since we can write $q_1 = S(T(\boldsymbol{\alpha}))$ by properly choosing a_1, a_2 and a_3, q_1 is convex. Similarly, q_2 can also be proved convex by letting $T(\boldsymbol{\alpha}) = \alpha_0$.

Appendix E: Proof of Lemma-3

Since $D_1^{(j)} \le D_2^{(j)}$ for all j, one has

$$\mathbf{D}_1^T \boldsymbol{\alpha} = \sum_{j=0}^{R} D_1^{(j)} \alpha_j \le \sum_{j=0}^{R} D_2^{(j)} \alpha_j = \mathbf{D}_2^T \boldsymbol{\alpha}, \tag{15}$$

for any $\boldsymbol{\alpha}$ with non-negative entries, and thus,

$$\hat{M}(\boldsymbol{\alpha}) = \min_{\mathbf{D} \in \Psi} \mathbf{D}^T \boldsymbol{\alpha} = \min_{\mathbf{D} \in \{\Psi \setminus \mathbf{D}_2\}} \mathbf{D}^T \boldsymbol{\alpha}. \tag{16}$$

One can remove $\mathbf{D}_2^T$ from $\overline{\Psi}$ without changing $\hat{M}(\boldsymbol{\alpha})$. Q.E.D.

Bibliography

[1] W. C. Y. Lee, *Mobile Communications Engineering*, McGrawHill, 1998.

[2] T. S. Rappaport, *Wireless Communications: Principles and Practice*, Prentice Hall, 1996.

[3] D. Tse and P. Viswanath, *Fundamentals of Wireless Communication*. New York: Cambridge University Press, 2005.

[4] John G. Proakis, *Digital Communications*, 4th edition, McGraw-Hill, 2001.

[5] G. J. Foschini Jr., "Layered space-time architecture for wireless communication in a fading environment when using multi-element antennas," *Bell Labs. Tech. J.*, vol. 2, pp. 41–59, 1996.

[6] I. E. Telatar, "Capacity of multi-antenna gaussian channels," *Europ. Trans. Telecommu.*, vol. 10, pp. 585–595, Nov./Dec. 1999.

[7] V. Tarokh, H. Jafarkhani, and A. R. Calderbank, "Space-time block code from orthogonal designs," *IEEE Trans. Inform. Theory*, vol. 45, pp. 1456–1467, July 1999.

[8] G. Foschini, G. Golden, R. Valenzuela, and P. Wolniansky, "Simplified processing for high spectal efficiency wireless communication employing multi-element arrays," *IEEE J. Select. Areas Commun.*, vol. 17, pp. 1841–1852, Nov. 1999.

[9] R. Heath, Jr. and A. Paulraj, "Switching between multiplexing and diversity based on constellation distance," in *Proc. Allerton Conf. Communication, Control and Computing*, Oct. 2000.

[10] L. Zheng and D. N. C. Tse, "Diversity and multiplexing: A fundamental tradeoff in multiple-antenna channels," *IEEE Trans. Inf. Theory*, vol. 49, no. 5, pp. 1073–1096, May 2003.

[11] A. Sendonaris, E. Erkip and B. Aazhang, "User cooperation diversity—Part I: System description," *IEEE Trans. on Commun.*, vol. 51, pp. 1927-1938, Nov. 2003.

[12] A. Sendonaris, E. Erkip and B. Aazhang, "User cooperation diversity—Part II: Implementation aspects and performance analysis," *IEEE Trans. on Commun.*, vol. 51, pp. 1939-1948, Nov. 2003.

[13] V. Emamian and M. Kaveh, “Combating shadowing effects for systems with transmitter diversity by using collaboration among mobile users,” in *Proc. Int. Symp. Communications, (ISC’01)*, Taiwan, R.O.C., Nov. 2001, pp. 105.1–105.4.

[14] H. Yanikomeroglu, “Fixed and mobile relaying technologies for cellular networks,” *in Proc. 2ndWorkshop on Applications and Services inWireless Networks (ASWN’02)*, Paris, France, July 2002, pp. 75–81.

[15] J. N. Laneman and G. W. Wornell, “Distributed space-time coded protocols for exploiting cooperative diversity in wireless networks,” *IEEE Trans. on Inform. Theory*, vol. 49, pp. 2415-2425, Oct. 2003.

[16] J. N. Laneman, D. N. C. Tse and G. W. Wornell, “Cooperative diversity in wireless networks: Efficient protocols and outage behavior,” *IEEE Trans. on Inform. Theory*, vol. 50, pp. 3062-3080, Dec. 2004.

[17] J. N. Laneman and G. W. Wornell, “Exploiting distributed spatial diversity in wireless networks,”in *Proc. 40th Allerton Conf. Communication, Control, and Computing (Allerton’00)*, Allerton Park, IL, Sept. 2000, pp. 775–785.

[18] M. Grossglauser and D. Tse, “Mobility increases the capacity of ad-hoc wireless networks,” in *Proc. IEEE Conf. Computer Communications (INFOCOM’01)*, Anchorage, AK, April 2001, pp. 1360–1369.

[19] 3GPP TS 36.300 V9.2.0 (2009-12), "Evolved Universal Terrestrial Radio Access (E-UTRA) and Evolved Universal Terrestrial Radio Access Network (E-UTRAN); Overall description; Stage 2 (Release 9)".

[20] Part 16: Air Interface for Fixed and Mobile Broadband Wireless Access Systems: Multihop Relay Specification, IEEE Std. P802.16j/D9, Feb. 2009.

[21] B. Q. V.-Nguyen, T. Q. Duong and N. N. Tran, “Ergodic capacity of cooperative network using adaptive transmission and selection combining,” in *Proc. IEEE ICSPCS 2009*, pp.1-6, Sept. 2009.

[22] K. G. Seddik, A. K. Sadek, W. Su and K. J. R. Liu, “Outage Analysis and Optimal Power Allocation for Multinode Relay Networks”, IEEE Signal Process. Lett., vol.14, no.6, pp.377–380, Jun. 2007.

[23] M. Hasna and M. S. Alouini, “End-to-end performance of transmission systems with relays over Rayleigh-fading channels,” *IEEE Trans. Wireless Commun.*, vol. 2, no. 6, pp. 1126–1131, Nov. 2003.

[24] S. Ikki and M. H. Ahmed, “Performance analysis of cooperative diversity wireless networks

over Nakagami-*m* fading channels," *IEEE Commun. Lett.*, vol. 11, no. 4, pp. 334–336, Apr. 2007.

[25] B. Maham and A. Hjorungnes, "Asymptotic performance analysis of amplify-and-forward cooperative networks in a Nakagami-*m* fading environment," *IEEE Commun. Lett.*, vol. 13, no. 5, pp. 300–302, May 2009.

[26] S. Ikki and M. H. Ahmed, "Performance of cooperative diversity using equal gain combining (EGC) over Nakagami-*m* fading channels," *IEEE Trans. Wireless Commun.*, vol. 8, no. 2, pp. 557–562, Feb. 2009.

[27] M. Hasna and M. S. Alouini, "A performance study of dual-hop transmissions with fixed gain relays," *IEEE Trans. Wireless Commun.*, vol. 3, no. 6, pp. 1963–1968, Nov. 2004.

[28] H. Shin and J. B. Song, "MRC analysis of cooperative diversity with fixed-gain relays in Nakagami-*m* fading channels," *IEEE Trans. on Wireless Commun.*, vol. 7, pp. 2069-2074, June 2008.

[29] M. Nakagami, "The *m*-distribution, a general formula of intensity distribution of rapid fading," in *Statistical Methods in Radio Wave Propagation*, W. G. Hoffman, ed. Oxford, U.K.: Pergamon, 1960.

[30] W. W. Peterson and D. T. Brown, "Cyclic Codes for Error Detection." In *Proc. of the IRE*, January 1961, 228–235.

[31] S. Lee, M. Han and D. Hong, "Average SNR and ergodic capacity analysis for opportunistic DF relaying with outage over Rayleigh fading channels," *IEEE Trans. on Wireless Commun.*, vol. 8, pp. 2807-2812, June 2009.

[32] Y. Zhao, R. Adve, and T. J. Lim, "Outage probability at arbitrary SNR with cooperative diversity," *IEEE Commun. Letter*, vol. 9, pp. 700-702, Aug. 2005.

[33] N. C. Beaulieu and J. Hu, "A closed-form expression for the outage probability of decode-and-forward relaying in dissimilar Rayleigh fading channels," *IEEE Commun. Letter*, vol. 10, pp. 813-815, Dec. 2006.

[34] W. Su, A. K. Sadek, and R. J. K. Liu, "SER performance analysis and optimum power allocation for decode-and-forward cooperation protocol in wireless networks," in *Proc. IEEE WCNC'05*, vol. 2, pp. 984-989, Mar. 2005.

[35] A. K. Sadek, W. Su, and R. J. K. Liu, "Performance analysis for multi-node decode-and-forward relaying in cooperative wireless networks," in *Proc. IEEE ICASSP'05*, vol. 3, pp. 18-23, Mar. 2005.

[36] Y. Lee and M.-H. Tsai, “Performance of decode-and-forward cooperative communications over Nakagami-m fading channels,” *IEEE Trans. on Vehicular Tech.*, vol. 58, pp. 1218-1228, March 2009.

[37] S. Amara, H. Boujemaa and N. Hamdi, “SEP of cooperative systems using amplify and forward or decode and forward relaying over Nakagami-m fading channels,” in *Proc. IEEE Signals, Circuits and Systems (SCS) 2009*, Medenine, Tunisia, Nov. 2009, pp. 1-5.

[38] Y. Lee and M.-H. Tsai, “Performance of decode-and-forward cooperative communications with multiple dual-hop relays over Nakagami-m fading channels,” *IEEE Trans. on Wireless Commun.*, vol. 8, pp. 2853-2859, June 2009.

[39] S. S. Ikki and M. H. Ahmed, “Performance analysis of multi-branch decode-and-forward cooperative diversity networks over Nakagami-m fading channels,” in *Proc. IEEE ICC 2009*, Dresden, Germany, pp. 1-6. June 2009.

[40] F. Xu, F.C.M. Lau, D.-W. Yue and S.F. Hau, “Error rate and diversity order of multinode cooperative communications in dissimilar Nakagami fading channels,” *IET Commun.*, vol. 3, pp. 1843-1850, Dec. 2009.

[41] W. Su and X. Liu, “On optimum selection relaying protocols in cooperative wireless networks,” *IEEE Trans. on Commun.*, vol. 58, pp. 52-57, Jan. 2010.

[42] M. R. Souryal and B. R. Vojcic, “Performance of amplify-and-forward and decode-and-forward relaying in Rayleigh fading with turbo codes,” in *Proc. IEEE ICASSP*, Toulouse, France, May 2006, pp. 681-684.

[43] X. Bao and J. Li, “Decode-amplify-forward (DAF): a new class of forwarding strategy for wireless relay channels," in *Proc. IEEE Workshop on SPAWC*, NY, USA, pp. 816-820, June 2005.

[44] J. Ch. Fricke, M. M. Butt, and P. A. Hoeher, “Quality-oriented adaptive forwarding for wireless relaying," *IEEE Commun. Lett.*, vol. 12, pp. 200-202, Mar. 2008.

[45] T. E. Hunter and A. Nosratinia, “Diversity through coded cooperation," *IEEE Trans. on Wireless Commun.*, vol. 5, pp. 283-289, Feb. 2006.

[46] M. Janani, A. Hedayat, T. E. Hunter and A. Nosratinia, “Coded cooperation in wireless communications: Space-time transmission and iterative decoding," *IEEE Trans. on Signal Processing*, vol. 52, pp. 362-371, Feb. 2004.

[47] M. N. Khormuji and E. G. Larsson, “Rate-optimized constellation rearrangement for the relay channel,” *IEEE Commun. Lett*. vol. 12, pp. 618-620, Sep. 2008.

[48] M. N. Khormuji and E. G. Larsson, “Improving collaborative transmit diversity by using constellation rearrangement,” in *Proc. IEEE WCNC 2007*, Hong Kong, China, Mar. 2007, pp. 804-808.

[49] Z. Si, R. Thobaben and M. Skoglund, “Instantaneous relaying with bit-interleaved coded modulation: Design and optimization, ” in *Proc. IEEE ISTC2010*, Brest, France, Sept. 2010, pp. 221-225.

[50] T.-W. Yu, W.-H. Sheen and C.-H. Wang, “Power allocation for cooperative bit-interleaved coded modulation systems with decode-and-forward relaying,” I*EEE Trans. on Wireless Commun.*, Accepted, Jan. 2012.

[51] H. Samra, Z. Ding and P. M. Hahn, “Symbol mapping diversity design for multiple packet transmissions,” *IEEE Trans. on Commun.*, vol. 53, no. 5, pp. 810-817, May. 2005.

[52] L. Szczcinski and M. Bacic, “Constellations design for multiple transmissions: Maximizing the minimum squared Euclidean distance,” in *Proc. IEEE WCNC 2005*, Orleans, LA, USA, Mar. 2005.

[53] G. Ungerboeck, “Channel coding with multilevel/phase signals,” *IEEE Trans. Inform. Theory*, vol. IT-28, pp. 56–67, Jan. 1982.

[54] S. H. Jamali and T. Le-Ngoc, *Coded-Modulation Techniques for Fading Channels*. New York: Kluwer, 1994.

[55] E. Biglieri, D. Divsalar, P. J. McLane, and M. K. Simon, *Introduction to Trellis-Coded Modulation with Applications*. New York: MacMillan, 1991.

[56] A. J. Viterbi, J. K. Wolf, E. Zehavi, and R. Padovani, “A pragmatic approach to trellis-coded modulation,” *IEEE Commun. Mag.*, vol. 27, pp. 11–19, July 1989.

[57] E. Zehavi, “Eight-PSK trellis codes for a Rayleigh channel,” *IEEE Trans. Commun.*, vol. 40, pp. 873-884, May 1992.

[58] G. Caire, G. Taricco and E. Biglieri, “Bit-interleaved coded modulation,” *IEEE Trans. on Inform. Theory*, vol. 44, pp. 937-946, May 1998.

[59] *IEEE Standard for Local and Metropolitan Area Networks, Part 11: Wireless LAN medium access control (MAC) and physical layer (PHY) specifications, Amendment 5: Enhancements for higher throughputs*, IEEE Std 802.11n-2009, 2009.

[60] *IEEE Standard for Local and Metropolitan Area Networks, Part 16: Air interface for broadband wireless access systems*, IEEE Std 802.16e-2009, 2009.

[61] R. Hoshyar and R. Tafazolli, “BER performance analysis of a cooperative BICM system

based on post-BSC model," in *Proc. IEEE PIMRC 2008*, Cannes, France, Sept. 2008, pp. 1–5.

[62] R. Hoshyar and R. Tafazolli, "Achievable full decode and forward rates for cooperative MIMO BICM system," in *Proc. 2008 IEEE PIMRC*, Cannes, France, Sept. 2008, pp. 1–5.

[63] G. M. Kraidy, N. Gresset, and J. J. Boutros, "Coding for the nonorthogonal amplify-and-forward cooperative channel," *IEEE Trans. Inf. Theory*, vol. 56, pp. 2601–2610, June 2010.

[64] T. Islam, R. Schober, R. K. Mallik, and V. K. Bhargava, "Analysis and design of cooperative BICM-OFDM systems," *IEEE Trans. Commun.*, vol. 59, pp. 1742–1751, June 2011.

[65] T. Islam, A. Nasri, R. Schober, and R. K. Mallik, "Analysis and relay placement for DF cooperative BICM-OFDM systems," in *Proc. IEEE WCNC 2011*, pp. 1670–1675.

[66] L. J. Rodríguez, N. H. Tran. and T. L.-Ngoc, "Bandwidth-efficient bit-interleaved coded modulation over NAF relay channels: Error performance and precoder design," *IEEE Trans. Vehicular Technology.*, vol. 60, pp. 2086–2101, June 2011.

[67] S. A. K. Tanoli, I. Khan and N. Rajatheva, "Asymptotic BER bounds for BICM-based multiple relay cooperative network under AWGN and Rayleigh fading channels," in *Proc. IEEE ChinaCOM 2009*, Xi'an, China, Aug. 2009, pp. 1–5.

[68] D. J. Costello, Jr., J. Hagenauer, H. Imai, and S. B. Wicker, "Applications of Error-Control Coding," *IEEE Trans. Inform. Theory*, vol. 44, pp. 2531-2560, Oct. 1998.

[69] Z. Qi, et al., "Power allocation for regenerative relay channel with rayleigh fading," in *Proc. IEEE VTC-2004 Spring*, Milan, Italy, May 2004, pp. 1167–1171.

[70] X. J. Zhang and Y. Gong, "Joint power allocation and relay positioning in multi-relay cooperative systems," *IET Commun*. vol. 3, pp. 1683-1692, Sep. 2009.

[71] F. Ke, S. Feng and H. Zhuang, "Relay selection and power allocation for cooperaitve network based on energy pricing," *IEEE Commun. Lett.*, vol. 14, pp. 396-398, May. 2010.

[72] G. Zheng, Y. Zhang, C. Ji and K.-K. Wong, "A stochastic optimization approach for joint relay assignment and power allocation in orthogonal amplify-and-forward cooperative wireless networks," *IEEE Wireless Commun.*, vol. 10., pp. 4091-4099, Dec. 2011.

[73] V. Mahinthan, J. W. Mark and X. Shen, "Performance analysis and power allocation for M-QAM cooperative diversity systems," *IEEE Wireless Commun.*, vol. 9, pp. 1237-1247, March 2010.

[74] D. Wang, Z. Li and X. Wang, "Joint optimal subcarrier and power allocation for wireless

cooperative networks over OFDM fading channels," *IEEE Trans. Vehicular Technology.*, vol. 61, pp. 249–257, Jan. 2012.

[75] T.-W. Yu, W.-H. Sheen and C.-H. Wang, "A low-complexity power allocation for cooperative bit-interleaved coded modulation systems with adaptive decode-and-forward relaying," in *Proc. IEEE PIMRC 2011*, Toronto, Canada, Sept. 2011, pp. 904-908.

[76] I. S. Gradshteyn and I. M. Ryzhik, *Tables of integrals, series, and products*, 7th ed., Burlington, MA: Academic Press, 2007.

[77] P. Robertson, E. Villebrun, and P. Hoeher, "A comparison of optimal and sub-optimal decoding algorithms in the log domain," in *Proc. IEEE ICC'95*, Seattle, WA, USA, Jun. 1995, pp. 1009-1013.

[78] S. Lin and D. J. Costello, Jr., *Error control coding: Fundamentals and applications.* Englewood Cliffs, NJ: Prentice-Hall, 1983.

[79] C. W. Helstrom, *Elements of Signal Detection and Estimation*. New Jersey: PTR Prentice Hall, 1995.

[80] S. P. Boyd and L. Vandenberghe, *Convex Optimization*. Cambridge University Press, 2003.

[81] G. B. Dantzig, *Linear Programming and Extensions.* Princeton University Press, Princeton, New Jersey, 1963.

[82] L. Szczecinski, F.-K. Diop, M. Benjillali, A. Ceron and R. Feick, "BICM in HARQ with mapping rearrangement: Capacity and performance of practical schemes," in *Proc. IEEE GLOBECOM 2007*, Washington, DC, USA, Nov. 2007, pp. 1410-1415.

[83] N. Z. Shor, *Minimization Methods for Non-differentiable functions*. Springer Series in Computational Mathematics. Springer, 1985.

[84] Z. Qi, et al., "Power allocation for regenerative relay channel with Rayleigh fading," in *Proc. VTC-2004 Spring*, Milan, Italy, May, 2004, pp. 1167-1171.